FZR-400

Annual Report 2003

Institute of Radiochemistry

Forschungszentrum
Rossendorf

Annual Report 2003

Institute of Radiochemistry

Editor: Prof. Dr. G. Bernhard

Editorial staff: Dr. H.-J. Engelmann

Forschungszentrum Rossendorf

Cover picture

Bacteria-based bioceramics for bioremediation of uranium mining waste waters

Left side   top: Atomic force micrograph of the uranium mining waste pile isolate *Bacillus sphaericus* JG-A12 (bar 1 µm)

                            middle: Stereomicroscopic picture of biological ceramic (biocer) after incubation with uranium (bar 100 µm)

                            bottom: Scanning electron micrograph of *B. sphaericus* JG-A12 cells embedded in a SiO_2 matrix

Right side   Sorption kinetics of uranium by different types of biocers (200 mg dry weight), *B. sphaericus* JG-A12 cells (36 mg dw) and the SiO_2 matrix itself (164 mg dw)

Preface

The Institute of Radiochemistry (IRC), one of the five institutes of the Forschungszentrum Rossendorf (FZR), performs basic and applied research in the fields of radiochemistry and radioecology. The motivation and background of our research are environmental processes relevant to the installation of nuclear waste repositories, for the remediation of uranium mining and milling sites, and radioactive contamination caused by nuclear accidents and fallout. Because of their high radiotoxicity and long half-life, actinides are of special interest. The research is focused on a better understanding of the chemical behavior of actinides in the in environment at a molecular level. Current topics of our research work are:

- Aquatic chemistry of the actinides
- Actinides in biosystems
- Interaction of actinides with solid phases
- Reactive transport of the actinides

About 60 scientists, technicians and PhD students are employed at the Institute of Radiochemistry.

Many new scientific results obtained in the past year are presented in this Annual Report, although only very few of them can be highlighted in the preface.

Further progress has been achieved in understanding the photochemical reactions of organic ligands in the process of measuring actinide complexes with our new fs- laser-spectroscopic system. In the field of basic research we determined the stability constants of various uranium complexes with bioligands, such as phosphate-containing sugars, amino acids, proteins, and peptides, so as to improve our understanding of uranium binding in biological systems. For the first time we were able to show by spectroscopy that uranium (VI) is reduced to uranium (IV) by special synthetic humic acids.

The number and quality of data sets and the functionality of our mineral-specific database RES^{3}T for surface complexation have been increased considerably.

We obtained some first results concerning the isolation and characterization of various bacteria in ground water samples from a Russian radioactive waste repository.

The formation of colloids during the flooding of uranium mines was experimentally tested on a pilot scale.

We proudly report that Dr. Andre Roßberg has been awarded the prize of the Nuclear Chemistry Section of the German Chemical Society for his doctoral thesis "Anwendung der Faktorenanalyse auf die Röntgenabsorptionsspektroskopie zur Bestimmung der Speziation von Uran in Lösungen" (Use of Factor Analysis in X-ray Absorption Spectroscopy for Determination of Uranium Speciation in Solutions).

This past year also brought some changes at the Institute. In November 2003 I was honoured by being appointed the new director of the Institute of Radiochemistry. I particularly wish to thank Professor Frank-Peter Weiß (Director of the Institute of Safety Research, FZR) who was acting director of the Institute for almost two years.

Further, I would like to thank our visitors, both from Germany and abroad, for their interest in our research and for their participation in the Institute's seminars. Thanks are also due to our scientific collaborators and the visiting scientists for coming to Rossendorf / Dresden in 2003 to share their knowledge and experience with us.

In the future this collaboration by visiting scientists will be strongly encouraged by us.

Special thanks for their support go to the Executive Board of the Forschungszentrum Rossendorf, the Ministry of Science and Arts of the Free State Saxony, the Federal Ministries of Education and Research and of Economics and Employment, the German Research Association (Deutsche Forschungsgemeinschaft), the European Commission as well as other organizations.

Prof. Dr. Gert Bernhard

CONTENT

I. SCIENTIFIC CONTRIBUTIONS

1. AQUATIC CHEMISTRY OF ACTINIDES / RADIONUCLIDES

2. ACTINIDES / RADIONUCLIDES IN BIOSYSTEMS

3. INTERACTION OF ACTINIDES / RADIONUCLIDES WITH SOLID PHASES

4. REACTIVE TRANSPORT OF ACTINIDES / RADIONUCLIDES

II. PUBLICATIONS, LECTURES, POSTERS, PH.D. AND DIPLOMA THESES, PATENTS, AWARDS

I. SCIENTIFIC CONTRIBUTIONS

Aquatic Chemistry of Actinides / Radionuclides

FLUORESCENCE PROPERTIES OF URANIUM(IV)

G. Geipel

The fluorescence of uranium(IV) was studied, using an Nd:YAG pumped OPO system as the excitation source and a combination of a 270 mm spectrograph with an ICCD -camera system as the detector. The fluorescence emission maxima were confirmed. The fluorescence lifetime at room temperature was found to be 2.69 ± 0.08 ns.

The fluorescence of uranium(IV) in aqueous solution was first described by Kirishima et.al. /1/, who found the fluorescence emission bands to be in agreement with the absorption spectrum of uranium(IV) in per-chloric acid. However, an exact determination of the fluorescence lifetime was not possible due to the pulse duration of the excitation laser.

To confirm these results and to determine the fluorescence lifetime of uranium(IV), we carried out time-resolved laser-induced fluorescence measurements, using a uranium(IV) solution prepared by electrochemical reduction of a uranium(VI) stock solution in perchloric acid. The solution was then diluted to 1.0E-04 M in uranium and to 0.1 M in perchloric acid. The absence of uranium(VI) was confirmed by laser-induced fluorescence measurement, using 266 nm laser excitation.

As reported in /1/, the excitation wavelength of uranium(IV) fluorescence was found to be 245 nm. After excitation in the wavelength range between 244 nm and 251 nm, we studied the fluorescence emission of uranium(IV), using an OPO-tunable laser system.
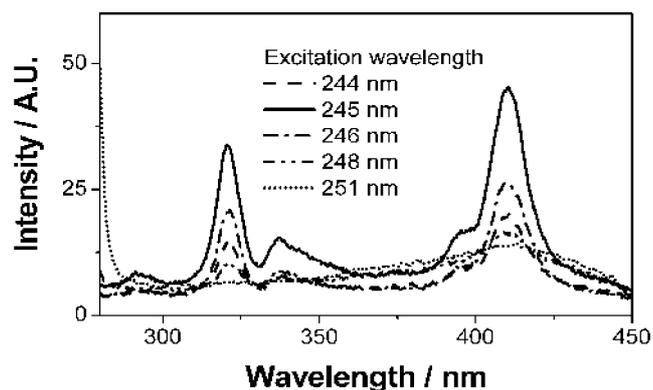
Fig. 1: Fluorescence spectrum of uranium(IV) in perchloric acid

Fig. 1 shows the fluorescence spectra of uranium(IV) as a function of the excitation wavelength. It turned out that the fluorescence of uranium(IV) was only excited in a very small wavelength range. The FWHM (Full Width at Half Maximum) of the absorption peak at excitation wavelength was found to be 2.7 nm.

Eight emission lines of the fluorescence of uranium(IV) were observed in the wavelength range between 290 nm and 550 nm. These peaks were located at 290, 318, 332, 338, 350, 389, 403 and 525 nm. The peaks at 290 nm and at 318 nm were unable to be resolved. Fig. 2 shows the time resolved fluorescence spectrum of the uranium(IV) solution. A fluorescence-decay time of less than 20 ns was expected in /1/. It was found to be 2.69 ± 0.08 ns.

We also studied the fluorescence spectra of uranium(IV) complexes. Fig. 4 shows, for example, the fluorescence spectrum of the uranium(IV) phosphate complex. At room temperature only one peak was ob-

tained at 308 nm. A broad unstructured fluorescence was found in the wavelength range 300 - 420 nm. Similarly broad and little structured spectra were obtained in sulphate, chloride and arsenate media.
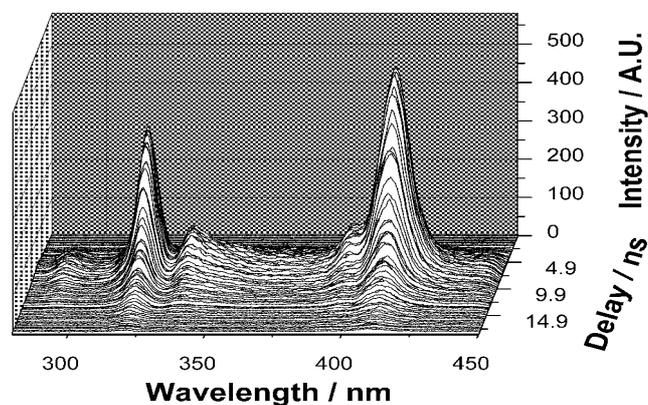
Fig. 2: Time-resolved fluorescence spectrum of uranium(IV) in perchloric acid
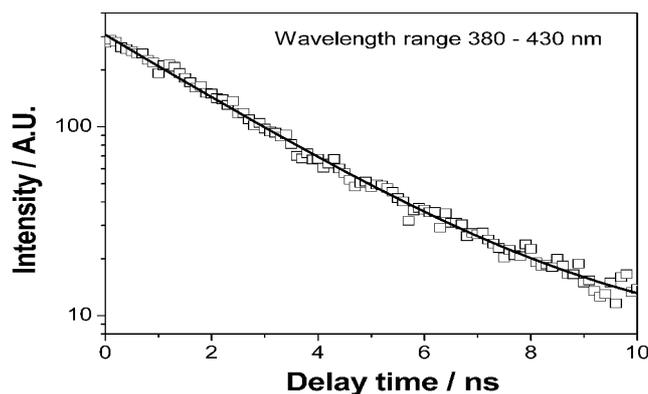
Fig. 3: Fluorescence decay of uranium(IV) in perchloric acid
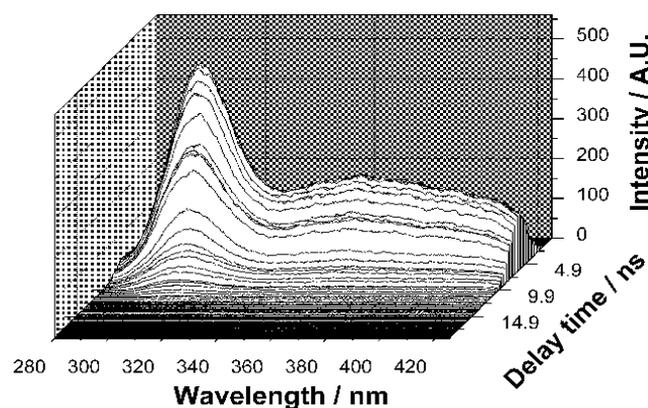
Fig. 4: Fluorescence of uranium(IV) in phosphoric acid

The fluorescence properties of uranium(IV) make it, however, possible to study the behavior of tetravalent actinide ions in lower concentrations than are required when using laser-induced photoacoustic spectroscopy.

References

/1/ Kirishima, A. et. al., Chem. Comm. 910 (2003)

EXAFS INVESTIGATION OF URANIUM COMPLEXATION BY GLUCOSE 6-PHOSPHATE AND FRUCTOSE 6-PHOSPHATE

A. Koban, A. Roßberg, G. Bernhard

The complex systems of U(VI) with glucose 6-phosphate and fructose 6-phosphate show a monodentate complexation of the uranium via the phosphate group.

To obtain further information concerning the binding properties and the structure of actinides in biological systems, we investigated selected bioligands with relevant functionalities such as sugar phosphates as model compounds. Potentiometric measurements show that the uranyl ion builds two complexes with the ligands glucose 6-phosphate G6P and fructose 6-phosphate F6P ($C_6H_{11}O_6PO_3^{2-}$ each), with a metal-to-ligand ratio of 1:1 $[UO_2(C_6H_{11}O_6PO_3)]$ and 1:2 $[UO_2(C_6H_{11}O_6PO_3)_2^{2-}]$ /1/.

The EXAFS measurements were carried out on solutions containing 10^{-3} M uranyl (sample U-F6P pH 5.5 5×10^{-3} M) with ligand concentrations from 5×10^{-3} to 5×10^{-2} M and various pH values (Tab.1) in polyethylene tubes of 13 mm diameter. Measurements were performed on the Rossendorf Beamline (ROBL) at the European Synchrotron Radiation Facility (ESRF) in Grenoble. The U L_{III}-edge spectra were measured in fluorescence modus. The EXAFS spectra were analyzed, using the suite of programs EXAFSPAK. The theoretical scattering phase and amplitude functions used in data analysis were calculated, using x-ray data from uranyl nitrate trimethylphosphate $UO_2(NO_3)_2(PO_4(CH_3)_3)$ /2/ by the FEFF8 program.

Fig. 1 shows the raw U L_{III}-edge k^3-weighted EXAFS spectra and the corresponding Fourier transform (FT) including the best theoretical fits for the uranyl sugar phosphate systems. The EXAFS structural parameters are summarized in Table 1.

Three peaks are visible in the FT of the complexed samples. The first and the second peak correspond to the scattering contribution of the two axial oxygen atoms (O_{ax}) of the uranyl ion and the scattering contribution of the equatorial oxygen atoms (O_{eq1}). The third peak is probably caused by backscattering from a light element such as carbon or oxygen. In view of the significant possibilities in the molecules, we assumed an oxygen shell (O_{eq2}) in our fit.

The U-O_{eq1} distances of the complexed species are much shorter than those of the pure uranyl hydrate $UO_2(H_2O)_5^{2+}$. This is due to coordination of the uranyl ion *via* the phosphate group in monodentate fashion. However, in this case a backscatterer contribution of phosphorus should be visible in the FT. As the U–P path and the three-fold U–O–P multiple scattering path nearly mutually extinguish themselves /3/, the small amplitude of the U–P and the U–O–P backscatterer contribution is strongly superimposed by the noise and was therefore not fitted.

The average U–O_{eq1} bond distance depends on the coordination number of the equatorial shell of U(VI). According to Burns et al. /4/ a five-fold coordination sphere seems to be most likely.

The peak at 2.3 Å in the FT cannot be reproduced only by coordinated water molecules and monodentate coordinated phosphate groups alone. We have modeled this backscatterer contribution with oxygen atoms (O_{eq2}). However, the origin of this scattering contribution is not yet understood and is currently under investigation.

Sample	Shell	N	R [Å]	σ^2 [10^{-3}Å^2]
UO_2^{2+}, pH 1.0	U-O_{ax}	*2f*	1.754(3)	1.1(2)
	U-O_{eq}	4.7(4)	2.402(5)	4.(7)
U-G6P, pH 3.5	U-O_{ax}	*2f*	1.768(2)	0.7(2)
92% UO_2(G6P),	U-O_{eq1}	7(1)	2.34(1)	19(3)
3% UO_2(G6P)$_2^{2-}$	U-O_{eq2}	1.4(3)	2.84(1)	*4f*
U-G6P, pH 4.0	U-O_{ax}	*2f*	1.773(3)	1.2(2)
68% UO_2(G6P),	U-O_{eq1}	5.2(9)	2.33(1)	12(2)
32% UO_2(G6P)$_2^{2-}$	U-O_{eq2}	1.0(6)	2.90(2)	1(3)
U-G6P, pH 5.5	U-O_{ax}	*2f*	1.771(3)	1.0(2)
7% UO_2(G6P),	U-O_{eq1}	5.9(8)	2.31(1)	13(1)
93% UO_2(G6P)$_2^{2-}$	U-O_{eq2}	0.9(3)	2.90(2)	*4f*
U-F6P, pH 3.5	U-O_{ax}	*2f*	1.773(3)	0.9(1)
78% UO_2(F6P),	U-O_{eq1}	5.7(9)	2.37(1)	16(2)
5% UO_2(F6P)$_2^{2-}$	U-O_{eq2}	1.3(3)	2.87(1)	*4f*
U-F6P, pH 4.0	U-O_{ax}	*2f*	1.773(3)	1.4(2)
30% UO_2(F6P),	U-O_{eq1}	5.2(8)	2.32(1)	12(2)
70% UO_2(F6P)$_2^{2-}$	U-O_{eq2}	1.6(3)	2.88(2)	*4f*
U-F6P, pH 5.5	U-O_{ax}	*2f*	1.773(2)	1.3(1)
2% UO_2(F6P),	U-O_{eq1}	4.8(5)	2.30(1)	20(4)
98% UO_2(F6P)$_2^{2-}$	U-O_{eq2}	1.3(2)	2.88(1)	*4f*

Standard deviations of variable parameters are given in parenthesis; N - coordination number; R – Radial distance; σ^2 – Debye-Waller factor, *f*: parameter fixed during the fitting procedure.

Tab. 1: Summary of the EXAFS structural parameters.
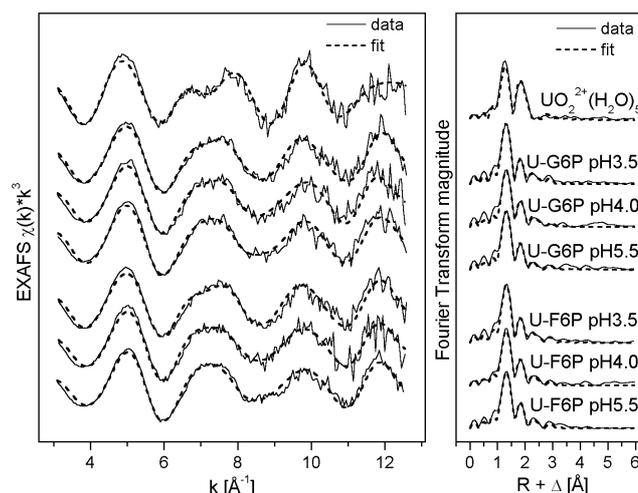
Fig. 1: Raw U L_{III}-edge k^3-weighted EXAFS spectra (left) and the corresponding Fourier transform (FT) (right).

References
/1/ Koban, A. et al., Radiochim. Acta, accepted (2004)
/2/ Agostini, G. et al., Inorg. Chim. Acta **62**, 237 (1982)
/3/ Den Auwer, C. et al., Polyhedron **17,** 4507 (1998)
/4/ Burns, P.C. et al., Can. Mineral. **34** 845 (1996)

COMPLEX FORMATION OF URANIUM(VI) WITH GLYCEROL 1-PHOSPHATE

A. Koban, G. Bernhard

TRLFS measurements of the complex system show an increase of the fluorescence intensity connected with a red shift of the fluorescence maxima. Formation constants for the complexes $UO_2(C_3H_7O_3PO_3)$ and $UO_2(C_3H_7O_3PO_3)_2^{2-}$ were determined by TRLFS and potentiometric titration.

Introduction

Glycerol 1-phosphate is widely distributed in biological systems, as constituent of phospholipids or as intermediate of metabolism. Because of its simple and clear structure it can serve as model for the interaction of actinides with more complex biological systems, such as phospholipids.

We studied the complexation behavior of uranium(VI) with glycerol 1-phosphate ($C_3H_7O_3PO_3^{2-}$), using TRLFS and potentiometric titration /1/.

TRLFS

The TRLFS measurements were performed at a fixed uranyl concentration (10^{-5} M) as a function of the ligand concentration (10^{-5} to 2×10^{-3} M) at pH = 4.00 $\pm$ 0.05, I = 0.1 M (NaClO$_4$) and T = 25 $\pm$ 2 °C.

Fig. 1 shows the fluorescence spectra of uranium(VI) as a function of the concentration of glycerol 1-phosphate. With increasing ligand concentration we notice a strong increase in fluorescence intensity, connected with a red shift of about 9 nm compared to the uranyl ion.

The TRLFS spectra show tri-exponential decays indicating a mixture of three species. The lifetimes are (averaged about all measurements) 155 $\pm$ 30 ns, 800 $\pm$ 160 ns, and 7 $\pm$ 3 µs. The lifetime of 7 µs with a very low but constant intensity can be assigned to uranyl hydroxide, which is always present in small amounts under such experimental conditions. The intensity of the second lifetime (800 $\pm$ 160 ns) decreases with increasing ligand concentration, whereas the intensity of the shortest lifetime (155 $\pm$ 30 ns) increases. A lifetime of 800 ns seems to be quite short for UO_2^{2+}(aq), but test solutions of UO_2^{2+}(aq) at pH 4 and 1 under same conditions showed lifetimes of 761 $\pm$ 46 ns (pH 4) and 784 $\pm$ 31 ns (pH 1), respectively. Therefore we assign the lifetime of 800 $\pm$ 160 ns to the free uranyl ion and the lifetime of 155 $\pm$ 30 ns to the uranyl(VI) glycerol 1-phosphate complex.

To estimate the stoichiometry of this complex a slope analysis for reaction (1) was made using the mass action law in its transformed linear form (2):

$$UO_2^{2+} + n\ C_3H_7O_3PO_3H_2 \leftrightarrow UO_2(C_3H_7O_3PO_3)_n^{(2-2n)+} + 2n\ H^+ \qquad \log \beta_{1n}* \qquad (1)$$
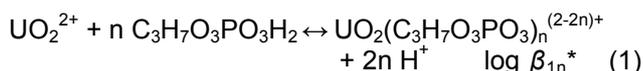
$$\log \frac{[complex]}{[UO_2^{2+}]_{free}} = n\log[ligand]_{free} + \log \beta_{1n}* + 2n\ pH \qquad (2)$$

The concentrations of the free uranyl ion were determined on the basis of the measured absorption spectra using conventional peak deconvolution.

These data were used to calculate the corresponding concentrations of the complex and the non complexed ligand. The slope of 1.24 $\pm$ 0.04 indicates a predominant formation of the 1 : 1 complex $UO_2(C_3H_7O_3PO_3)$.
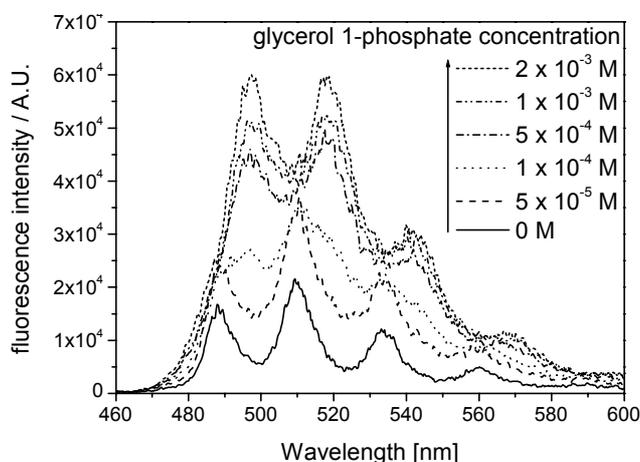
Fig. 1: TRLFS spectra of uranium(VI) (10^{-5} M) as a function of the ligand concentration at pH=4.0.

Taking into account the dissociation of glycerol 1-phosphoric acid, the complexation reaction can be written as follows:

$$UO_2^{2+} + C_3H_7O_3PO_3^{2-} \leftrightarrow UO_2(C_3H_7O_3PO_3) \quad \log\beta_{11} \quad (3)$$

The complex stability constant of $UO_2(C_3H_7O_3PO_3)$ results to be $\log\beta_{11}$ = 6.15 $\pm$ 0.05.

The spectra of the uranyl glycerol 1-phosphate complex can be isolated from the composite spectra using conventional peak deconvolution. The peak maxima of the complexed uranyl species are located at 497, 518, 543, 569, and 599 nm.

Potentiometric titration

The potentiometric titration experiments were carried out at a starting volume of 50 mL with two different uranyl concentrations (1×10^{-4} and 5×10^{-4} M) and glycerol 1-phosphate concentrations (5×10^{-4} M and 10^{-3} M) each at T = 25.0 $\pm$ 0.1 °C, I = 0.1 M (NaClO$_4$) under carbonate free conditions like described in /2/.

The measured titration data were analyzed in the pH range from 3 to 8 using the Hyperquad 2000NT least squares program, version 2.1 /3/.

Two complexes with a metal-to-ligand ratio (M:L) of 1:1 and 1:2 could be observed. The equilibrium constants were determined to be $\log\beta_{11}$ = 6.23 $\pm$ 0.09 for $UO_2(C_3H_7O_3PO_3)$ and $\log\beta_{12}$ = 10.22 $\pm$ 0.13 for $UO_2(C_3H_7O_3PO_3)_2^{2-}$. Besides at almost all titration curves any other complexes with a 1:3 or 2:3 stoichiometry or protonated species could be fitted to improve the fit parameter. Thus still more species seems to exist in this system. Further investigations are necessary to validate this presumption.

References

/1/ Koban, A. et al., Polyhedron, accepted (2004)
/2/ Koban, A. et al., Radiochim. Acta **91**, 393 (2003)
/3/ Gans, P. et al., Talanta **43**, 1739 (1996)

COMPLEX FORMATION OF URANIUM (VI) WITH L-THREONINE BY TRLFS

A. Günther, G. Geipel, G. Bernhard

We studied the complex formation of uranium (VI) with the amino acid L-threonine at pH 4 . We found a fluorescent 1:1 complex. The formation constant was assigned to be log K = 2.71 ± 0.12.

The object of this study was to determine the fluorescence properties of U(VI) complexes with several amino acids, e.g. with L-threonine in aqueous solution. The fluorescence data were used for identification of uranium complexes formed in biological systems (plants, bacteria).

The measurements were performed on $5 \cdot 10^{-5}$ M uranium. The concentration of L-threonine varied between 0 and $1.5 \cdot 10^{-2}$ M. All fluorescence measurements were performed at an ionic strength of I=0.1M ($NaClO_4$) and pH 4. The setup of the time-resolved laser-induced fluorescence spectroscopy is described in /1/.

Fig. 1 shows the spectra of uranium(VI) as a function of the total L-threonine concentration. We found an increasing fluorescence intensity with increasing ligand concentration and a small red shift.
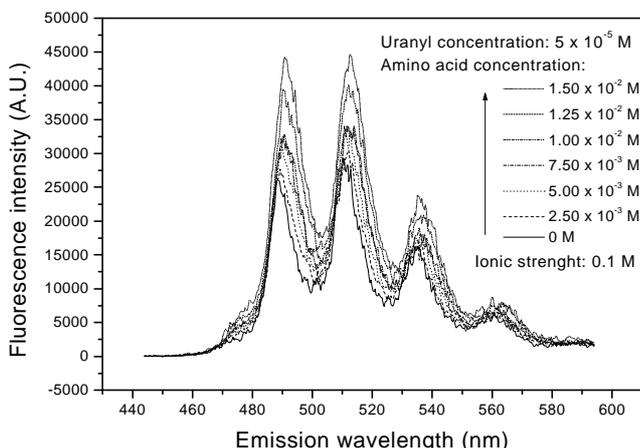
Fig. 1: Fluorescence spectra of uranium (VI) as a function of the L-threonine concentration at pH 4
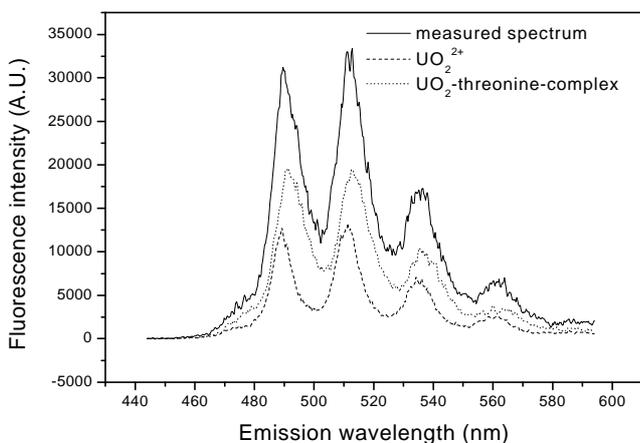
Fig. 2: Peak deconvolution of the fluorescence spectrum of a solution containing $5 \cdot 10^{-5}$M uranyl and $5 \cdot 10^{-3}$M L-threonine at pH 4.

The time-resolved spectra showed a bi-exponential fluorescence decay indicating a mixture of two species. The longer lifetime (~1700 ns) is typical for the free uranyl ion. The shorter lifetime (~880 ns) can be assigned to the uranyl-L-threonine complex.

The single spectra of the various species were determined from the composite spectrum using conventional peak deconvolution (Fig. 2). The main fluorescence emission bands of the uranyl-L-threonine complex are located at 476, 492, 514, 537 and 565 nm.

The reaction of UO_2^{2+} and L-threonine at pH 4 can be written as:

$$UO_2^{2+} + x \; [^+NH_3CHCOO^-$$
$$| \qquad\qquad \Leftrightarrow \; UO_2[L\text{-threonine}]_x^{2+}$$
$$CH(OH)CH_3]$$
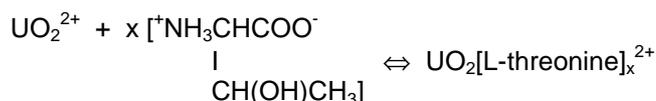
After rearranging and transforming the mass action law, we obtain the following equation:

$$\log \frac{[(UO_2(L-threonine)_x)^{2+}]}{[UO_2^{2+}]} = \log K + x \log[L\text{-threonine}]$$

The concentration of the free uranyl ion was determined on the basis of the fluorescence spectra measured. These data were used to calculate the corresponding concentration of the complex and the non-complexed ligand.
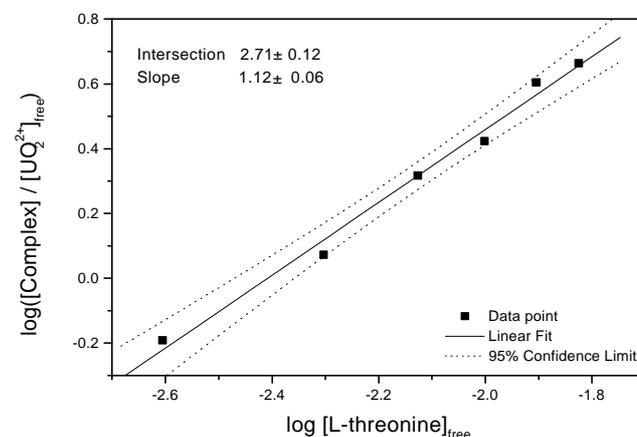
Fig. 3: Slope analysis of the complex formation at pH 4 and ionic strength of 0.1 M

The validation of complex formation is shown in Fig.3. By plotting the log ($[UO_2complex]$ / $[UO_2^{2+}]_{free}$) vs. the log ($[L\text{-threonine}]_{free}$) we obtain the stoichiometry of the complex reaction from the slope. The value x is found to be 1.12 ± 0.06, which clearly shows a 1:1 complex formation. From the intersection the formation constant at an ionic strength of 0.1 M is obtained to be log K = 2.71 ± 0.12.

References

/1/ Geipel, G. et al. Radiochim. Acta **75**, 199-204 (1996)

COMPLEX FORMATION OF URANIUM (VI) WITH O-PHOSPHO-L-THREONINE BY TRLFS

A. Günther, G. Geipel, J. Raff, G. Bernhard

We studied the complex formation of uranium (VI) with O-phospho-L-threonine at pH 4, using time-resolved laser-induced fluorescence spectroscopy. We found two complex species with a high fluorescence yield.

In continuation of our studies concerning the complex formation of U(VI) with amino acids /1,2/, we investigated the uranyl - phosphorus containing L-threonine system at pH 4. Studies of the surface layer (S-layer) protein from the uranium mining waste pile isolate *Bacillus spaericus* JG-A12 indicate the presence of O-phospho-L-threonine (p-threonine) in its primary structure.

The TRLFS spectra were recorded with a pulsed Nd:YAG laser system. The excitation wavelength of the uranyl fluorescence was 266 nm at a laser energy of 200 – 350 µJ. The experiments were performed at a fixed uranyl concentration of $5 \cdot 10^{-5}$ M. The ligand concentration of p-threonine varied between $1 \cdot 10^{-5}$ and $1 \cdot 10^{-2}$ M. Using $NaClO_4$, the ionic strength of the complex solutions was adjusted to 0.1 M. The pH value was constant at 4. The complex forming reaction can be written as :

$$UO_2^{2+} + x \ [\text{p-threonine}] \Leftrightarrow UO_2[\text{p-threonine}]_x^{(2-y)+} + yH^+ \quad (1)$$
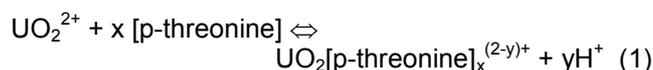
with

$$\log \frac{[(UO_2(p-threonine)_x)^{(2-y)+}]}{[UO_2^{2+}]}$$

$$= \log K + x \log[\text{p-threonine}] - y \log [H^+] \quad (2)$$

At a constant hydrogen ion concentration is

$$\log K' = \log K - y \log [H^+] \quad (3)$$

The complex formation of the uranyl cation is possible by the carboxyl and/or the phosphate group.

Fig.1 shows the fluorescence spectra of uranium (VI) as a function of the total p-threonine concentration.
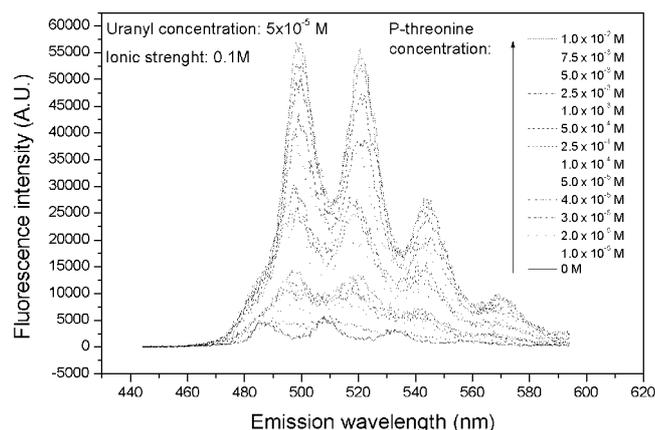
Fig. 1: Fluorescence spectra of uranium (VI) as function of the O-Phospho-L-threonine concentration at pH 4

We found an increase of the fluorescence intensity and a red shift of the emission bands compared to the measurement of the uranyl test solution of $5 \cdot 10^{-5}$ M already at low uranium p-threonine concentration.

In addition to the free uranyl we determined two uranyl complex species by analysis of the fluorescence decay (Fig. 2). The lifetimes are ~ 1600 ns for the free UO_2^{2+} (aq) and ~700 ns for the 1:1 complex. The lifetime of ~ 4400 ns is attributed to the 1:2 complex.
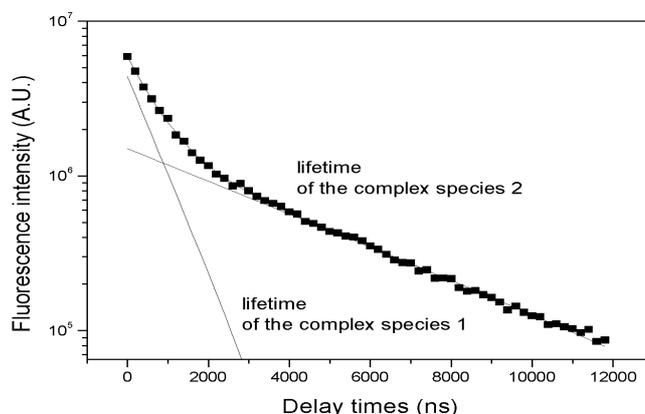
Fig. 2: Bi-exponential fluorescence decay of the solution with $5 \cdot 10^{-5}$ M uranium and $1.25 \cdot 10^{-4}$ M p-threonine (1:25) at pH 4
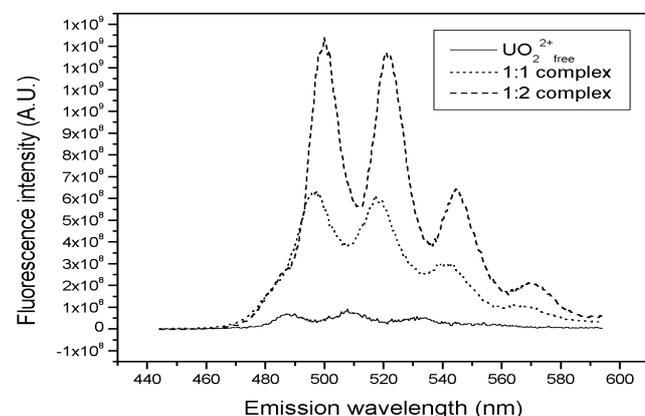
Fig. 3: Peak deconvolution of the spectra of the U(VI) / p-threonine system at pH 4.

The main emission bands of the first uranyl-p-threonine complex are 481.4, 496.6, 517.7, 541.0 and 567.0 nm. 483.7, 500.1, 521.5, 544.6 and 569.3 nm are the emission bands for the second complex species (Fig. 3). Compared with the uranyl-sulphate system /3/ the difference of the emission bands of the complex species is very small. That is why it was not possible in the first formulation to calculate the complex formation constant by slope analysis (equation 2 and 3), using fluorescence intensity of the deconvoluted spectra of the single species and the lifetimes too. With the factor analysis calculation program SPECFIT /4/ the formation constants were calculated to be log K'_{11}= 4.40 ± 0.09 for the 1:1 complex and log K'_{12}= 6.84 ± 0.17 for the 1:2 complex. The model used can only provide information on log K' as no data on the dependence of the spectra on pH are available.

References

/1/ Günther, A. et al.; this report p.4

/2/ Günther, A., Roßberg, A., Bernhard, G. Report FZR-373, p.3 (2002)

/3/ Geipel, G. et al. Radiochim. Acta **75**, 199-204 (1996)

/4/ SPECFIT 32, Spectrum Software – Associates 2003

VALIDATION OF THE COMPLEX FORMATION BETWEEN URANIUM(VI) AND 2,5-DIHYDROXYBENZOIC ACID

G.Geipel, S. Nagasaki

To validate the complex formation between uranium(VI) and 2,5-dihydroxybenzoic acid the fluorescence properties of uranium were used. A dynamic quench process occurs besides the static quench process caused by the complex formation. A 1:1 complex forming reaction was found and the stability constant was assigned to be log K = 3.79 ± 0.06.

In a former study /1/ we used the fluorescence properties of the 2,5-dihydroxybenzoic acid to study the complex formation between uranium(VI) and 2,5-dihydroxybenzoic acid. Taking into account the dynamic quench effect of the uranium onto the fluorescence of the 2,5-dihydroxybenzoic acid and effects of excited state reactions of the ligand a 1:1 stoichiometry was found. In the pH range 2.5 - 4.5 the complex forming reaction was found to be independent on the pH. Therefore the reaction equation was assigned to be

$$UO_2^{2+} + H_2L^- <=> UO_2H_2L^+ \qquad (1)$$
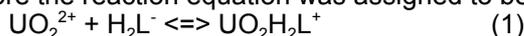
The stability constant was assigned to be log K = 3.59 ± 0.08.

As the uranylion also emitts fluorescence after excitation this can be used to validate the complex formation. As found already in /1/ the formed complex does not emitt any fluorescence at room temperature. Therefore only the fluorescence of the non-complexed uranylion can be used to determine the complex formation.

Using the following model

$$UO_2^{2+} + x\ H_2L^- <=> UO_2(H_{(2-y)}L)_x^{(2+2x-y)+} + xy\ H^+ \quad (2)$$
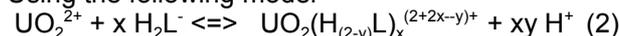
The stability constant can be determined by scanning over the concentration of the added ligand and over pH. Experiments were carried out in the pH range 2.5 - 4.0.

A strong pH dependent dynamic quench effect of the ligand system on the fluorescence of the non-complexed uranium(VI) was observed.

The dynamic quench constant K_{SV} was found to follow the equation

$$K_{SV} = 36000 - 8000 \cdot pH \qquad (3)$$

From this behavior we conclude that mainly the non-dissociated ligand H_3L is responsible for the dynamic quenching.

In Fig. 1 a time-resolved fluorescence spectrum of uranium is shown. The uranium concentration in the measured solution was 5.0E-05 M, the concentration of the added ligand 8.0E-05 M. The ionic strength was adjusted to 0.1 M with $NaClO_4$ and the pH was 3.5.
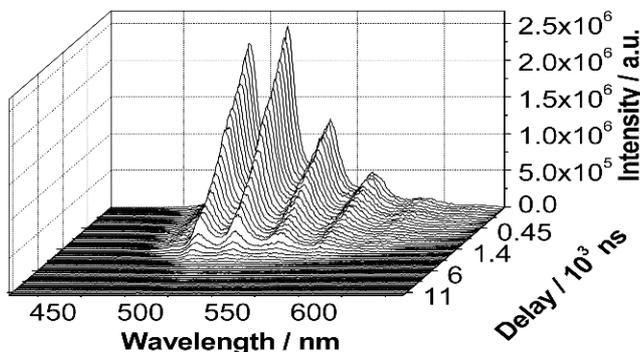
Fig. 1: Time-resolved fluorescence spectrum of uranium(VI)

Nevertheless the fluorescence decay was found to be diexponentiell. This behavior is shown in Fig. 2 for the same solution. The fluorescence decay times were found to be 0.927 ± 0.001 µs and 8.19 ± 0.005 µs. The fluorescence intensity of the long decaying species is very low and reaches about 3%. The fluorescing species responsible for this emission was therefore assigned to be $UO_2(OH)^+$.
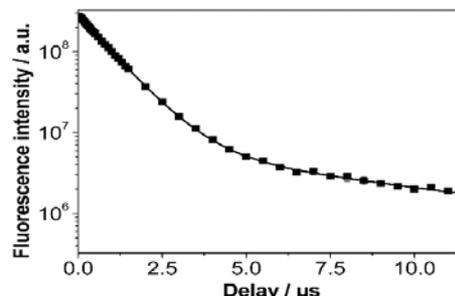
Fig. 2: Fluorescence decay of uranium(VI) species

A 1:1 complex stoichiometry was derived from the slope analysis. The stability constants vary between 3.49 ± 0.13 and 3.93 ± 0.12 in the studied pH range.
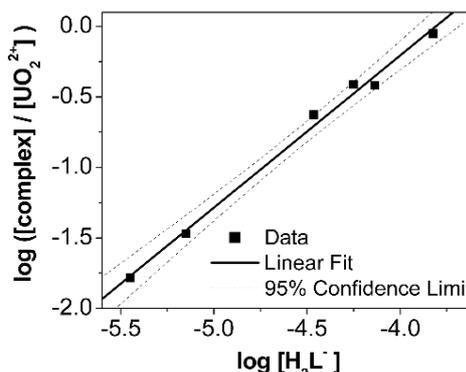
Fig. 3: Slope analysis of the complex formation at pH 3.5
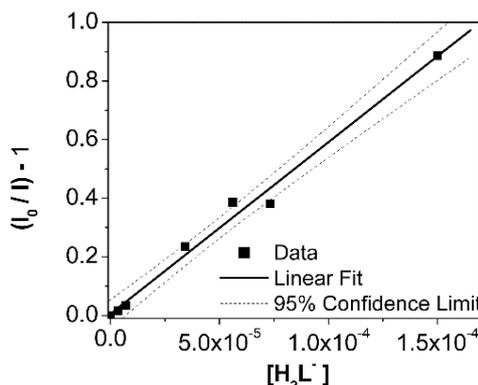
Fig. 4: Stern-Volmer plot at pH 3.5

No dependence of the stability constant could be observed. Therefore we conclude, that the reaction equation (1) could be confirmed. The stablity constant by use of the uranium measurements was assigned to be log K = 3.79 ± 0.06. This is in good agreement with the data derived from the measurements of the ligand fluorescence.

References
/1/ Geipel, G., Nagasaki, S., Report FZR-373, p.9

EXCITED STATE REACTIONS OF ORGANIC LIGANDS

G. Geipel, D. Vulpius, G. Bernhard

We studied the complex formation between uranium(VI) and 2,3-dihydroxybenzoic acid /1/. The estimation of the stability constant resulted in a difference of 0.8 orders of magnitude using the fluorescence properties of uranium and of the ligand, respectively. To explain this difference we have to include an excited state reaction of the non-complexed ligand

Recently we reported on studies of complex formation between uranium and 2,3-dihydroxybenzoic acid (2,3-DHBA) /1/. The stability constant obtained from the fluorescence properties of the uranyl ion (dynamic and static quenching process) differs by about 0.8 orders of magnitude from that derived from fluorescence measurements of the ligand (only static quenching).

It is obvious that during the excitation the formed complex is not changed /2/.

The ligand may undergo several photochemical processes during the excitation.

If the solvent water acts as proton acceptor the following scheme can be applied to excited state reactions:

$$A^* \underset{k_b}{\overset{k_a}{\rightleftharpoons}} H^+ + B^*$$

$$k_f + k_d \downarrow\uparrow \qquad\qquad \downarrow k'_f + k'_d$$

$$A \qquad\qquad\qquad B$$
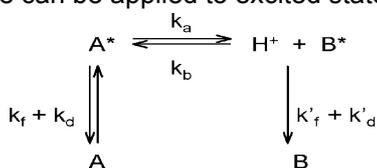
The kinetic constants k_a and k_b can be derived as follows /3/:

$$\frac{\Phi/\Phi_0}{\Phi'/\Phi'_0} = \frac{1}{k_a\tau_0} + \frac{k_b\tau'_0}{k_a\tau_0}\left[H^+\right] \qquad (1)$$

Fluorescence spectra at low pH demonstrate that the non-deprotonated ligand does not emit fluorescence.

In strong acid media occurs upon excitation an excited state proton transfer reaction and a fluorescing species is formed. The fluorescence lifetime of this species is extremely short (~ 70 ps) (Fig. 1).
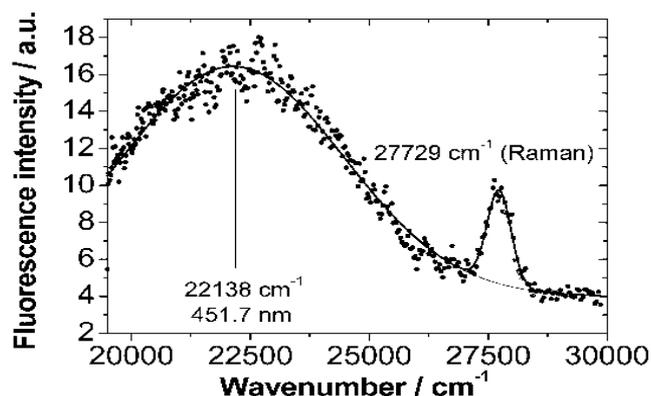
Fig. 1: Fluorescence spectrum of 2,3-dihydroxybenzoic acid in 1 M HClO$_4$

At pH > 2 this species cannot be observed. The phenolic OH group becomes more acidic and starts to dissociate at low pH values in the excited state. This effect is well-known from naphthol /4/.

It is not clear, whether the reaction equilibrium is reached or not during the lifetime of the excited state.

We used the fluorescence decay data of the 2,3-dihydroxybenzoic acid in the pH range 2.0 to 6.8 to perform a global analysis. From this we obtain a rate constant k_a of $1.0 \cdot 10^{10}$ L· Mol^{-1} · s^{-1} and k_b of $2.8 \cdot 10^{10}$ L · Mol^{-1} · s^{-1}. However, these constants have to be
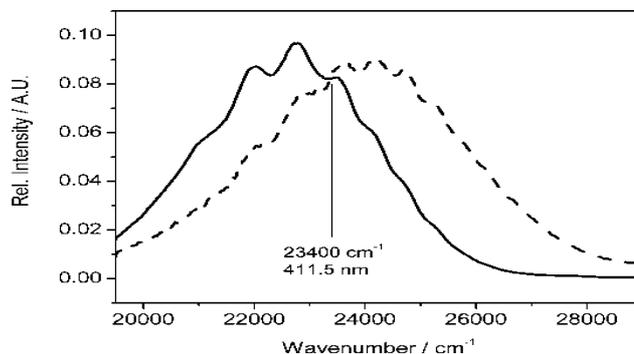
Fig. 2: Component analysis of the fluorescence spectra
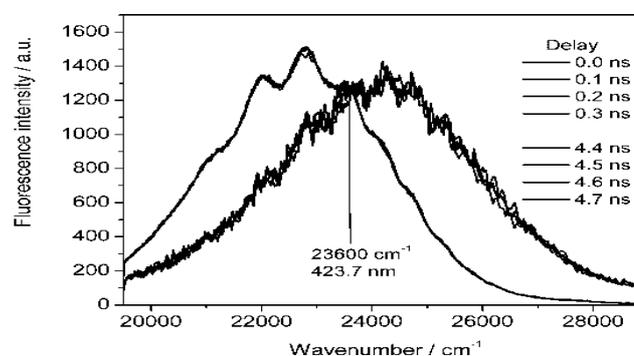
Fig. 3: Construction of the isoemissive point of a time-resolved spectrum
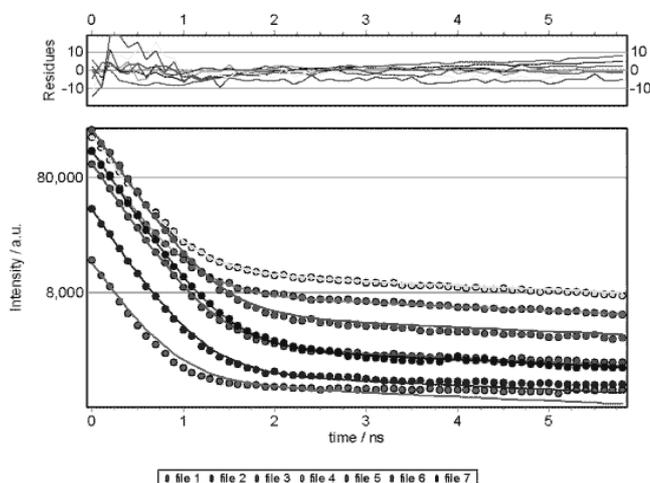
Fig. 4: Global analysis of the fluorescence decay

confirmed by steady state fluorescence measurements.

References:
/1/ Geipel, G. et al., Spectrochim. Acta A **60**, 417-424 (2003)
/2/ Lakowicz, J.R., *Principles of Fluorescence Spectroscopy*, 2nd Ed. Kluwer Academic (1999)
/3/ Valeur, B., *Molecular Fluorescence*, Wiley-VCH (2002) p.105
/4/ Webb, S.P. et al., J. Amer. Chem. Soc. **106**, 7286 (1984)

EXCITED-STATE PROTON TRANSFER OF 3-HYDROXYBENZOIC ACID, 4-HYDROXYBENZOIC ACID, AND VANILLIC ACID

D. Vulpius, G. Geipel, L. Baraniak, G. Bernhard

The excited-state proton transfer of 3-hydroxybenzoic acid (1), 4- hydroxybenzoic acid (2), and vanillic acid (3) was studied as preliminary work for the determination of complex formation constants of these ligands with actinide elements.

In a previous contribution /1/ we reported on the determination of the complex formation constant of uranium(VI) with 3-hydroxybenzoic acid using the fluorescence properties of the organic ligand. We asserted that 3-hydroxybenzoic acid undergo a proton transfer by excitation with ultraviolet light and that this reaction must be considered in the calculation of the complex formation constant.

Now we studied the excited-state proton transfer of some ligands in detail. The following reaction schemata show our results. A kinetic calculation of these reactions is not yet possible at present. Therefore, complex formation constants of these ligands cannot be determined also because a mathematical way from the fluorescence signal of these ligands to their steady state concentration in the energetic ground state is not well-known. As consequence, we are searching for experimental boundary conditions which let assume a simple linear relationship between fluorescence and concentration.
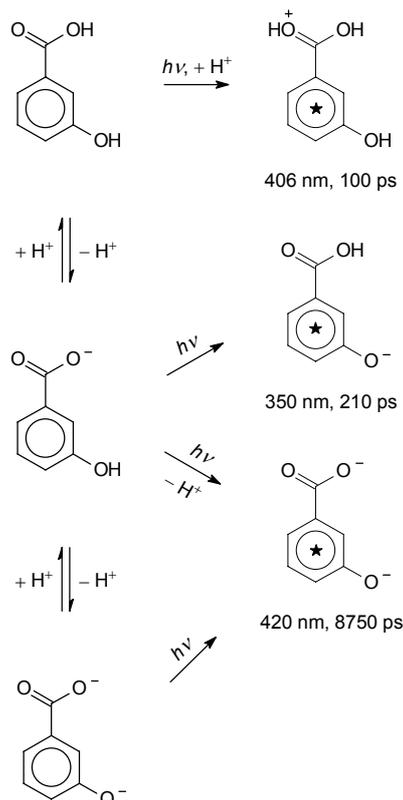
(1)

(2)

(3)

References

/1/ Vulpius, D. et al., Report FZR-373 (2003), p.10

8
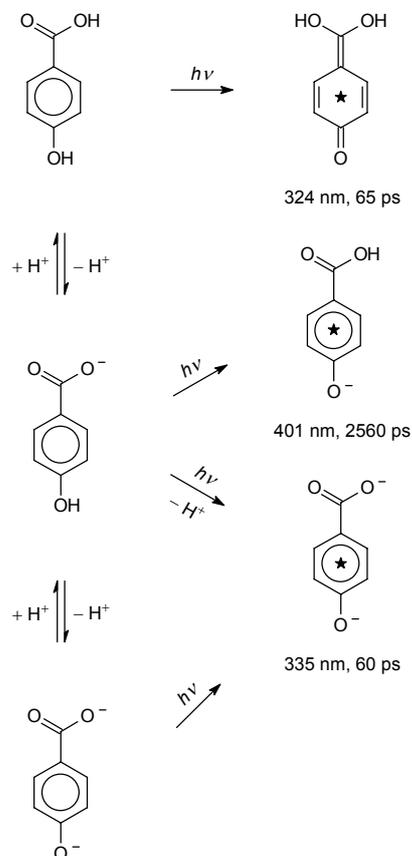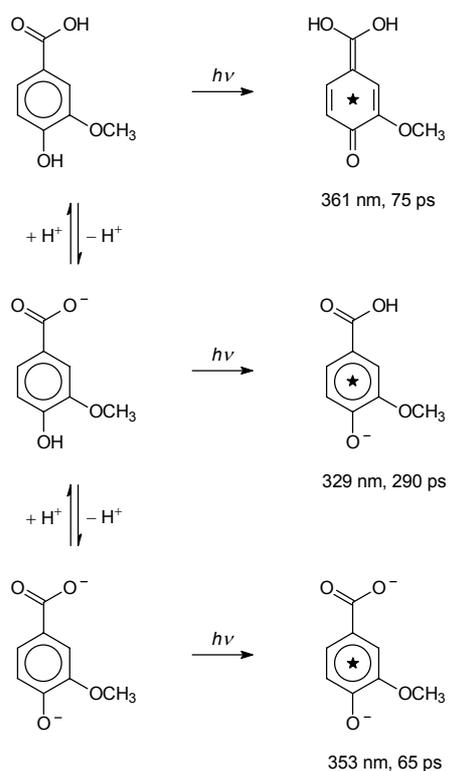
CHARACTERIZATION OF Cu(II)-CYCLAM COMPLEXES BY LASER-INDUCED FLUORESCENCE SPECTROSCOPY

D. Appelhans[1], D. Tabuani[1], B. Voit[1], G. Geipel, G. Bernhard, H. Spies[2], H. Stephan[2]
[1]Institut für Makromolekulare Chemie, IPF Dresden
[2]Institut für Bioanorganische und Radiopharmazeutische Chemie

Time-resolved laser-induced fluorescence spectroscopy (TRFLS) has been used to study the interaction of copper(II) with different cyclam derivatives. The fluorescence emission and lifetime are strongly depended on the structure of the complexes formed.

Introduction

Copper complexes with cyclam **1** have applications in radiopharmaceutical chemistry /1-3/. We have chosen cyclam as core unit for the synthesis of novel dendritic molecules. Here, we want to report on the spectroscopic (TRFLS) properties of star-like cyclams **2** and **3**.
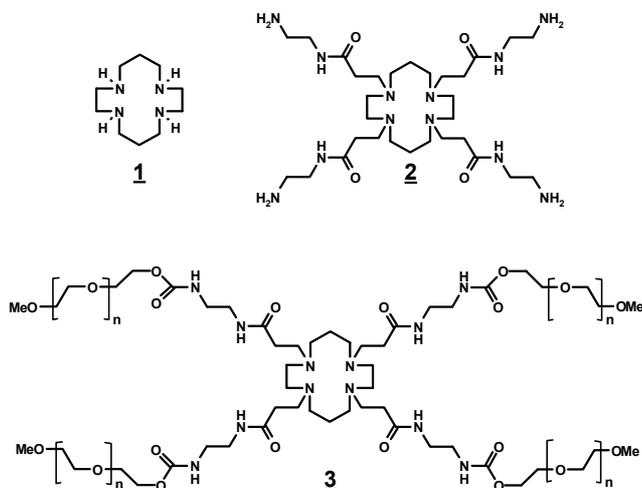
Fig. 1: Cyclam derivatives investigated

Results and Discussion

Cyclam **1** was purchased from Aldrich. **2** was prepared according to the known procedure /4/. The PEG (polyethylene glycol having an average molecular weight of 550) appended cyclam derivative **3** was obtained via hydroxy group activation of polyethylene glycol using 4-nitrophenylchloroformate. This intermediate was finally treated with the cyclam tetraamine **2**. To form the copper complexes, $Cu(CF_3SO_3)_2$ dissolved in MeCN was added to a MeCN solution of cyclam derivative (0.023 M) until Cu was equimolar. The complexation process was maintained overnight at room temperature. TRFLS experiments were performed as described recently /5/. The excitation wavelength was set to be 266 nm. As can be seen from Fig. 2 the intensity of the emitted fluorescence signal increases with changes of the ligand. Also a change of fluorescence decay times and a small change of the maximum of the fluorescence emission was found. This can be interpreted by a decrease of the quench effect of the metal ion on the fluorescence of the ligand due to increasing shielding of the metal ion.
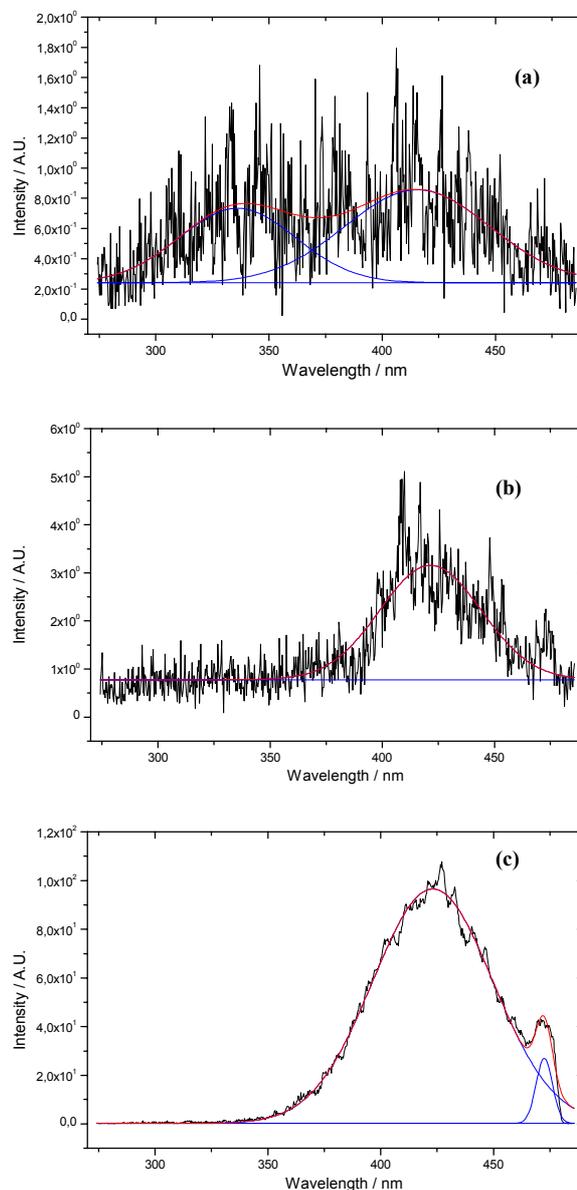
Fig. 2: Time resolved fluorescence spectra of **1** (a), **2** (b) and **3** (c) with $Cu(CF_3SO_3)_2$ in acetonitril

References

/1/ Parker, D., Chem. Soc. Rev. **19**, 271-291 (1990)
/2/ Blower, P. J. et al., Nucl. Med. Biol. **23**, 957-980 (1996)
/3/ Sun, X. et al., J. Med. Chem. **45**, 469-477(2002)
/4/ Zhuo, R. X. et al., J. Contr. Release **57**, 249-257 (1999)
/5/ Geipel, G., Report FZR-343 (2002) p.7

INFLUENCE OF ALKALINE EARTH METAL IONS ON THE URANIUM(VI) EXTRACTION FROM AQUEOUS SOLUTION BY CALIX[6]ARENE

K. Schmeide, R. Ludwig[1], G. Bernhard

[1] Freie Universität Berlin, Institute of Chemistry / Inorganic and Analytical Chemistry

The influence of competing ions (Mg^{2+}, Ca^{2+}, Ba^{2+}) on the uranium extraction from aqueous solution by p-tert-octyl-calix[6]arene hexacarboxylic acid (denoted as LH_6), as a model system for environmental remediation after uranium mining, was studied as a function of pH and ligand concentration by means of solvent extraction experiments.

Experimental

Conditions of solvent extraction experiments: aqueous phase: $[UO_2^{2+}] = 1 \times 10^{-5}$ M, $[Mg^{2+}] = 1 \times 10^{-2}$ M, $[Ca^{2+}] = 5 \times 10^{-3}$ M, $[Ba^{2+}] = 5 \times 10^{-3}$ M, organic phase: as stated in figure captions.

Results and discussion

In the absence of competing ions the uranium extraction increases with pH and reaches a maximum near pH 4 (Fig. 1). In the presence of alkaline earth metal ions the uranium extraction is enhanced in the order Mg < Ca $\leq$ Ba. Previously, an enhancement of metal ion extraction in the presence of competing alkali ions was observed for the lanthanide and copper extraction by calix[4]arenes, never for calix[6]arenes /1-3/. The curve slope in the plot log D_U versus pH ($D = c_{metal,org}/c_{metal,aq}$) is about 2 in the absence of competing ions and in the presence of Ba and about 3 in the presence of Mg and Ca. A curve slope of 3 shows, that in addition to one uranyl ion one alkaline earth metal ion together with one nitrate ion is extracted. This assumption is supported by the curve slope of about 1 in the plot log $D_{Mg,Ca,Ba}$ versus pH and by data from elemental analysis (not shown).
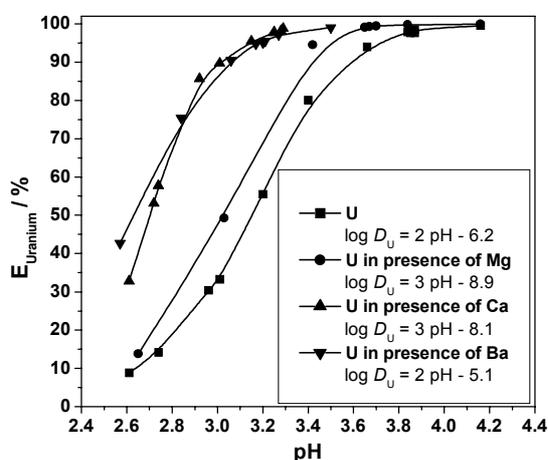
Fig. 1: Uranium extraction by LH_6 in absence and presence of competing ions as a function of pH value. Organic phase: $[LH_6] = 5 \times 10^{-4}$ M, CH_2Cl_2.

The plots of log D versus ligand concentration have a slope of about one for uranium (Fig. 2) and alkaline earth metal ion extraction (not shown). This means that one uranyl ion and one alkaline earth metal ion is bound per calixarene molecule. For the uranium extraction in the presence of calcium ions the following complexation equation is postulated where the solid line denotes the species in the organic phase:

$$UO_2^{2+} + Ca^{2+} + \overline{H_6L} + NO_3^- \leftrightarrow \overline{(UO_2CaH_3L)^+NO_3^-} + 3H^+$$
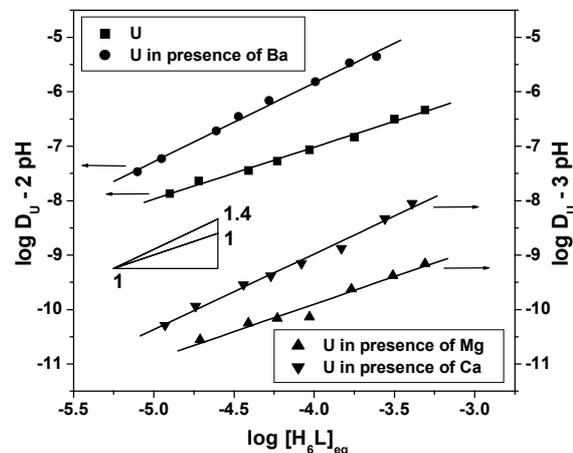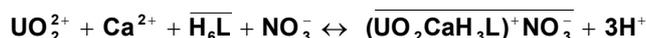
Fig. 2: Uranium extraction by LH_6 in absence and presence of competing ions at $pH_{0.5}$ as a function of ligand concentration. Organic phase: $[LH_6] = 1.3 \times 10^{-5}$ to 5×10^{-4} M, CH_2Cl_2. (Due to different pH and pH-dependencies the order seen in Fig. 1 is not reflected here.)

Conclusion

- The extraction of alkaline earth metal ions by calixarene and their influence on uranium extraction correlates with the ionic diameter of the competing ions as well as with their affinity to carboxyl groups of the ligand. The ionic radius of Ba^{2+} (1.35 Å) fits best the cavity size of the calix[6]arene (about 3 × 7 Å /4/). This agrees well with the extraction constants reported for alkaline earth metal ion extraction by this ligand /5/ which increase in the order: Mg < Ca < Ba with $K_{ex} = 2.7 \times 10^{-8}$, 7.8×10^{-6} and 1.1×10^{-4} mM, respectively.

- Alkaline earth metal ions are co-extracted together with uranyl ions due to cation exchange which represents a new mechanism for U(VI) complexation.

- The uptake of the alkaline earth metal ions into the calixarene molecule possibly causes structural changes within the calixarene molecule (e.g., a kind of molecular preorganization).

The calixarene selectivity towards UO_2^{2+} in real waters can be improved further applying α-halogenated acetic acid or hydroxamic acid calixarene derivatives.

Acknowledgment

References

/1/ Ludwig, R. et al., Solv. Extr. Ion Exch. **11**, 311 (1993)

/2/ Ohto, K. et al., Solv. Extr. Ion Exch. **14**, 459 (1996)

/3/ Ohto, K. et al., Poyhedron **16**, 1655 (1997)

/4/ Gutsche, C.D., *Calixarenes*, Royal Soc. Chem. 1989

/5/ Kakoi, T. et al., Anal. Sci. **14**(3), 501 (1998)

STUDY ON THE REDOX STABILITY OF URANIUM(VI) COMPLEXES WITH SYNTHETIC AND NATURAL HUMIC ACIDS

S. Sachs, G. Geipel, G. Bernhard

The redox stability of U(VI) complexes with synthetic humic acids (HA) and natural HA Aldrich was studied. A first spectroscopic evidence for the reduction of U(VI) by synthetic HA with distinct redox functionality is provided.

Introduction

The migration behavior of actinides strongly depends on their oxidation state that can be influenced by humic acids (HA). Therefore, the detailed description of the effects of HA on the mobility of actinides in the environment requires the understanding of the influence of HA on the oxidation state of actinides in addition to knowledge on the HA-actinide-complexation. Based on the oxidation of phenolic compounds we developed synthetic HA model substances with pronounced redox functionalities in order to study the redox properties of HA and the redox stability of actinide humate complexes /1/. In this work we studied the redox stability of U(VI) humate complexes using these synthetic HA which are characterized by significant higher Fe(III) redox capacities than natural HA Aldrich.

Experimental

The redox stability of U(VI) humate complexes of HA type Hyd-Glu (oxidation product from hydroquinone and glutamic acid /1/) and type Cat-Gly (oxidation product from catechol and glycine /1/) was studied at pH 9 (0.1 M $NaClO_4$) in comparison to natural HA Aldrich (AHA). According to /2/, U(VI) humate solutions with initial U(VI) and HA concentrations of $1 \cdot 10^{-4}$ M and 0.4 g/L, respectively, were prepared under N_2 atmosphere and exclusion of light using CO_2-free solutions. Laser-induced photoacoustic spectroscopy was applied for detection of U(IV) in the sample solutions. The wavelength range between 600 and 675 nm was studied. To separate the HA and to decompose possibly formed U(IV) humate complexes, the samples were acidified with H_2SO_4 prior to its analysis.

Results

In Fig. 1 the photoacoustic spectra of the studied solutions are shown together with their peak deconvolution. Comparing the spectra it becomes obvious that the spectra of the synthetic products are characterized by a high background absorption. This is due to an incomplete HA exclusion from the solutions which results in a HA contribution to the absorption signal. However, from these spectra it becomes clear that no absorption signals were detected for the solution of AHA, whereas for both synthetic products two absorption bands were determined. Thus, we conclude that after 93 days reaction time no detectable U(IV) concentration (detection limit: 10^{-5}–10^{-6} mol/L /2/) was formed by an AHA-mediated U(VI) reduction. In absence of HA, the solvated U^{4+} ion shows characteristic absorption maxima at 629.5 nm, 649.1 nm and 671.7 nm /3/. These absorption wavelengths are close to those determined in the solutions with synthetic HA type Hyd-Glu and Cat-Gly. This result points to the occurrence of detectable U(IV) quantities in the solutions with the HA-like oxidation products from hydro-

quinone and catechol. Therefore, it can be concluded that U(IV) was reduced by both synthetic HA.
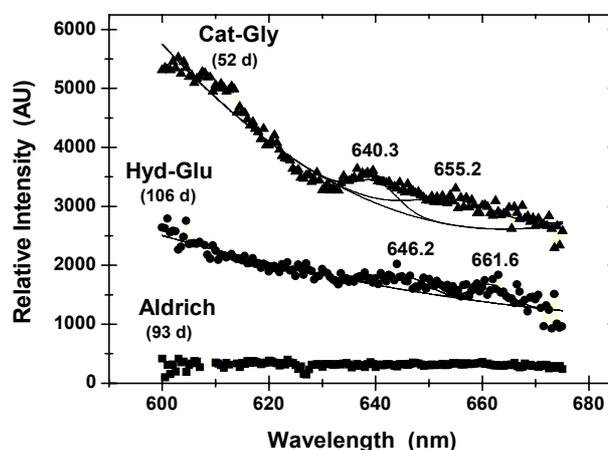
Fig. 1: Photoacoustic spectra of the studied HA solutions. Numbers in brackets indicate the equilibration time of the samples.

The shift of the absorption bands observed for HA type Hyd-Glu and Cat-Gly could be due to the formation of U(IV) sulfate complexes in the studied solutions. Similar peak shifts were found for U(IV) complexes with arsenate /3/. Furthermore, the spectra which were obtained for both synthetic HA are similar to that of an uranium solution with wood degradation products published in /2/, where the reduction of U(VI) by these substances was spectroscopically observed.

From our spectroscopic results we conclude that the synthetic HA with pronounced redox functionalities show both, higher Fe(III) /1/ and U(VI) redox capacities than AHA. The obtained results represent a first qualitative and spectroscopic proof for the reduction of U(VI) by HA. Further studies are performed in order to quantify the U(VI) redox capacities of the HA alike oxidation products from hydroquinone (Hyd-Glu) and catechol (Cat-Gly).

Acknowledgment

References

/1/ Sachs, S. et al., Final Report, Project No. 02E9299 (2003)

/2/ Abraham, A., PhD Thesis, TU Dresden (2002)

/3/ Geipel, G. et al., In: *Uranium in the Aquatic Environment* (Merkel, B.J., Planer-Friedrich, B., Wolkersdorfer, C., eds.) Springer, Berlin (2002) p. 369-376

PH-INDUCED FT-IR DIFFERENCE SPECTROSCOPY OF HUMIC ACIDS IN AQUEOUS SOLUTIONS

H. Foerstendorf, K. Muschter, S. Sachs

Solutions of humic acids (HA) were investigated by pH-induced FT-IR spectroscopy. The spectra clearly show the different protonation states of the carboxyl and phenolic groups of the HAs. This spectroscopic technique is promising for further structural investigations of HA dissolved in water.

Vibrational spectroscopy of environmental samples is a special challenge due to their frequent molecular complexity and the aqueous medium which is a strong absorbing solvent over a wide spectral range of interest. A solution for these difficulties is the combination of reaction-induced difference spectroscopy with the attenuated total reflection (ATR) technique.

In difference spectroscopy only changes of the system under investigation occurring during a selective induced reaction are measured. All constant contributions are eliminated which makes it possible to detect changes of functional groups at a submolecular level. The ATR-technique provides the possibility to record samples in aqueous solution without the limitation of total absorption. The infrared light propagates through a suitable crystal under total reflection angle. Since fractions of the IR light are absorbed during reflection at the crystal's surface, absorption spectra of the medium which is in direct contact to the crystal are available. In this study we investigate the structural changes of humic acids (HA) during changing the pH of the aqueous solvent as a preliminary test for further studies of sorption experiments with HA substances.

Experimental

Aqueous solutions with distinct pH values of purified commercial HA from Aldrich (AHA) and synthetic HA type R4 (oxidation product from catechol and glycine /1/) with increased content of phenolic groups were measured in a diamond ATR-flow cell (Vol.: 200 µl) at room temperature. Difference spectra (spectral resolution 4 cm^{-1}) were calculated from the single beam spectra recorded every 90 s (scan time: 60 s) under a constant flow rate of 0.25 ml/min.
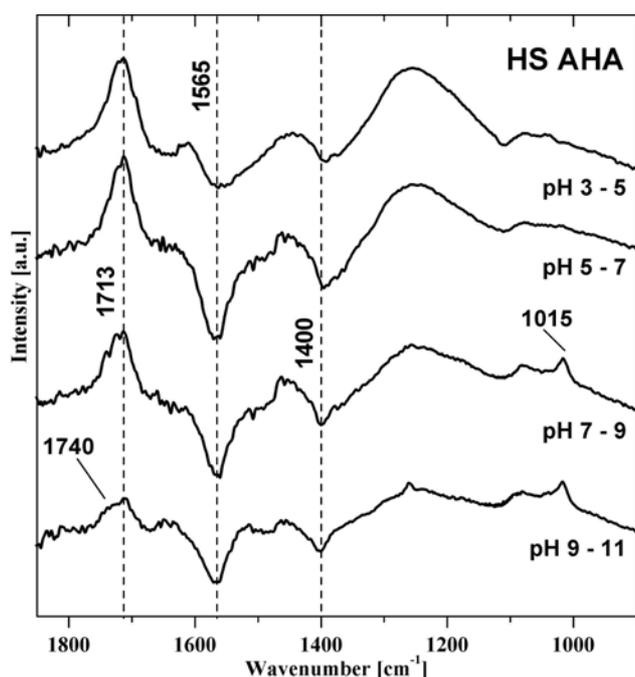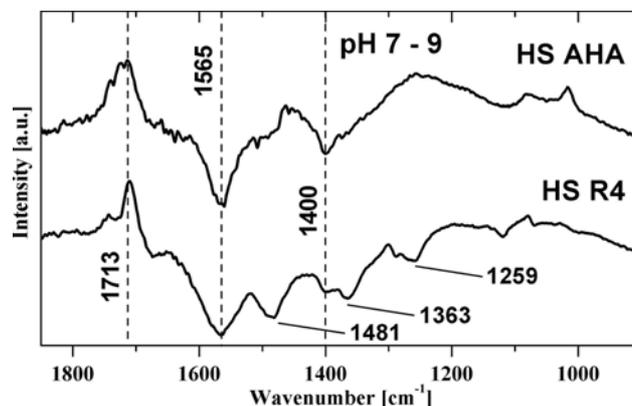
Fig. 2: pH induced FT-IR difference spectra of AHA and R1-03.

Results

The infrared difference spectra are characterized by positive and negative bands representing HA at lower and higher pH values, respectively. All spectra show positive bands at 1713 cm^{-1} which can be assigned to protonated carboxyl groups whereas the negative bands at 1565 and 1400 cm^{-1} represent the deprotonated form of these functional groups (v_{as} and v_s). The amplitude of the difference spectra decreases with increasing pH (Fig. 1) since most of the carboxyl groups are deprotonated at pH > 7. The shoulder at 1740 cm^{-1} showing up in the spectrum of AHA at pH 7-9 and especially at pH 9-11 indicates the deprotonation of carboxyl groups in a more hydrophobic environment which generally absorb at higher frequencies than COOH-groups in a hydrophilic surrounding. The bands below 1100 cm^{-1} cannot unequivocally be assigned today. They possibly represent OH-groups which are deprotonated at pH > 7.

The spectrum of the synthetic HA R4 containing an increased number of phenolic groups in the pH range 7 to 9 shows additional bands around 1481, 1363 and 1259 cm^{-1} (Fig. 2). These bands obviously represent changes which are mainly due to the increased number of phenolic groups. From the synthesis of R4 it can be expected that there is an increased content of still unspecified amino groups which may also contribute to the spectral changes observed in Fig. 2.

In future times interaction of actinide ions (*e.g.* UO_2^{2+}) with HA substances will be investigated by this spectroscopic technique for identification of the functional groups involved in sorption processes.

References

/1/ Sachs, S. et al., final report, BMWA project No. 02E9295, Rossendorf (2003)

Fig. 1: pH induced FT-IR difference spectra of AHA dissolved in H_2O. The pH change is given in the figure.

CHARACTERISATION OF A SPECTRO ELECTROCHEMICAL CELL - SAFETY CONDITIONS AND BASIC ELECTROCHEMICAL PRINCIPLES

J. Tutschku, C. Hennig, G. Bernhard

An electrochemical cell for in-situ XAFS measurements has been successfully tested for various electrolytes .

Introduction

An electrochemical cell was developed for in-situ XAFS investigations of radioactive materials /1/.
To meet the requirements of radio protection, the cell is equipped with a double containment in order.

It consists of a massive body of chemically resistant materials without any separate windows. Two independent cover plates serve for containment and include all electrical connectors (Fig.1).

The cables are passed through the cover plates. In addition to being chemically resistant, the body material also has to be mechanically robust as well as resistant to radiation. Various materials were tested in a number of experiments. Polytetrafluoroethylene (PTFE) were found to be suitable for alkaline and acidic solutions and Polyvinylidenefluoride (PVDF) for acidic media. Polypropylene was also tested and can be used as an alternative for both. The constructed cell has a volume of approximately 10 mL.

The working electrode is a piece of platinum gauze, which is squeezed into the cell during fitting and expand inside. In contrast to a former design with a Pt counter electrode, we used Ag as the electrode material (a silver wire of 1 mm thickness). Ag has a lower redox potential than OH⁻ and is therefore dissolved and precipitated as AgCl. A sufficiently high concentration of Cl⁻ in the solution is needed for this reaction. No gas is deposited but silver will be dissolved at a lower potential. With an electrode of second type, no diaphragm is needed for this arrangement.

A additional silver wire is used as a reference electrode. The potential of the Ag/AgCl electrode is measured in terms of redox potential in the solution containing chloride ions.

A pH-electrode (glass electrode), a redox electrode and a temperature sensor are also located in the cell.

The samples were prepared by dissolving UO_3 in 0.1 M H_2SO_4 or 0.1 M $HClO_4$ to a final concentration of 0.01 M UO_2^{2+}.

Fig. 1:
Electrochemical cell (exploded design)

Experimental

Before carrying out the XAFS experiments, the redox behavior of the uranium has to be investigated. First of all the current – voltage curve is measured in order to determine the redox potential of the electrolytic system (Fig. 2). The result of the electrolyte $UO_2(ClO_4)_2$ is shown in Fig. 2. As can be seen, a potential of -300 mV can be used for complete reduction of U(VI) to U(IV).
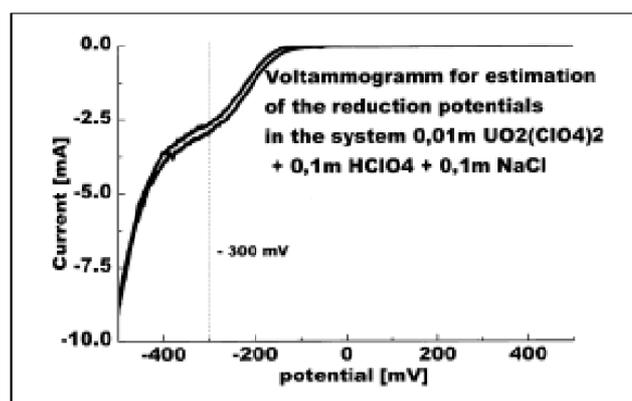
Fig.2: Current-potential curve for estimation of the reduction potential for uranium

The reduction is determined by measuring the current against time. This makes it possible to estimate the electric charge during reduction.

The dissolution of uranium (IV) was determined by the UV/VIS spectroscopy. Subsequent sampling in defined time steps showed the increase in U(IV) concentration and the decrease of U(VI) concentration. This procedure was used to ascertain the processes taking place in the cell (Fig. 3). In this way we estimated the conditions in the cell.
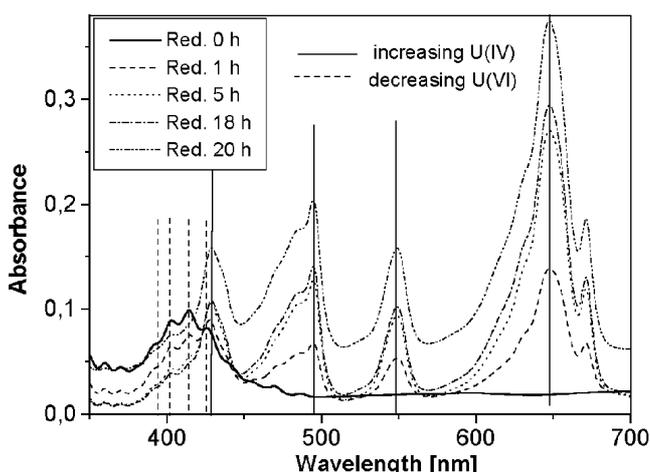
Fig. 3: UV/VIS spectra for reduction of uranium

After this preparation the cell was ready for XAFS experiments.

/1/ Rettig, D. et al. Report FZR-343 (2001) p.51

UV/VIS-INVESTIGATION OF URANIUM REDUCTION IN SOLUTIONS
THE INFLUENCE OF VARIOUS ANIONS

J. Tutschku, C. Hennig, G. Bernhard

The influence of several anions on the complex formation with uranium in different valence states was investigated by electrochemistry and UV/VIS spectroscopy with the spectrochemical cell projected for XFAS measurements

Introduction

The combination of XAFS and electrochemistry can provide important information about the redox behavior and the coordination of species in aqueous solution. Here we report the determination of the redox states of uranium by UV/VIS spectroscopy. These experiments were needed to find out which electrolytes are suitable for XAFS measurements.

Experimental

The samples were prepared by dissolving UO_3 in 0.1 M acids. Solutions of $UO_2^{2+} A^{2-}$ with ClO_4^-, SO_4^{2-}, CO_3^{2-}, CH_3COO^- and $HCOO^-$ were thus obtained.
The reduction was carried out in a previously described electrochemical cell /1,2/. The conditions for the electrolyte were estimated by electrochemical and spectroscopic (UV/VIS) methods.

A small amount of chloride was added to all solutions, to facilitate the electrochemical reduction of uranium using an Ag/AgCl – electrode as a counter electrode. It was shown by UV/VIS spectra that the Cl^- has no influence on the complexation of the chosen anions.

Results and discussion

In Fig. 1 the UV-VIS spectra of UO_2SO_4 are presented. The sample was probed during the electrochemical reduction with – 300 mV.
The spectra show the stepwise reduction of the spectral features, increasing U(IV) and decreasing U(VI), respectively.
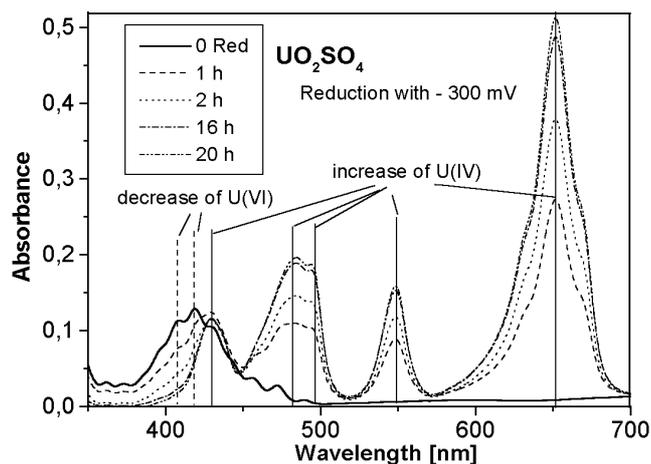
Fig. 1: UV/VIS spectra during reduction of 0.01M UO_2SO_4 , 0,02 M NaCl, pH = 0,78 with H_2SO_4

This experiments were carried out with solutions of various anions. In this way we obtained spectra for U(VI) and U(IV) for solutions with the anions:

ClO_4^-, SO_4^{2-}, CO_3^{2-}, CH_3COO^- and $HCOO^-$
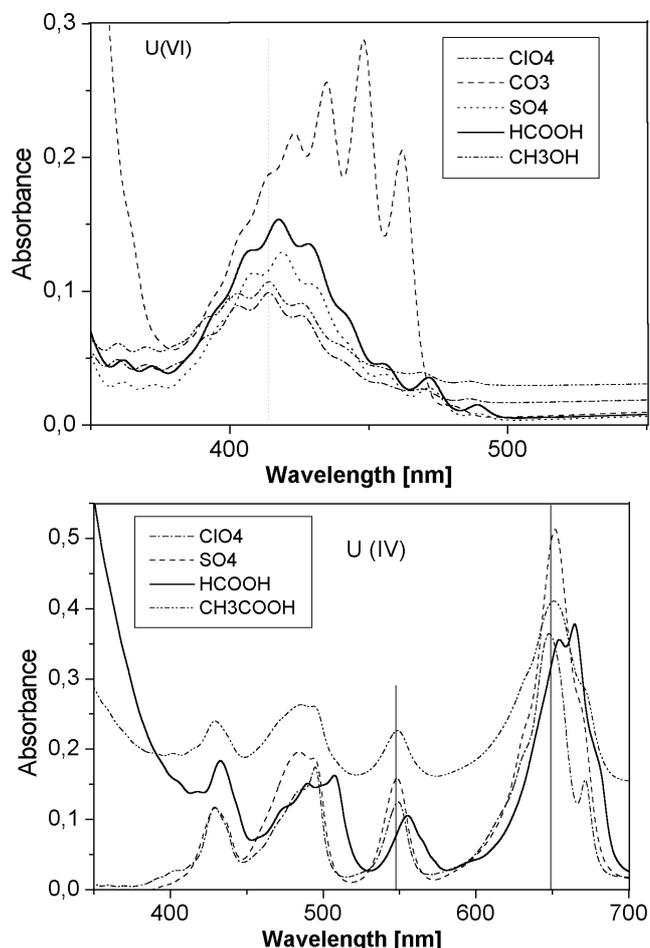
Fig. 2: UV/VIS spectra for U(VI) (stock solution) and U(IV) (completely reduced solutions) with various anions

The complex formation strength is related to the position of the absorption peaks. The stronger the complexes, the higher are the wave numbers. This makes it possible to distinguish the stronger complex formation in the case of sulphate, carbonate and formiate anions from the non-complexing perchlorate anions.
The U(IV) ion is only soluble in solutions with a high concentration of H^+ (pH < 1) . It should be mainly coordinated with H_3O^+ ions. The position of the absorption bands is the same for ClO_4^-, SO_4^{2-} and CH_3COO^-.
The shifted absorption band for U(IV) formiate points to an inner sphere complex for U(IV) ion. Proof of this assumption may be provided by XAFS measurements.

References
/1/ Rettig, D. et al. Report FZR-343 (2001) p.51
/2/ Tutschku, J. et al. this report p.13

ELECTROCHEMICAL URANIUM REDUCTION EXPERIMENTS IN THE PRESENCE OF FORMIC ACID

J. Tutschku, C. Hennig, A. Roßberg, G. Bernhard

The electrochemical reduction of uranium in the presence of formic acid was investigated by UV/VIS and XANES spectroscopy.

Introduction

The design of an electrochemical cell /1/ was adapted to the conditions of in situ XAFS measurement on radionuclides.

Experimental

The sample was prepared by dissolving UO_3 in 2 M formic acid. 0.1 M NaCl was added to create the conditions for the electrolyte as described in /2/.

The electrochemical behavior of electrolyte was analysed by preliminary UV/VIS measurements.

Results and discussion

UV/VIS investigation

During the reduction process 1 mL of the solution was taken from the electrochemical cell for the UV/VIS measurement. Fig. 1 shows that the increasing peaks related to U(IV) at 654 nm and 664 nm have been shifted to higher wavelengths. The decrease in the group of peaks related to U(VI) at about 420 nm indicates a reduction in uranium (VI).

A reduction in U(VI) by auto-oxidation of formic acid was even observed without electrochemical treatment. To obtain a pure UV/VIS spectrum of U(VI) the redox procedure was reversed.
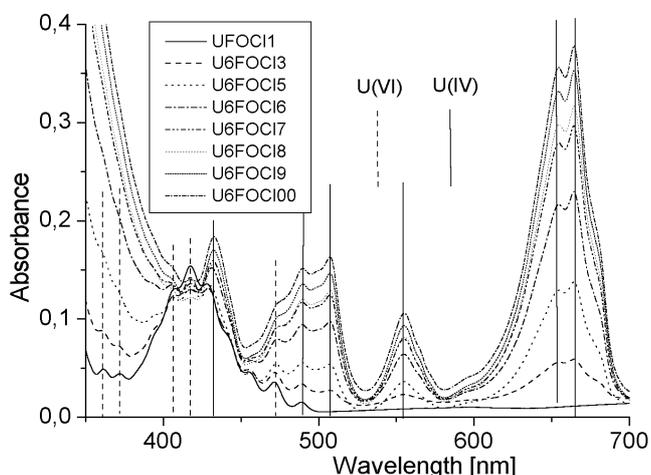
Fig. 1: Reduction of U(VI) to U(IV) in formic acid

XANES measurement

The reduction procedure *in situ* was coupled with XANES measurements performed at ROBL .

A XANES measurement was carried out every 30 minutes, while the reduction process was uninterrupted. Fig. 2 shows a series of XANES spectra indicating transition from U(VI) to U(IV).

The composition of the species as a function of the reduction time was calculated, using factor analysis /3/.
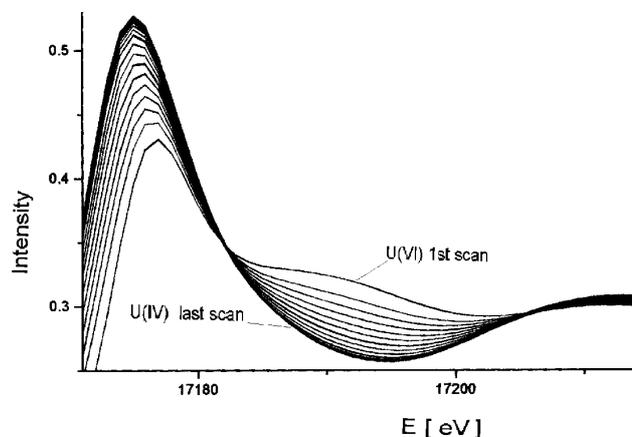
Fig. 2: U L_3-edge XANES spectra taken in situ during the reduction process

The quantitative relation of U(VI) and U(IV) was calculated and is shown in Fig. 3.
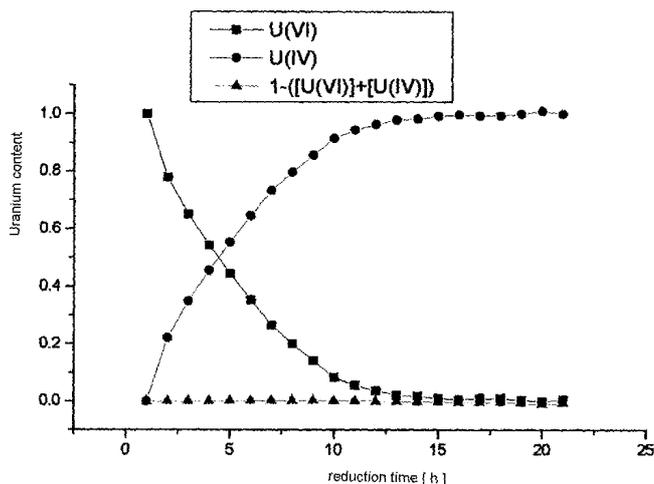
Fig. 3: Composition of U(VI) and U(IV) during reduction

These XANES measurements demonstrate the *in situ* electrochemical reduction of uranium.

References
/1/ Rettig, D., et al. Report FZR-343 (2001) p.51
/2/ Tutschku, J., et al. this report p.14
/3/ Roßberg, A., et al. Anal. and Bioanal.Chem. **376**, 631 (2003)

FIRST URANIUM L_{III} EXAFS MEASUREMENTS WITH THE SPECTRO-ELECTROCHEMICAL CELL

C. Hennig, J. Tutschku, A. Scheinost, G. Bernhard

The structure of aqueous U complexes at oxidizing and reducing redox potentials was investigated by in situ XAFS spectroscopy using an spectro-electrochemical cell. We found that under reducing conditions, U^{4+} is coordinated to water only in presence of ClO_4^-, but is additionally coordinated to one or two sulfate groups in the presence of SO_4^{2-}.

Introduction

During migration in soils and sediments, U ions may undergo various changes in redox potential, which influence the speciation and hence the transport behavior of U. Some of these species are unstable, and can be investigated only *in situ* using an electrochemical cell. Therefore, we have developed an spectro-electrochemical cell for the in-situ determination of U speciation by XAFS spectroscopy. Details of this cell are given by Tutschku et al. (this issue).

Experimental

The samples were prepared by dissolving enough UO_2 in 0.1 M SO_4^{2-} or 0.1 M ClO_4^- to achieve a final concentration of 0.01 M U. The oxidation state and structure of the U complexes was determined by XAFS measurements in transmission mode at ROBL. The spectra were acquired before and after an 8 hour reduction at –350 mV in presence of SO_4 and at –300 mV in presence of ClO_4 (vs. Ag/AgCl).
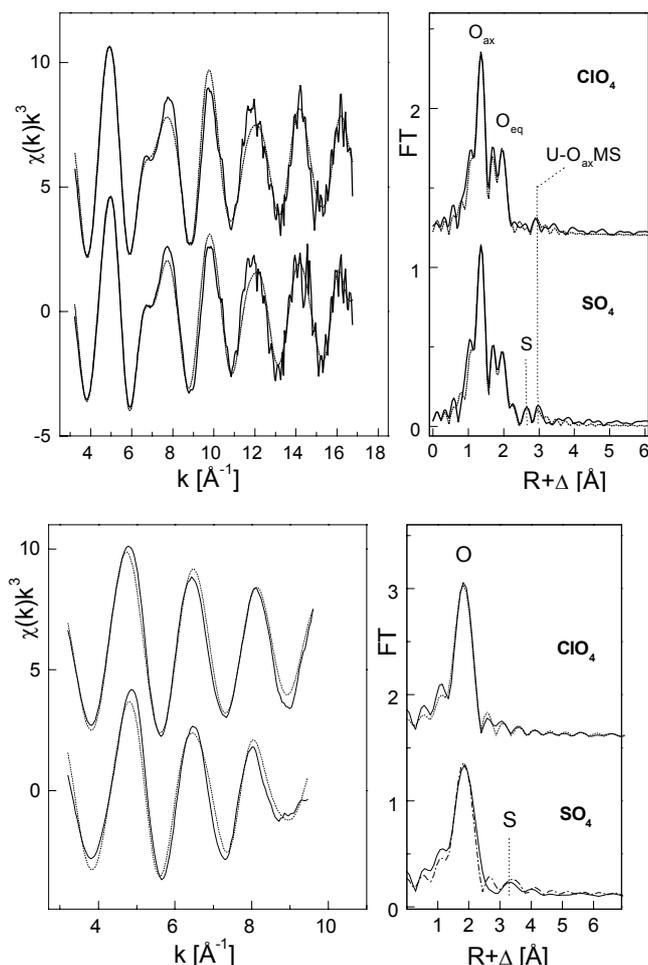
Results and discussion

At the beginning of the experiment, both XANES (not shown) and the EXAFS Fourier transforms (FT, Fig. 1, top) indicate hexavalent U only. In the non-complexing 0.1 M ClO_4^- solution, 5 equatorial O atoms at a distance of 2.42 Å confirm that the uranyl ion is coordinated to water /1/ (Table 1). The spectrum of U in sulfuric acid is very similar, indicating a dominant coordination to water. However, the weak feature at $R+\Delta R = 2.7$ Å can be fitted with one S atom at a distance of 3.07 Å. This distance is in agreement with the U-S bond length of 3.07 Å in the solid $UO_2SO_4 \cdot 2CH_3CON(CH_3)_2$, where UO_2^{2-} is bidentately coordinated to [SO_4] /4/. In contrast, a monodentate U-S complex would yield a distance of 3.63 Å /5/. Hence our results clearly indicate formation of a binary aqueous complex $UO_2(SO_4)_n^{2-2n}$.

After 8 hours of reducing redox potential, only tetravalent U can be observed (Fig. 1, bottom). The U atom is coordinated to 8 O atoms at a distance of 2.41 Å. This result is in contrast to Moll et al. /2/ who found 9 to 11 neighboring atoms, but is in agreement with that by Pocev /3/ derived from LAXS. Previous investigations showed that a cumulant approximation did not change the coordination numbers /2/.

Tab. 1: EXAFS structural parameters

sample	Shell	R [Å]	N	σ^2 [Å^2]
U^{6+}-[ClO_4]	U-O_{ax}	1.76	1.9	0.0015
	U-MS	3.52	1.9	0.0030
	U-O_{eq}	2.42	4.9	0.0075
U^{6+}-[SO_4]	U-O_{ax}	1.77	1.8	0.0016
	U-MS	3.53	1.8	0.0032
	U-O_{eq}	2.43	5.4	0.0087
	U-S	3.07	1.0	0.0070
U^{4+}-[ClO_4]	U-O	2.41	8.1	0.0074
U^{4+}-[SO_4]	U-O	2.42	8.5	0.0095
	U-S	3.85	1.5	0.0090

While no further backscattering atoms were found for non-complexing U-ClO_4, U-SO_4 contains a signal at $R+\Delta R = 3.4$ Å, which could be fitted with one or two S atoms at a distance of 3.85 Å. This distance is in line with a monodentate coordination. To the best of our knowledge, this is the first structural determination of the aqueous U^{4+}-SO_4 complex.

References

/1/ Sémon, L. et al., Chem. Phys. Chem. **2**, 591 (2001)

/2/ Moll, H. et al., Inorg. Chem. **38**, 1795 (1999)

/3/ Pocev, S. et al., Acta Chem. Scand. **27**, 2146 (1973)

/4/ Blatsov, V.A. et al., Z. Strukt. Khim. **31**, 131 (1990)

/5/ Moll, H. et al., Radiochim. Acta **88**, 55 (2000)

Fig. 1: U L_{III}-edge EXAFS spectra and their Fourier transforms before (top) and after (bottom) reduction

EXAFS ANALYSIS OF THE Cm³⁺ AQUO ION BY AN OPTIMIZED REGULARIZATION METHOD

M. Kunicke, I. Kamensky[1], Yu. Babanov[1], H. Funke
[1]Institute of Metal Physics, RAS, Ekaterinburg, Russia

A new method for determining the optimized regularization parameter for EXAFS analysis was developed. The method is applied to the spectrum of the Cm³⁺ aquo ion and compared with results from standard EXAFS data evaluation procedures.

Introduction

The regularization method was recommended for EXAFS data analysis nearly two decades ago /1/ and substantially improved in the last years /2/. The regularization procedure is applied to the EXAFS spectrum of the Cm³⁺ aquo ion /3/ and compared with the standard data evaluation procedure.

The numerical treatment of the inverse problem arising in the EXAFS data analysis has a free parameter: the regularization parameter α. Up to now the determination of α was an unresolved problem. Now, based solely on the L-curve-criterion an optimized value of α can be determined for each spectrum /2/. The optimized regularization parameter leads to a stable solution with a good convergence of the iterative process.

The L-curve

In general, the L-curve is a log-log plot of the norm of a regularized solution versus the norm of the corresponding residual. Both norms depend parametrically on α. The resulting curve shows a shape like the capital letter "L". The optimal regularization parameter is chosen as the maximum of the L curve curvature, corresponding to the corner of the "L". Further details can be found in /2/.
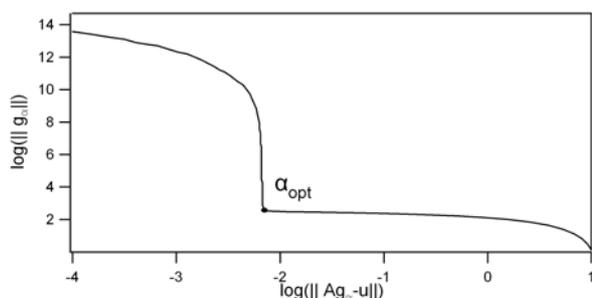
Fig. 1: The L-curve for experimental data of Cm³⁺

Figure 1 shows a typical L-curve. The function g_α is the partial distribution function, u is the measured EXAFS spectrum, and A is the EXAFS integral operator /1,2/.

Experimental and results

Besides plutonium, the long-lived isotope curium plays a crucial role for long-term performance assessment of nuclear waste repositories. In order to predict the mobilization and retardation of this nuclide, it is necessary to know the structures of the actinide species that are involved in the process of migration. Thereby, the characterization of the Cm³⁺ aqua-ion forms the base for further investigations. For details see /3/.

The sample was prepared in non-complexing 1.0 *M* perchloric acid. The Cm L_{III}-edge (18970 eV) EXAFS spectrum was collected in transmission mode at ROBL/ESRF.

The optimized regularization parameter for the present spectrum is: $\alpha_{opt} = 6.3 \times 10^{-6}$. Figure 2 shows the excellent agreement between the experimental data $\chi(k)$ and the solution by the regularization method.

To obtain structural information from the experimental data, both the regularization method and conventional data fitting using EXAFSPAK was applied. In both cases the backscattering phase and amplitude, the mean free path, and the reduction factor were calculated using FEFF8.

The structural parameters obtained from EXAFS data by both methods, and including an earlier UV-Vis measurement /4/, are summarized in Table 1.
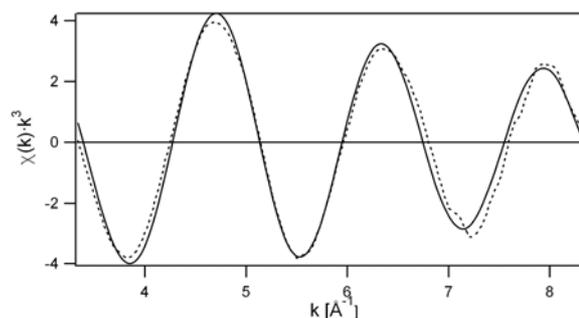
Fig. 2: Comparison of the experimental EXAFS data (dotted line) and the spectrum obtained from the regularization method (solid line)

Tab. 1: Fit parameters

Method	N	R (Å)	Σ^2 (Å²)
UV-Vis /4/	9		
Fitting (S_0^2=0.9)	9.3	2.46	0.0075
Regularization	9.2	2.45	0.0080

The agreement of the structural parameters obtained by both methods is excellent. Hence, if only one type of backscatterer atoms is present, the regularization method may be successfully applied to EXAFS data evaluation without any *a priori* model assumptions.

References

/1/ Babanov, Yu.A. et al., Phys. Stat. Sol. *(b)*, **105**, 747 (1981); **108**, 103 (1981)

/2/ Kunicke, M. et al., Physica Scri*pta*, accepted; Report FZR-343, p. 46 (2002)

/3/ Funke H. et al., Proceedings of the 32èmes Journées des Actinides, Ein-Gedi, Israel (2002)

/4/ Carnall, W.T., J. Less-Common Met. **156**, 221 (1989)

Actinides / Radionuclides in Biosystems

MOLECULAR BACTERIAL DIVERSITY IN URANIUM CONTAMINATED SOILS AND WATERS

S. Selenska-Pobell, G. Radeva, K. Flemming, G. Satschanska, A. Geißler, T. Tzvetkova

A comparative analysis of natural bacterial communities occurring at different uranium mining wastes demonstrated that they are site-specific and consist of very diverse phylogenetic groups.

Natural bacterial communities were analyzed in soil and water samples collected from different sites and depths of the following uranium wastes, Johanngeorgenstadt (JG), Gittersee/Coschütz (Gitt), Schlema (Schl) in Germany and from Gunnison, Colorado (Gunn) and Shiprock, New Mexico (Sh) in the USA.

Three bacterial rDNA libraries were prepared by using the following universal bacterial PCR amplification primer sets: 16S rDNA$_{7F-1513R}$; 16S rDNA$_{43F-1404R}$ and 16S rDNA$_{968F}$-23S rDNA$_{130R}$ (RISA).

The results of these analyses are summarized in Tables 1 and 2. As evident from the data presented in the Tables the composition of bacterial communities in soil and water samples is site-specific. In the soils of the German uranium mining waste pile JG, for instance, mainly α-proteobacteria and representatives of *Holphaga/Aci-dobacterium* (H/A) phylum were identified in samples collected from three different depths. This result was independent from the primer set used (compare in Table 1 JG34$_{7f-1513R}$ and JG36$_{7f-1513R}$ to JG34 $_{43f-1404R}$ and JG36$_{43f-1404R}$, respectively). In the soil samples of the uranium mill tailings Gitt no representatives of the H/A phylum were identified and the α-proteobacteria were not predominant. Instead, the number of the γ-proteobacterial sequences was extremely high (about 50 % of all clones per a library) and the *Cytophaga/Flavobacterium/Bacteroides* (CFB) sequences represented a significant part of the bacterial community in contrast to the JG. The γ-proteobacteria were predominant also in the Gunn uranium mining depository site. In this case, however, representatives of the H/A phylum were retrieved as well (see Table 1).

Tab. 1: Bacterial groups (given in %) found in soil samples collected from JG, Gitt, Gunn, and Sh

Origin rDNA library	Proteobacteria				H/A	Act	Bac	CFB	GNS	N/L	PI
	α	β	γ	δ							
JG34$_{7f-1513R}$ (1-2 m depth)	24	20	4	-	25	7	-	9	-	7	4
JG34$_{43F-1404R}$ (1-2 m depth)	35	-	9	10	24	6	-	-	2	-	-
JG36$_{7f-1513R}$ (2-3 m depth)	25	14	14	-	31	-	-	1	-	7	4
JG36$_{43f-1404R}$ (2-3 m depth)	29	8	21	12	25	-	-	-	2	3	-
JG37$_{3F-1404R}$ (3-4 m depth)	47	3	6	5	32	-	-	3	-	-	-
Gitt$_{7f-1513}$ (2-3 m depth)	15	14	48	-	-	3	3	17	-	-	-
Gitt$_{43F-1404R}$ (2-3 m depth)	7	15	54	-	-	-	4	20	-	-	-
Gunn$_{43F-1404R}$ (2-3 m depth)	15	6	45	6	11	-	-	4	-	-	-
Sh$_{43F-1404R}$ (2-3 m depth)	7	2	17	9	3	3	31	-	17	5	3

The composition of the bacterial communities in the soils of the uranium mill tailings Sh was extremely complex. The main bacterial groups there were affiliated to the Gram positive *Bacillales* (Bac). In addition, the amount of the green non-sulfur bacteria (GNS) and of the γ-proteobacteria was relatively high.

Tab. 2: Bacterial groups (given in %) found in water samples collected from Gitt, Sh and Schl

Origin rDNA library	Proteobacteria				CFB	Act	Ver	GSB	GNS	N/L	PI
	α	β	γ	δ							
Gitt$_{43F-1404R}$ (20 m depth)	14	11	46	11	18	-	-	-	-	-	-
Gitt$_{RISA}$ (20 m depth)	-	-	14	10	14	5	5	-	-	10	38
Sh$_{43F-1404R}$ (2 m depth)	-	-	83	5	12	-	-	-	-	-	-
Sh$_{RISA}$ (2 m depth)	-	97	-	3	-	-	-	-	-	-	-
Schl$_{43F-1404R}$ (20 m depth)	8	-	9	58	-	-	1	10	7	-	-
Schl$_{RISA}$ (20 m depth)	-	-	-	59	-	-	-	41	-	-	-

The 16S rDNA analysis of the water samples of the Gitt mill tailings confirmed the predominance of the γ-proteobacteria and also of the CFB in that environment (see Table 2). Interestingly, applying the RISA retrieval for the analysis of the same water samples we were able to identify representatives of several very diverse bacterial groups such as *Planctomycetales* (Pl), *Nitrospira/Leptospirillum ferrooxidans* (N/L), *Verucomicrobia* (Ver) and *Actinobacteria* (Act) in addition to the two above mentioned groups. Moreover, the Pl population which consisted exclusively of anaerobic ammonia oxidizers was evaluated by RISA as predominant.

The RISA retrieval provided results complementary to those obtained by the 16S rDNA analyses all cases studied. In the Sh environment the 16S rDNA retrieval demonstrated a very strong predominance of γ-proteobacteria, whereas the RISA retrieval indicated the presence mainly of β-proteobacteria. In the case of Schl both approaches indicated a strong predominance of delta proteobacteria. However, the two retrievals identified different (almost not overlapping) parts of the rest of the bacterial community. Via RISA a large number of green sulfur bacteria (GSB) was found in the Schl samples. By using the 16S rDNA retrieval GSB were also identified in Schl but in a much lesser number. Instead, representatives of α- and γ-proteobacteria as well as green non sulfur (GNS) bacteria and Ver were found.

Our results show the importance of using more than one PCR primer pair in the construction of environmental 16S rDNA libraries.

BACTERIAL DIVERSITY IN SOILS OF THE URANIUM MINING WASTES

A. Geißler, T. Tzvetkova, K. Flemming, S. Selenska-Pobell

Bacterial diversity was investigated by using the 16S rDNA retrieval in soil samples collected from one uranium mining waste pile and two uranium mill tailings. A considerable diversity and significant differences were found in the composition of the natural bacterial communities at the three studied environments.

Natural bacterial communities were analyzed in soil samples collected from one uranium mining waste pile called Haberland near the town of Johanngeorgenstadt (JG37), Germany, and from two uranium mill tailings at Gunnison, CO (GUBH2) and Shiprock, NM (Sh765B), both in the USA. The 16S rDNA retrieval was applied as described in /1/. The results of this analysis are summarized in Table 1. As shown in the table, significant differences were observed in the composition of the natural bacterial communities at the three studied environments.

Table 1: Size of bacterial populations (given in %) in the samples from the studied uranium wastes

	JG37	GUBH2	Sh765B
Proteobacteria			
α	**47**	15	7
β	3	6	2
γ	6	**45**	17
δ	5	6	9
Holophaga/Acidobacterium	32	11	3
Cytophaga/Flavobacterium/Bacteroides	3	4	-
Bacilli	-	-	**31**
Actinobacteria	-	-	3
Nitrospira/Leptospirillum	-	-	5
Green non-sulfur bacteria	-	-	17
Planctomycetales	-	-	3
Novel[1)]	4	13	2

[1)]Novel lineages, Candidate divisions OP8 and OP11

Mainly α-Proteobacteria and representatives of the *Holophaga/Acidobacterium* phylum were found in the sample JG37. The part of α-Proteobacteria was the highest, especially of those acting as plant symbionts, namely *Bradyrhizobium* species. In agreement with the analysis of several other samples from this uranium mining waste pile, the representatives of the *Holophaga/Acidobacterium* phylum seem to be characteristic for this site /4/. This bacterial phylum is poorly studied and is represented by only a few cultured isolates. Because *Holophaga/Acidobacteria* are predominant in the JG samples, we put efforts to culture representatives of this phylum in order to study their activity and to elucidate their role in the geo-microbiological processes at the uranium waste near Johanngeorgenstadt.

In the soil sample of the Gunnison uranium mill tailings (GUBH2) γ-Proteobacteria were numerically predominant. They were represented by *Pseudo-monas* and *Acinetobacter* species.

The composition of the bacterial community in the soil sample of the Shiprock uranium mill tailings (Sh765B) was more complex. The predominant bacterial populations were those of *Bacilli,* green non-sulfur bacteria and γ-Proteobacteria. It was published that some *Bacillus* strains recovered from uranium wastes demonstrate an ability to bind selectively and reversibly high amounts of U, Al, Pb, Cu and Cd /3/. Green non-sulfur bacteria were represented by clones which were affiliated with uncultured representatives of this phylum. The γ-Proteobacteria were predominated by *Pseudomonas* and *Acinetobacter* species as in the case of the GUBH2 sample. It was demonstrated by others /2/ that the addition of acetate to the highly saline uranium-contaminated aquifer sediments of the Shiprock mill tailings stimulated a removal of U(VI) from the groundwater and that this was associated with an enrichment of the sediments, mostly with microorganisms closely related to *Pseudomonas*. Interesting is the presence of *Planctomycetales* (ANAMMOX) in the soil sample Sh765B. These bacteria are possibly involved in an anaerobic oxidation of ammonium to molecular nitrogen.

The observed differences in the composition of the bacterial communities in the studied environments are possibly connected to their different grade of contamination with heavy metals, and also to their different geographic and geologic origin /1/.

As expected β- and δ-Proteobacteria were found in all studied samples. The bacterial group of δ-Proteobacteria consists mainly of sulfate and metal-reducing bacteria and their presence is an indication for metal reduction at that sites. Surprisingly, the number of δ-Proteobacteria clones was not very high. Most of the retrieved sequences were related to not yet cultured bacteria, and some of them were moreover affiliated to novel bacterial divisions. Efforts to cultivate some bacterial isolates from the uranium wastes are in progress in our laboratory.

References
/1/ Geißler, A., Report FZR-377 (2003)
/2/ Nevin, K. P. et al., Appl Environ Microbiol **69**, 3672-3675 (2003)
/3/ Selenska-Pobell, S. et al., FEMS Microbiol. Ecology **29**, 59-67 (1999)
/4/ Selenska-Pobell, S. et al., Uranium in the aquatic environment, editors Merkel, B. J., Planer-Friedrich, B. & Wolkersdorfer, C. , Springer-Verlag, p. 455-464 (2002)

IDENTIFICATION OF *GEOBACTER* SPECIES AND OTHER DELTA-PROTEOBACTERIA IN URANIUM MINING WASTES

A. Geißler, S. Selenska-Pobell

Geobacter-specific primers were used for generation of 16S rDNA libraries for soil samples collected from the uranium mining waste pile Haberland near Johanngeorgenstadt (JG37) in Germany and from the uranium mill tailings near Shiprock (Sh765B) in the USA. Most of the retrieved sequences were affiliated to Geobacter species, however sequences related to other δ-Proteobacteria were identified as well.

Representatives of the bacterial genus *Geobacter* belong to the family *Geobacteracea* in the δ subdivision of the Proteobacteria and are able to reduce and immobilize a large number of heavy metals and radionuclides /3/. Because of this they play a major role in geomicrobiological processes occurring at the uranium mining wastes. However, we filed to find these bacteria in the soil sample JG37 and only a limited number of them was identified in the sample Sh765B, when the universal-primer-based 16S rDNA approach was applied /4/. These results indicate that the populations of *Geobacter* are possibly below the limit of detection of the used 16S rDNA retrieval, most probably due to the structure of the universal primers or because the *Geobacter* populations are not dense enough.

In order to overcome the problems of the universal 16S rDNA retrieval we generated 16S rDNA libraries for the mentioned samples by using the *Geobacter*-specific primers Geo561f and Geo825r /6/. The results of this analysis are presented in Fig. 1. As shown in the Fig. 1 most of the retrieved sequences were affiliated to *Geobacter* species. The clone JG37-GeoIII-01 was related to *Geobacter* sp. CdA-2, which was isolated from mining-impacted sediments of Lake Coeur d'Alene, Idaho and was also capable of respiratory Fe(III) reduction /1/. These sediment samples were investigated also by the 16S rDNA approach which demonstrated the presence of the uncultured *Geobacteracea* C109 and C130 /2/. Our clone JG37-GeoIII-04 was closely related to these sequences. The mentioned authors presented that iron reducing bacteria and especially the *Geobacteraceae* are inhabiting metal-polluted environments /2/. As seen in the Fig. 1 most of the sequences from Sh765B were affiliated to a sequence of an uncultured bacterium Geo-83, which was identified in a petroleum-contaminated aquifer located in Bemidji, Minn. where benzene oxidation under in situ Fe(III)-reducing conditions occurs /5/.

The 16S rDNA genes of *Geobacter* species were however, not the only templates amplified. Also amplified were sequences related to the genera *Stigmatella*, *Anaeromyxobacter* and *Myxobacter*, all members of the δ-Proteobacteria. Interestingly, some of the clones (Sh765B-GeoI-44, JG37-GeoIII-36) were affiliated to sequences of uncultured δ-proteobacteria which were identified in our clone library of JG37 constructed by using universal bacterial primers /4/.

In this work the presence of *Geobacter* species in the soil samples of the uranium mining wastes was demonstrated. Their quantification by using Real-Time PCR is in progress in our laboratory.

References

/1/ Cummings, D.E. et al., Appl. Environ. Microbiol. **66**, 154-162 (2000)

/2/ Cummings, D.E. et al., Microb. Ecol. **46**, 257-269 (2003)

/3/ Finneran, K.T. et al., Soil and Sediment Contamination **11**, 339-357 (2002)

/4/ Geißler, A., Report FZR-377 (2003)

/5/ Rooney-Varga, J.N. et al., Appl. Environ. Microbiol. **65**, 3056-3063 (1999)

/6/ Stults, J.R. et al., Appl. Environ. Microbiol. **67**, 2781-2789 (2001)
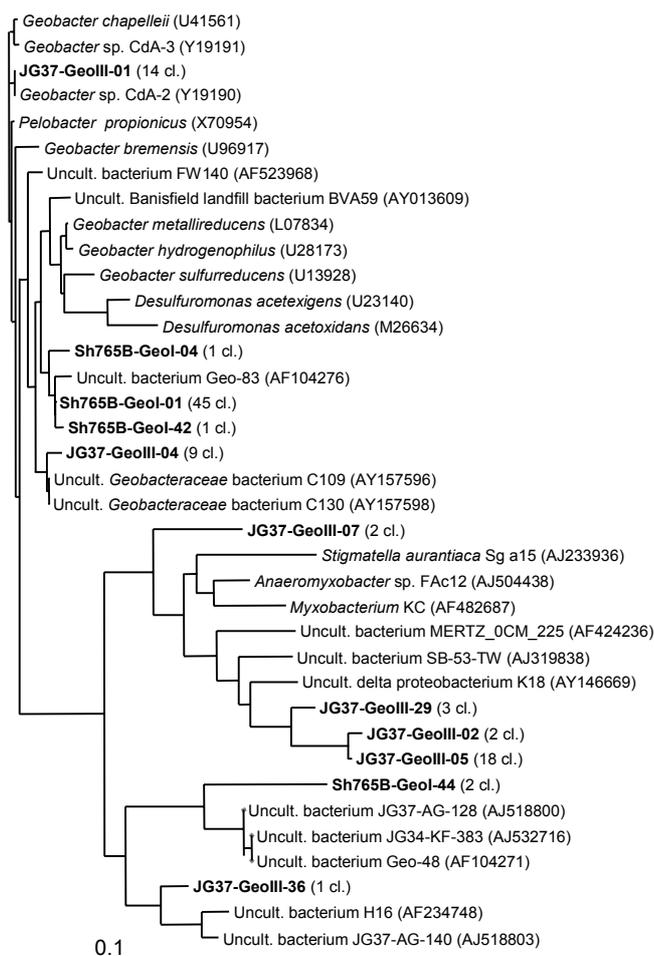
Fig.1: Delta–Proteobacteria identified by using *Geobacter*-specific primers in the soil samples JG37 and Sh765B.

BACTERIAL AND ARCHAEAL DIVERSITY IN WATERS AT THE SIBERIAN DEEP-WELL MONITORING SITE TOMSK-7

M. Nedelkova, S. Selenska-Pobell

Microbial diversity was studied in deep underground waters near the radioactive waste injection site Tomsk-7 by using the 16S rDNA retrieval. The bacterial populations of Dechlorosoma sp. as well as of Chrysobacterium sp. were found to be predominant there. The archaeal populations were represented by sequences which were affiliated to Euryarchaeota and Crenarchaeota.

Recently, we demonstrated a large bacterial diversity in a water sample collected from depths of 290 to 324 m at the monitoring site S15 near the city of Tomsk, Siberia, Russia /1, 2/. The biomass from that sample was concentrated via consequent filtration on a glass fiber filter and on two filters with pore sizes of 0.45μm and 0.22μm. Total DNA was isolated from the whole biomass collected on the tree filters and analyzed /1, 2/.

In this work, a parallel sample from the same site was studied. In order to achieve more detailed characterization of the indigenous bacterial communities at that site, two bacterial clone libraries were generated: one for the DNA isolated from the biomass collected on the 0.45μm filter and another one for those collected on the 0.22μm filter. The comparative analysis of the two libraries revealed significant differences in the predominant groups and in the species composition. As shown in Table 1, 41 % of the sequences of the 0.45μm clone library were affiliated to β–Proteobacteria.

A relatively dense and microdiverse population of not yet cultured *Cyanobacteria* was found in both the 0.45μm and the 0.22μm libraries. This group of sequences was not identified in our previous analysis /1, 2/. Interestingly, similar cases of microdiversity were observed for different species in other uranium contaminated environments /3/.

In addition, one archaeal clone library was generated for the water sample analyzed in our previous work /1, 2/. As seen in Fig. 1 the Archaeal populations are represented by microdiverse sequences affiliated to Crenarchaeota and Euryarchaeota. Most of them were related to the uncultured archaeons HTA-B10 and ARC3, which were identified in different metal-rich environments /4]/. Interestingly, one of the Crenarchaeota clusters was closely related to the uncultured archaeon Gitt-GR-78, found in the uranium mining wastes /5/.

Bacterial groups		Clone libraries	
		0.45μm	0.22μm
Proteo-bacteria	α	5.3	7.1
	β	**41**	8.2
	γ	6	13.7
	δ	2.3	-
CFB		4.5	**55.2**
Gramm +	Low G+C	9.8	-
	High G+C	5.3	1.1
Holophaga/Acidobacteria		1.5	-
Cyanobacteria		20.4	13.7
OP11		-	0.5
OP8		1.5	-
TM7		0.7	-
Termite group		0.7	0.5
Deinococcus/Thermus		0.7	-

Tab. 1: Bacterial groups (given in %) identified in the 0.45μm and 0.22μm 16S rDNA libraries

The main part of these clones showed high levels of identity to *Dechlorosoma* sp. This result is in agreement with our previous studies /1,2/. However, in contrast to that analysis, where the *Dechlorosoma* sp. represented 65 % of the clones, now its predominance was not too strong. Instead, larger variety was identified of Gramm positive bacteria, of α–, γ–, and δ–Proteobacteria, and also of members of Candidate divisions OP8, TM7, *Deinococcus/Thermus* and of the Termite group. In the 0.22μm clone library *Dechlorosoma* sp. was not identified any more. In this case populations of *Cytophaga/ Flavobacterium / Bacteroides* (CFB) group, namely the *Chrysobacterium* spp., were predominant (Table 1).

Fig. 1: Archaea identified at the S15 site. The number of clones is given in brackets.

References

/1/ Nedelkova, M. et al., Report FZR-373, p.30 (2003)

/2/ Nedelkova, M. et al., in press (2004)

/3/ Selenska-Pobell, S., In: *Interactions of Microorganisms with Radionuclides*. Elsevier Sciences, Oxford, UK, pp. 225-253, (2002)

/4/ Stein, L. et al., Env. Microb. **3**, 10-18 (2001)

/5/ Radeva, G., Selenska-Pobell, S. Report FZR-373, p.29 (2003)

MOLECULAR ANALYSES OF THE S-LAYER GENES AND PROTEINS OF *BACILLUS SPHAERICUS* JG-A12 AND NCTC9602

K. Pollmann, M. Schnorpfeil, G. Radeva, S. Selenska-Pobell

The seqences of the S-layer genes and of the S-layer proteins from the bacterial strains Bacillus sphaericus JG-A12 and 9602 were analysed. Besides the functional genes both strains contain a second S-layer gene like copy.

Introduction

The uranium mining waste pile isolate *Bacillus sphaericus* JG-A12 and its closest relative *B. sphaericus* 9602 are enveloped by surface layer proteins. The cells of these strains are capable of selective accumulating heavy metals such as U^{2+}, Pb^{2+}, Cd^{2+} and Al^{3+} /1/. Further, Pd nanoclusters are formed on the S-layers /2/ and on the bacterial cells in the presence of a reducing agent. In order to identify the potential metal binding sites and also to clone and express the S-layer genes in *E. coli*, the sequences of both S-layer genes and of the matured proteins were studied.

Sequence analysis of the S-layer genes

Sequencing of the S-layer genes from the strains *Bacillus sphaericus* JG-A12 and *B. sphaericus* NCTC9602 was finished using vectorette libraries (Sigma) which were constructed by using different restriction endonucleases. The ORF of the S-layer gene of the strain JG-A12 encodes a protein of 1238 amino acids with a theoretical molecular weight of 126 kDa, whereas the ORF of the S-layer gene of the strain 9602 encodes a protein of 1099 amino acids with a theoretical molecular weight of 113 kDa. The upstream regions of the genes of both strains contain ribosomal binding sites and strong promoters at positions -83 (-10, TATACT) and -106 (-35, TTGACA). Expression of both S-layer genes was confirmed by Northern Hybridisation using Dig labeled PCR probes which were specific to the central part of the S-layer genes and by RT-PCR using primers which are specific to the upstream regions.

The N-terminal and central domains of the S-layer proteins of the strains JG-A12 and 9602 show an unusual high identity between each other and differ significantly from the known S-layer proteins of other *Bacillus sphaericus* strains (Fig. 1). The two S-layer proteins differ significantly in their C-terminal parts. Interestingly, the C-terminal part of the S-layer protein of JG-A12 shows an unusual strong similarity to that of the strain *B. sphaericus* 2177 (Fig. 1). Moreover, the S-layer gene of JG-A12 is followed by a gene encoding a transposase. These results strongly indicate that the S-layer genes have evolved from different ancestors followed by genetic rearrangements.

Tab. 1: Amino acid composition of the S-layer proteins: The portion of Asp, Glu, Ser and Thr

	Aspartate	Glutamate	Serine	Threonine
*B.sph.*JG-A12	5 %	5 %	5 %	14%
B.sph. 9602	5%	5%	6%	12%
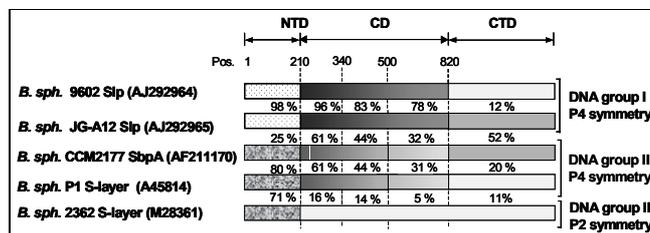
Fig. 1: Comparison of S-layer proteins of different *Bacillus sphaericus* strains. *B. sph.* = *Bacillus sphaericus* ; NTD = N-terminal domain; CD = central domain; CTD = C-terminal domain; Pos. = amino acid position.

The primary structure of both S-layer proteins show a high contents of the amino acids serine and threonine, which are potential phosphorylation sites, as well as aspartate and glutamate (Tab. 1). Since previous EXAFS analyses showed, that U(VI) is coordinated to phosphate and carboxyl groups /3/, it is probable, that these amino acids are involved in metal binding. Since especially in the C-terminal parts stretches of these amino acids are found, it is probable, that these parts determine the metal binding properties of the S-layer proteins.

Detection of a second S-layer gene like copy

In the strains *B. sphaericus* JG-A12 and NCTC 9602 large plasmids were detected by using gel electrophoresis and PFGE. Southern hybridisation using Dig labeled S-layer gene specific probes indicated, that both plasmids encode a second S-layer gene-like copy. Both copies were sequenced using vectorette libraries.

The S-layer gene-like copy of 9602 shows high identity to the functional gene, while the upstream region contains a modified ribosomal binding site and shows significant differences. In the case of the S-layer gene-like copy of JG-A12, a large part of the N-terminal domain, the signal peptide and a large part of the upstream region is deleted. These results indicate that the rearranged S-layer gene-like copies are non-functional.

Acknowledgements

References

/1/ Selenska-Pobell, S. et al., FEMS Microbiol. Ecol. 29: 59-67(1999)
/2/ Raff, J., PhD thesis, Report FZR-358 (2002)
/3/ Raff, J. et al., Report FZR-373, p. 36 (2002)

POSTTRANSLATIONAL MODIFICATION OF THE S-LAYER PROTEIN FROM *BACILLUS SPHAERI-CUS* JG-A12 AND ITS INFLUENCE ON URANIUM BINDING

J. Raff, S. Selenska-Pobell

Biochemical analysis of the B. sphaericus JG-A12 S-layer shows posttranslational modifications in a form of phosphorylation. Using concentrations of 1 to 10 mg uranium per liter the S-layer of B. sphaericus NCTC 9602 and bovine serum albumine show lower affinity to uranium than the S-layer of B. sphaericus JG-A12.

Posttranslational modifications of proteins as e.g. phosphorylation, glycosylation or cleavage of proteins are very common in nature. It is especially relevant for stability of proteins and regulation of the activity of enzymes. As outermost cell wall component surface layer (S-layer) proteins are the interface between the cell and the environment. The uranium mining waste pile isolate *B. sphaericus* JG-A12 possess also a S-layer protein /1/. Its primary structure differs significantly from all S-layer proteins known up to now /2/, but shows highest similarity to the S-layer protein of the reference strain *B. sphaericus* NCTC 9602.

In the present work recrystallized S-layer proteins of the *B. sphaericus* stains JG-A12 and NCTC 9602 were tested for phoshorylation using inductive coupled plasma mass spectroscopy (ICP-MS), a colourimetric method according to Ekman and Jäger /3/ and via phosphorous specific staining of proteins after SDS gelelctrophoresis with the GelCode kit (Piece Biotechnology). The DIG glycan detection kit (Roche Diagnostics Corporation) was additionally used to investigate glycosylation status of S-layer proteins. Then uranium binding properties was compared between the different phosphorylated S-layers and the non phosphorylated protein bovine serum albumine (BSA). All above mentioned methods show phosphorylation for the S-layer proteins of the *B. sphaericus* strains JG-A12 and NCTC 9602 (see table 1).

Tab. 1: Phosphorous content in mol P/ mol protein

	ICP-MS	colouri-metric method	phospho-protein staining
B. sphaericus JG-A12 S-layer	$0,65 \pm 0,01$	$0,26 \pm 0,02$	+
B. sphaericus NCTC 9602 S-layer	$0,11 \pm 0,01$	$0,05 \pm 0,01$	+
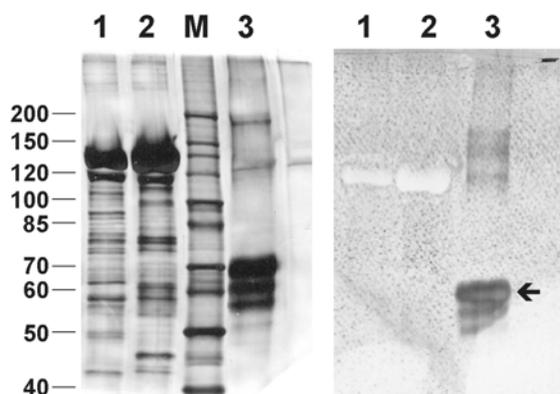
Fig. 1: Glycan specific staining of proteins. Silver stained SDS gel (left) and DIG stained blot of an equal SDS gel (right, arrow indicates glycosylation). Lanes: 1, JG-A12 S-layer; 2, NCTC 9602 S-layer; 3, glycosylated reference protein fetuin; M, molecular weight standard in kd (potein ladder 10-200 kd, MBI Fermentas)

Interestingly the S-layer protein of *B. sphaericus* JG-A12 possesses five to six times more phosphorous compared to the S-layer protein of *B. sphaericus* NCTC 9602. Besides that both S-layer proteins are not glycosylated (see Fig. 1).
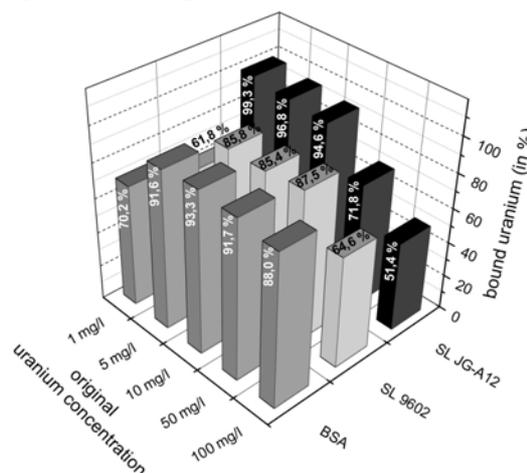
Fig. 2: Uranium binding of 1.5 g/l S-layer protein of the *B. sphaericus* strains JG-A12 and NCTC 9602 compared to that of 1.5 g/l serum bovine albumine.

Although the S-layer proteins of *B. sphaericus* JG-A12 and NCTC 9602 have a very similar molecular structure, the NCTC 9602 S-layer as well as the BSA possess significantly lower affinity to uranium in solution with a concentration of uranium between 1 and 10 mg/l than the JG-A12 S-layer protein. The latter binds 94,6 to 99,3 % of the uranium compared to 61,8 to 85,4 % and 70,2 to 93,3 % for the NCTC 9602 S-layer and BSA. This means that the S-layer of *B. sphaericus* JG-A12 is able to bind already all uranium in environmental relevant concentrations of 5 mg/l and below. As known from extended x-ray absorption fine structure (EXAFS) spectroscopy, uranium is mainly bound via phosphate and carboxyl groups to the S-layer /4/. As the content of amino acids having side chains with carboxyl groups is equal for the S-layer proteins of *B. sphaericus* NCTC 9602 and JG-A12 /2/, the different binding behavior can be ascribed to the higher phosphorylation degree of the JG-A12 S-layer. This may be an adaptation of *B. sphaericus* JG-A12 to its highly with heavy metals contaminated environment.

References
/1/ Raff, J., PhD thesis, University of Leipzig (2002)
/2/ Pollmann, K., this report p. 23
/3/ Ekman, P., Jäger, O., Analytical Biochemistry **214**, 138-141 (1993)
/4/ Raff, J. et al, Report FZR-373 (2003), p. 36

EXAFS STUDIES OF PALLADIUM NANOCLUSTERS FORMED AT THE CELLS AND S-LAYERS OF *BACILLUS SPHAERICUS* JG-A12

M. Merroun, K. Pollmann, J. Raff, A. Scheinost, S. Selenska-Pobell

EXAFS spectroscopy was used to characterize the Pd nanoclusters formed at the cells and S-layers of B. sphaericus JG-A12. The results demonstrate that cells of this bacterium are able to form Pd nanoclusters of about 19 to 43 atoms with a diameter range between 8.5 and 10 Å. In the case of S-layers however, the palladium is not fully reduced.

Metallic nanostructures are promising candidates for the development of sensors, catalysts and nanoscopic electrical connections. Palladium is one of the most widely used metals in transition metal catalyzed organic synthesis, as it is capable of catalyzing a wide variety of commercially important reactions. It has also been used as catalyst for removing nitrate ion from drinking water, for hydrogenation and for combustion reactions. In this work the formation of Pd nanoclusters at the cells and S-layers of *B. sphaericus* JG-A12 in anaerobic conditions were studied using EXAFS spectroscopy.

The samples were prepared as follows: *B. sphaericus* cells were grown in a batch culture to mid exponential phase and harvested by centrifugation at 10.000 rpm for 30 min. After worth, the cells were washed in MOPS/NaOH buffer pH 7.0 several times. To palladise *B. sphaericus* JG-A12 cells, 50 ml of Pd(II) solution (Na_2PdCl_4) were poured into 55 ml serum bottles, degassed under nitrogen for 15 min. In the case of the S-layers, the reduction of Pd(II) (K_2PdCl_4) was started by addition of NaN_3.

Palladium K-edge EXAFS spectra of the Pd nanoclusters formed at the cells of *B. sphaericus* JG-A12 at pH 2 und 4 in presence of H_2 and their corresponding Fourier transforms (FT) are shown in Fig. 1. Using Pd-Pd shell parameters of Pd foil all the peaks were attributed to 4 Pd-Pd shells with distances of 2.75, 3.88, 4.77 and 5.42 Å . A better estimate of the average cluster size is obtained from the number of first neighbours (6.3 and 7) which considerably lower than the coordination number of 12 of an infinite lattice.
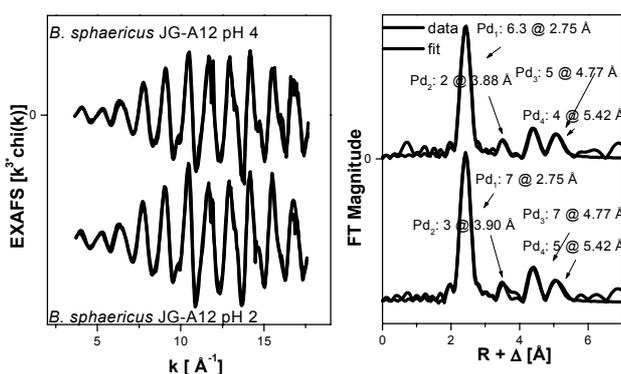
Fig. 1: Pd K-edge EXAFS spectra and their corresponding FT of the Pd nanoclusters formed at the cells of *B. sphaericus* JG-A12 at pH 2 and 4 in the presence of H_2.

According to Mojet B.L. /1/ the range coordination number between 6.3 and 7 of the first shell found in this work is reached in a cluster of about 19 to 43 atoms with a diameter range between 8.5 and 10 Å formed at a layer of nearest neighbors around a central atom. In the absence of H_2 (Fig. 2) the palladium is bound to carboxyl groups.
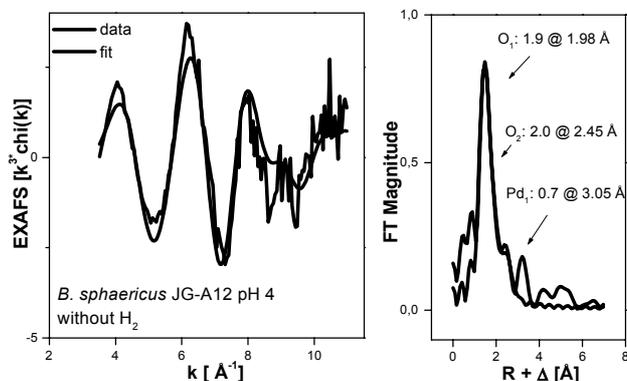
Fig. 2: Pd K-edge EXAFS spectra and their corresponding FT of the Pd nanoclusters formed at the cells of *B. sphaericus* JG-A12 at pH 2 and 4 in the absence of H_2.
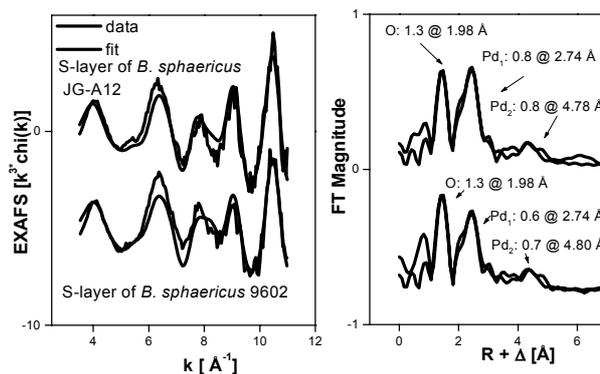
Fig. 3: Pd K-edge EXAFS spectra and their corresponding FT of the Pd nanoclusters formed at the S-layer of *B. sphaericus* JG-A12 and 9602.

However, the EXAFS spectra of the palladium complexes formed at the S-layer of *B. sphaericus* JG-A12 and its reference strain NCTC 9602 (Fig. 3) demonstrated that the palladium is not fully reduced.

Preliminary results obtained by laser induced Infrared spectroscopy analysis indicated that a part of Pd is bound to carboxyl groups of the S-layer.

References
/1/ Mojet, B.L . PhD Thesis 1997

TOXICITY OF URANIUM TOWARDS *Desulfovibrio äspöensis* DSM 10631: FLOW CYTOMETRY AND TRANSMISSION ELECTRON MICROSCOPE STUDIES

M. Merroun, H. Moll, M. Maitz[1], G. Bernhard, S. Selenska-Pobell
[1]Institut für Ionenstrahlphysik und Materialforschung

Flow Cytometry (FCM) and Transmission Electron Microscope (TEM) were used to investigate the toxicity of uranium towards the cells of D. äspöensis DSM 10631. The results demonstrated that the uranium at high concentration affects the integrity of the cell membranes and consequently is taken up into the cytoplasm.

Flow cytometry (FCM) is a powerful technique with great potential for performing both qualitative and quantitative analyses based on simultaneous measurements of structural and functional parameters of individual cells. In this study we used the LIVE/DEAD *Bac*Light Kit /1/ (stain mixture distinguishes viable bacterial cells from dead ones on the basis of membrane integrity) to investigate the toxicity of uranium on *D. äspöensis*. The kit contains two nucleic acid stains. The green fluorochrome (Syto 9) is a small molecule that penetrates intact plasma membranes, while the larger red fluorochrome (propidium iodide, PI) penetrates only compromised membranes. Both show fluorescence when bound to DNA, but PI has the higher affinity and replaces Syto 9, thus allowing a clear distiction between cells with intact membrane (green) and dead cells with destroyed membrane (red). In addition, to visualize the toxic effect of uranium we perform TEM studies.

The strain was grown under anaerobic conditions in 250 ml bicarbonate-buffered medium containing a trace amount of ferrous chloride (7.5×10^{-7} M) at 22 °C. The cell pellet was washed 3 times with 0.9% NaCl. To study the toxic effect of uranium on this bacterium, the cells were treated with 2 different concentrations of this metal (15 and 150 mg/l) during 3, 14, 20, 48 and 72 h. After the contact with uranium, cells (1ml) were mixed with 3 µl of a mixture of Syto 9 and propidium iodide (1:1), nucleic acid stains from LIVE/DEAD kit and were incubated in the dark for 15 min at room temperature. Bacterial suspensions incubated in the presence of both stains simultaneously were analysed by flow cytometry for green (i.e. viable) and red (i.e. dead) fluorescence.

For TEM analysis the cells were fixed in 2% (v/v) glutaraldehyde, dehydrated in ethanol and then embedded in Spurr resin.

Flow cytometry technique
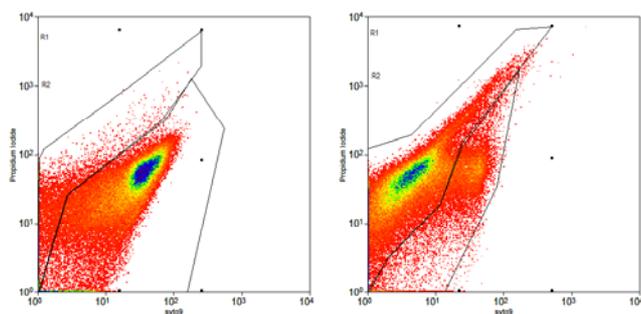
Fig. 1: FCM analysis of the viability of *D. äspöensis* in the absence (right) and in the presence of 150 mg/l of uranium (left) after 3 h of incubation.

In the absence of uranium, and after 48 and 72 h of incubation, 80 and 75% of the cells exclude propidium iodide. respectively. This fluorescent dye is concentrated by microbial cells in an energy-dependent fashion. Hence, staining with Syto 9 and subsequent flow cytometric analysis is one approach to measure metabolic active cells. However, after 72 h of cell incubation with 15 and 150 mg/l of uranium, only 30 and 5% of the cells exclude propidium iodide (live cells), respectively.

TEM and EDX analysis
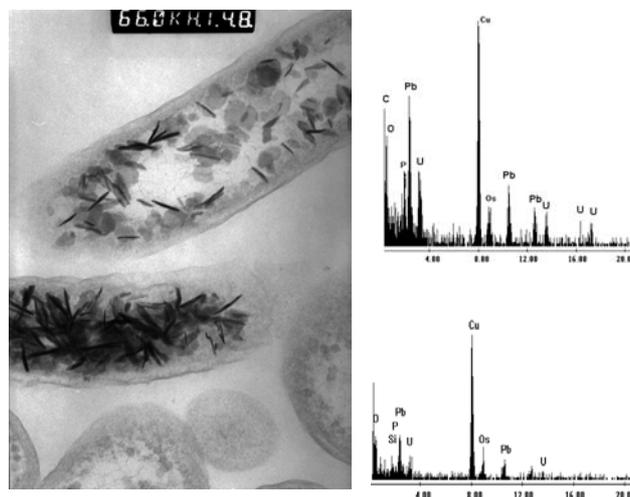
Fig. 2: TEM and EDX analysis of the cellular localization of uranium accumulated by the cells of *D. äspöensis*.

TEM and EDX analysis demonstrated that the cells of *D. äspöensis* accumulate uranium intracellularly, presumably, as phosphate compounds after 48 h contact with this metal.

Flow cytometry and TEM analysis showed that as a result of the uranium stress the cell membrane is damaged and uranium can penetrate inside the bacterial cells.

References
/1/ Alonso, JL. et al., Appl . Environ. Microbiol. **68**, 5151 (2002)

Desulfovibrio äspöensis DSM 10631^T AND URANIUM – FIRST LIPAS RESULTS

H. Moll, G. Geipel, M. Merroun, S. Selenska-Pobell, G. Bernhard

In continuation of the studies investigating the interaction of uranium(VI) with D. äspöensis DSM 10631^T, the LIPAS technique was used to explore the speciation of uranium associated with the biomass. The formation of U(IV) was demonstrated.

Introduction

We are investigating the interaction of selected actinides with the sulfate-reducing bacterial (SRB) strain *Desulfovibrio äspöensis* isolated at the Äspö HRL /1-5/. *Desulfovibrio* strains have the ability to immobilize heavy metals, e.g. uranium by reduction. In /2/ we demonstrated the formation of U(IV) due to the activity of the bacterial cells using the XAS technique with synchrotron radiation. In this study we are applying a new method, Laser-induced Photoacoustic Spectroscopy (LIPAS), for the identification of U(IV) associated with the biomass. To our knowledge there are no studies so far exploring the speciation of actinide-bacteria complexes / compounds using this spectroscopic technique. LIPAS is a powerful tool to study the spectroscopic properties of actinides at very low concentrations /3/. A further advantage of this method is the detection of U(IV) in the presence of U(VI).

Experimental

The anaerobic strain *D. äspöensis* DSM 10631^T was grown under anaerobic conditions in an optimized 250 mL bicarbonate-buffered mineral medium (DSMZ – Medium 721) containing resazurin as a redox indicator at 22 °C. The biomass was collected by centrifugation and washed three times with 0.9 % NaCl. To study the interaction of *D. äspöensis* with U(VI) the cells were grown to the mid-exponential phase. The collected biomass was 0.8 g$_{dry\ weight}$/L. The molecular analysis of the *D. äspöensis* cultures was performed using ARDREA as described in /4/. Two parallel samples were prepared. In sample A, the cells were incubated with 15 mg/L U(VI) in solution at pH 5. In sample B the uranium concentration used was 150 mg/L. After shaking the samples for 72 hours under nitrogen atmosphere, the LIPAS spectra were measured. The design of LIPAS is described in /3/.

Results

We are presenting the first interpretation of the LIPAS data measured in a biological system. The LIPAS spectra of samples A and B are summarized in the Figure 1. The spectra of the bacterial samples are different. In principle, the only difference between both samples is the uranium concentration present in the medium. The reasons for the observed varieties are not fully understood. In the spectrum of sample A we could identify two absorption bands centered at 628 and 650 nm. A comparison with the literature showed that U(IV) shows characteristic absorption maxima at 625.5, 649.1 and 671.7 nm /3/. Especially from the detected absorption band at 650 nm we are concluding the presence of U(IV) due to the activity of the cells of *D. äspöensis*. At the moment we can not quantify the amount of U(IV). When the sample A was exposed to air for 72 h, the absorption bands at 628 and 650 nm disappeared due to re-oxidation of U(IV) and because the bacteria are damaged by the oxygen. This gives further evidence that the

existence of U(IV) in the original sample A was connected to the activity of the bacterial cells. After the XAS results published in /2/, this is the second experimental proof that *D. äspöensis* bacteria are able to reduce U(VI) to U(IV) by an enzymatic reaction.
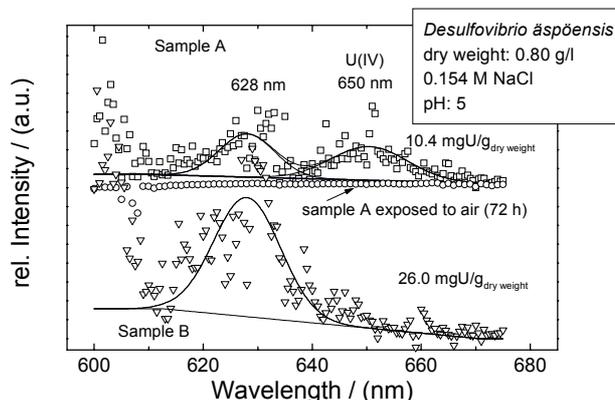
Fig. 1: LIPAS spectra of uranium in suspensions of *D. äspöensis.*

In sample B, where the amount of uranium was 10 times higher and possibly toxic to the bacterial cells, we could not clearly identify the formation of U(IV). The absorption band at 650 nm, which is a strong indication for U(IV), is missing. As a result from additional measurements we cannot clearly assign the absorption band at 628 nm to the presence of U(IV). The experiments are indicating that the reduction of U(VI) by this novel SRB strain is possibly related with the occurrence of vital cells. Using flow cytometry in combination with fluorescence microscopy we could demonstrate the toxicity of uranium at that concentrations to the cells of *D. äspöensis* /5/. In a system containing 150 mgU/L, more than 80 % of the cells showed damaged membranes already after a contact time of 3 h. If the uranium concentration in the medium is reduced to 15 mg/L approximately 30 % of the cells are still vital after 72 h of interaction. The toxicity of uranium at concentrations larger than 15 mg/l might be one reason why the detection of U(IV) failed in sample B.

This study shows again the complexity of the interaction mechanism of uranium with *D. äspöensis.*

Acknowledgement

References

/1/ Motamedi, M., et al., Int. Syst. Bacteriol. **48**, 311 (1998)

/2/ Moll, H. et al., Report FZR-373 (2003) p. 31, 32

/3/ Geipel, G. et al., Radiochim. Acta **82**, 59 (1998)

/4/ Moll, H. et al., Environ. Sci. Technol. **38**, 1455 (2004)

/5/ Merroun, M. et al., this report p. 26

INTERACTION OF ACTINIDES WITH *Desulfovibrio äspöensis* DSM 10631[T]. PART II: CURIUM

H. Moll, Th. Stumpf[1], M. Merroun, A. Roßberg, S. Selenska-Pobell, G. Bernhard
[1] Institut für Nukleare Entsorgung, Forschungszentrum Karlsruhe, Karlsruhe, Germany

We presenting the first results on interactions of the sulfate-reducing bacterium D. äspöensis DSM 10631[T] with curium(III). A biosorption of Cm(III) was observed forming an inner-sphere surface complex of Cm(III) onto the D. äspöensis cell envelope.

Introduction

Sulfate-reducing bacteria (SRB) are frequently distributed in the deep granitic rock aquifers at the Äspö hard rock laboratory (Sweden). We are focussing our work on the SRB strain *Desulfovibrio äspöensis* DSM 10631[T] recovered from a depth of 600 m at the Äspö site /1/. Compared to uranium /2/ much less is known about bacterial interactions with Cm(III).

The Gram-negative strain *D. äspöensis* was grown to the mid-exponential phase as described in /3/. The collected biomass was 0.8 $g_{dry\ weight}$/L. The molecular analysis of the *D. äspöensis* cultures was performed using ARDREA as described in /3/. The time-resolved laser-induced fluorescence spectra were recorded at 25 °C using a flash lamp pumped Ti:sapphire laser (Elight, Titania). Details on the experimental set-up are summarized in /3/.

Results

Figure 1 shows emission spectra of 3×10^{-7} mol/L Cm(III) in aqueous solution in presence of *D. äspöensis* at various pH.
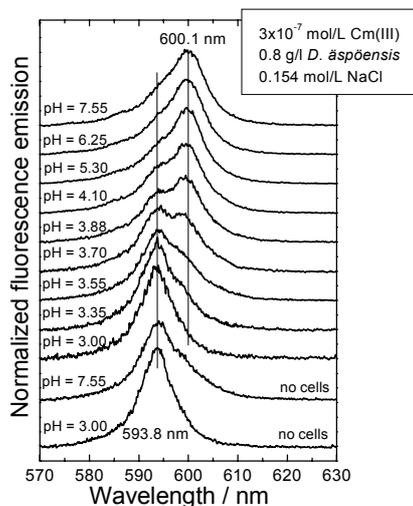
Fig. 1: Fluorescence emission spectra of Cm(III) in a suspension of *D. äspöensis* at different pH.

In all samples with cells at pH < 3.35 the emission band of the Cm(III) aquo ion dominates the emission spectra. Starting at pH 3.35 the intensity of the 593.8 nm peak decreases with increasing pH and a second peak appears with a peak maximum at 600.1 nm. We interpret the pH dependence of the emission spectra as biosorption, forming an inner-sphere surface complex of Cm(III) onto the cell envelope of *D. äspöensis*. The factor analysis technique was applied to calculate the contributions of the pure components to the measured composite spectra. The spectra of the single components derived by deconvolution of the mixed spectra (Fig. 1) are shown in figure 2.
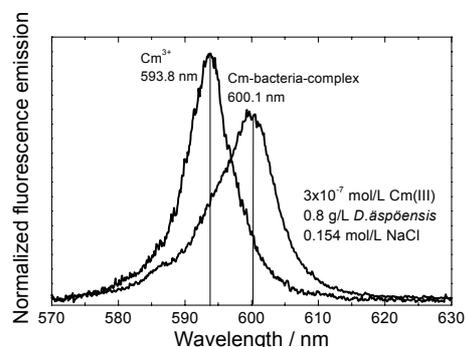
Fig. 2: Spectra of the single components of Cm(III) in suspensions of *D. äspöensis*.
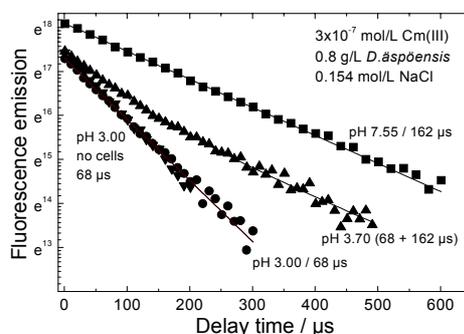
Fig. 3: Fluorescence lifetimes in the system Cm(III) - *D. äspöensis*; mono- and bi-exponential decay behavior.

Lifetime measurements revealed for the Cm[3+] aquo ion 68 µs whereas the Cm-*D. äspöensis*-surface complex is characterized by a long fluorescence emission lifetime of 162 +/- 5 µs. According to the Kimura & Choppin equation a lifetime of 68 µs corresponds to nine water molecules in the first Cm(III) coordination sphere and a lifetime of 162 µs corresponds to three water molecules in the actinide first hydration shell /4/. The dehydration of Cm(III) by sorption onto the bacteria can be explained by the interaction process of Cm(III) and the cell envelope of *D. äspöensis*. These findings and other investigations of Gram-negative bacteria with actinides may indicate an interaction of Cm(III) with organic phosphato-groups of the cell envelope. We found no indications for an uptake of Cm(III) inside the cells.

Acknowledgement

References
/1/ Motamedi, M. et al., Int. Syst. Bacteriol. **48**, 311 (1998)
/2/ Moll, H. et al., Report FZR-373 (2003) p. 31, 32
/3/ Moll, H. et al., Environ. Sci. Technol. **38**, 1455 (2004)
/4/ Kimura, T. et al., J. Alloys Comp. **213/214**, 313 (1994)

COLLOID FORMATION IN KÖNIGSTEIN FLOOD WATER MEDIATED BY BACTERIA ?

K.-U. Ulrich, S. Weiß, M. Merroun, H. Zänker

Two chemically very similar acid flood water samples of the Königstein uranium mine showed different Fe(II) oxidation rates and colloid formation behavior, mediated probably by bacteria. The key trigger of the processes and the responsible organisms remain to be identified.

In preparation of neutralization experiments /1/ we characterized two flood water samples (FW-1, FW-2) from the abandoned Königstein uranium mine for basic chemical parameters, iron speciation, colloids, and presence of bacteria. The samples were stored at 5°C in darkness without oxygen exclusion. ICP-MS and the phenanthroline method served for total Fe and Fe(II) analysis, with Fe(III) calculated by difference. Particle growth was followed in the supernatant after centrifugation (1h, 52000 g) by means of photon correlation spectroscopy (PCS). Bacteria were visualized by direct growth on a solid nutrient broth medium and by SEM on a 50 nm filter membrane with 50 mL of filtered sample volume.

Both FW samples had a pH of 3.0 and similar concentrations of O_2 (0.7 mg/L), sulfate (1.3 g/L), and total Fe (300 mg/L) which completely passed a 3 kD filter membrane even though 19% and 28% of the iron was ferric iron in FW-1 and FW-2, respectively (Fig. 1). EQ3/6 calculation verified Fe^{3+} to be oversaturated, i.e. there should be ultra-fine colloids that are able to pass 3 kD ultrafilters. However, PCS was not sensitive enough for their detection. Whereas iron speciation and transparency of the uncolored water sample FW-1 remained unchanged over 28 days, FW-2 showed distinct Fe(II) oxidation with a half-life of about 12 days (Fig. 1). After 9 days, 11% of total Fe was colloidal (>3 kD) and the water color had changed from light yellow to orange-brown. In the centrifugate, the median particle diameter increased linearly and the scattered light intensity logarithmically with time until a constant level was reached due to sedimentation of larger aggregates (Fig. 2). This is in analogy with results from acid rock drainage water /2/. Since the Fe(II) concentration did not decline simultaneously, aggregation of preexisting fine colloids should be the main reason for the rapid particle growth. This was in accordance with a near-zero particle surface charge at pH 3 (laser Doppler electrophoresis), i.e. a weak electrostatic stabilization of the colloids.

Microbial growth tests on a nutrient broth medium and SEM examination on filter membranes showed bacteria to be present only in sample FW-2 (Fig. 3), not in sample FW-1. Thus we hypothesize that microbial processes might have mediated the iron oxidation in FW-2. Though it is known that the Fe(II) oxidation rate, which is extremely low in air-saturated waters of pH ≤ 5 (half-life: 1625 days), can be accelerated by microbes and autocatalysis /3/, the key factor for starting Fe(II) oxidation and the responsible microorganisms are not yet identified in our case. Further investigations with biomolecular techniques are in progress.

References
/1/ Ulrich, K.-U. et al., this report p.45
/2/ Richter, W. et al., Report FZR-373, p. 27
/3/ Davison, W., De Vitre, R. (1992). Iron Particles in Freshwater. In: Buffle, J., van Leeuwen, H.P. (ed.), *Environmental Particles*. Vol. 1. Lewis, p. 315-355.
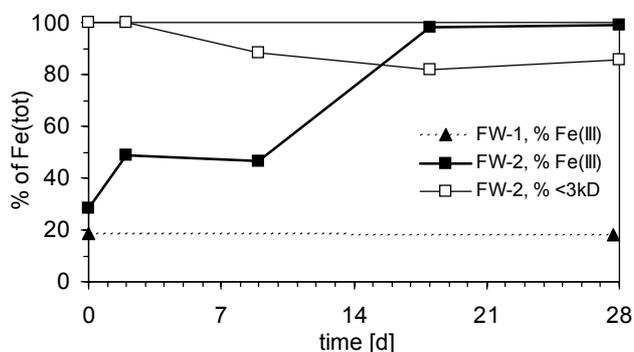
Fig. 1: Percentages of Fe(III) and <3kD fraction based on Fe(tot) concentration in the water samples FW-1 and FW-2 over time.
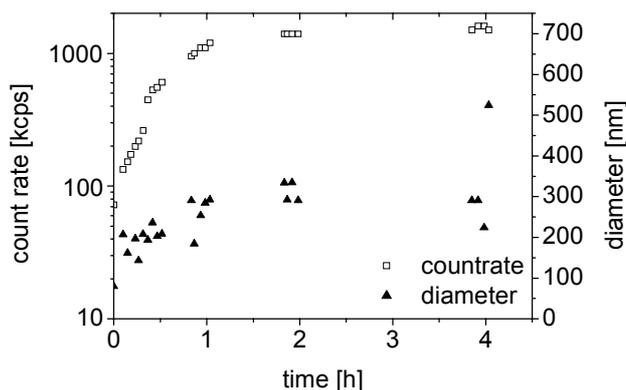
Fig. 2: Course of particle diameter (CONTIN deconvolution) and countrate in a 1h 52000 g centrifugate of sample FW-2.
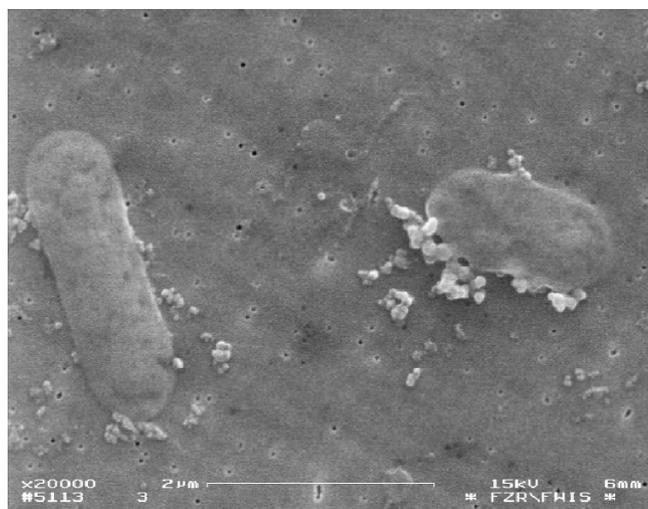
Fig. 3: SEM image (20000 x) of bacteria and colloids in FW-2 with 50 mL water filtered over a 50 nm membrane (Shot: E. Christalle).

MICROSCOPIC CHARACTERIZATION OF *PSEUDOMONAS AERUGINOSA* BIOFILMS

K. Großmann, T. Arnold, G. Bernhard

Scanning Electron Microscopy (SEM) and Scanning Confocal Laser Microscopy (SCLM) studies showed that the formation of a biofilm on a biotite surface can be classified in six stages, starting with reversible and irreversible adhesion and culminating in the dispersion of cells by sloughing and erosion.

Introduction

Bacteria in nature do not usually occur as single individual bacterial cells but rather in large communities of bacteria glued together by Extracellular Polymeric Substances (EPS). Such aggregates are called biofilms. They may significantly influence the transport of heavy metals in the geosphere by changing the geochemical conditions within the biofilm or simply by adsorption onto biological surfaces.

Experimental

Biotite platelets were placed in a mixed-flow reactor, and a bacteria cocktail was pumped through the reactor at 0.02 ml per minute. The experiments were performed at room temperature. Samples were taken at certain time intervals and studied by SEM and SCLM.

Results

The initial stages of colonization on the biotite surface were observed after five hours of wetting. At this stage individual bacteria colonized the surface by reversible and irreversible adhesion. After the initial phase another five biofilm stages occurred listed below:

1. reversible and irreversible adhesion to the surface of the substratum
2. formation of microcolonies
3. production of EPS as shown in Fig.1
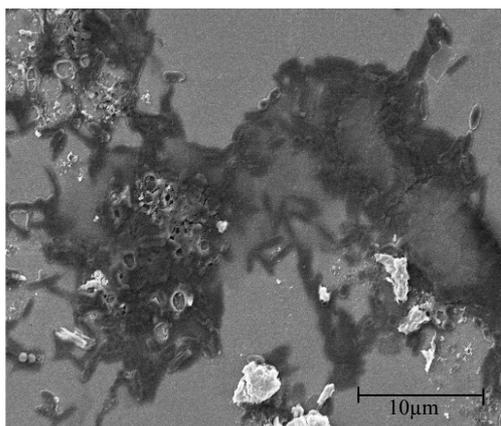
Fig.1: SEM picture showing the stage at which microcolonies are attached to the surface and the production of EPS has set in

4. adhesion of further bacteria to the already attached microcolonies as depicted in Fig.2
5. mature confluent biofilm
6. active flaking and more dispersion by sloughing and erosion
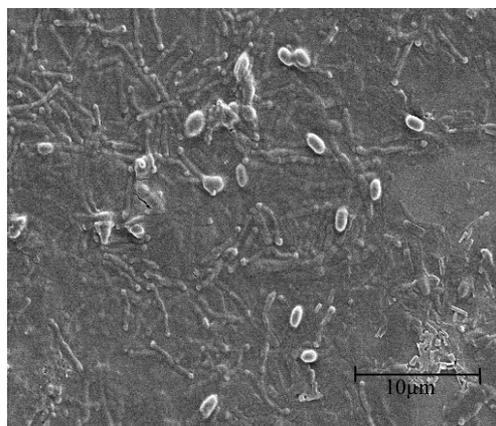
Fig.2: SEM picture showing the stage of adhesion of further bacteria to the attached microcolonies

The mature confluent biofilm was further characterized by using fluorochromes and fluorescent- labeled lectins in combination with SCLM. The characterization of living and dead eukaryotic cells within the biofilm was achieved with SYTO 9 and propidium iodite. The EPS in the *Pseudomonas aeruginosa* biofilm was visualized, using the lectins concanavaline A (ConA) and wheat germ agglutinin (WGA) (Fig.3). The fluorescent- labeled lectin ConA (attached to alginate) yielded cloudlike regions that were randomly distributed within the mucoid biofilms. In WGA- treated biofilms, the lectin was predominantly associated with bacterial cells[1]. In addition, the thickness of the biofilm was determined by SCLM and a value of 5.3µm was determined.
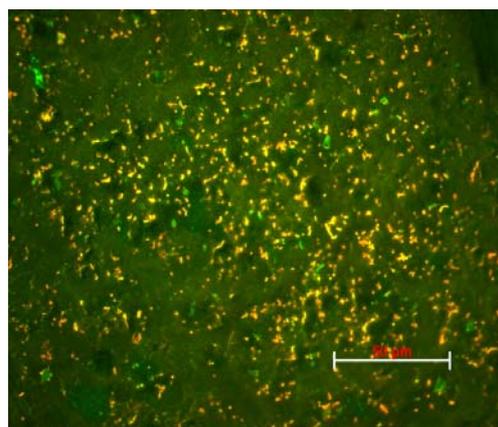
Fig.3: The EPS of a mature confluent biofilm was visualized using fluorescent- labeled lectins ConA (green) and WGA (red) as well as SCLM

References

/1/ Strathmann et al. Journal of Microbiological Methods **50**, 237–248 (2002)

EXAFS STRUCTURAL ANALYSIS OF THE LOCAL CHEMICAL ENVIRONMENT OF U(VI) IN PARTS OF PLANTS

A. Günther, A. Roßberg, G. Bernhard

We determined the EXAFS structural parameters of uranium(VI) complexes in the separated cell liquids and solid cell components of lupine and found that the uranium(VI)-coordination in the main species varied.

To determine the chemical speciation of uranium after the uptake into plants, we investigated several plant samples with TRLFS, EXAFS and REM /1/.The spectroscopic results showed that uranium(VI) is predominantly bound to inorganic and/or organic phosphorus groups inside the plants. Compared with the cell liquids, the solid cell components contain more uranium(VI). We conclude from this that uranium(VI) is mainly bound to the cell wall components and/or that it is precipitated as solid complex.

The goal of our study was to determine the structural parameters of the uranyl complex species in the liquids and solid components of the plant cells.

Lupines were grown in uncontaminated soil and then transferred into hydroponic solution. The uranium concentration in the hydroponic solution was $1 \cdot 10^{-2}$M at pH 3.5. After harvesting the plants were washed and separated into root, shoot and leaf. The cells of the section samples of the roots and shoots were destroyed in an oscillating mill while being cooled with liquid nitrogen. Then the green mass was centrifuged and the cell liquid separated from the solid cell components.

The EXAFS spectra of the cell liquids and solid cell components were recorded at the Rossendorf Beamline (ROBL) at ESRF in Grenoble. The U L_{III}-edge spectra were measured in fluorescence mode. The EXAFS spectra were analyzed using the EXAFSPAK program suite /2/. The theoretical scattering phases and amplitudes were calculated for m-autunite with the FEFF8 scattering code /3/.

Sample		Shell	N	R[Å]	$\sigma^2 \cdot 10^3$ [Å^2]
Cell liquid	r (A)	U-O$_{ax}$	2	1.77	0.9
		U-O$_{eq(1)}$	6.0	**2.41**	8.7
		U-O$_{eq(2)}$	-	-	-
		U-P	2.4	**3.60**	4
Solid cell components	r (B)	U-O$_{ax}$	2	1.78	1.5
		U-O$_{eq(1)}$	3	**2.31**	4
		U-O$_{eq(2)}$	2	2.50	10
		U-P	2	**3.61**	4
	sh (C)	U-O$_{ax}$	2	1.78	1.9
		U-O$_{eq(1)}$	5.4	**2.28**	5.7
		U-O$_{eq(2)}$	-	-	-
		U-P	4.6	**3.59**	4

The standard deviations are given in parenthesis. During the fitting procedure the coordination number of O_{ax} was held constant at N=2 (N-coordination number with an uncertainty of 25%, R-radial distance with an uncertainly of±0.02Å, σ^2- Debye-Waller factor, r-root, sh-shoot)

Tab. 1: EXAFS structural parameters of the uranyl complex species in several cell components of the lupine

The EXAFS spectra of the investigated plant samples vary (Fig. 1). The changes in the EXAFS spectra are attributed to structural changes in the equatorial plane of uranium(VI). For the cell liquid (A) we obtained similar structural parameters as for uranyl hydrate (Tab. 1), which is the main component in the hydroponic solution. Furthermore, the EXAFS spectrum of sample (A) shows a U–P interaction at 3.60 Å. For the solid cell components (C) we obtained a relatively short U-O$_{eq}$ bond with 2.28 Å. In the case of this sample the EXAFS structural parameters agree with those of m-autunite (inorganic uranyl phosphate). Sample (B) shows two structurally different types of coordinated O$_{eq}$ atoms. The short U-O$_{eq(1)}$ bond distance of 2.31 Å and the U-P interaction at 3.60 indicate a monodentately bound phosphate group. If sample (B) consists of one complex with one type of interacting ligand, the O$_{eq(2)}$ atoms could arise from the organic rest on the phosphate group.

Fig. 1: Raw U L_{III}-edge k^3-weighted EXAFS spectra (left) and their corresponding Fourier transform (right) of investigated cell components.

Fig. 1 shows the raw U L_{III}-edge k^3-weighted EXAFS spectra and corresponding Fourier transforms (FT) of several uranium containing cell components of the plant. The structure parameters are summarized in Table 1.

References

/1/ Günther, A., Bernhard, G., Geipel, G., Reich, T., Roßberg, A., Nitsche, H. Radiochim. Acta **91**, 319-328 (2003)

/2/ George, G.N., Pickering, I.J.: EXAFSPAK A Suite of Computer Programs for Analysis of X-Ray Absorption Spectra. Stanford Synchrotron Radiation Laboratory, Stanford, CA. USA. (1995)

/3/ Ankudinov, A.L., Ravel, B., Rehr, J.J., Conradson, S.D., Phys.Rev. **B 58**, 7565-7576 (1998)

QUANTITATIVE ANTIMONY SPECIATION IN SHOOTING-RANGE SOILS BY EXAFS SPEC-TROSCOPY AND ITERATIVE TRANSFORMATION FACTOR ANALYSIS

A.C. Scheinost, A. Roßberg, Ch. Hennig, D. Vantelon[1], R. Kretzschmar[1], A. Johnson[2]

[1]Institute of Terrestrial Ecology, ETH Zurich; [2]Swiss Federal Institute of Environmental Science and Technology (EAWAG), Switzerland

In 6 shooting range soils with a wide variety of pH, mineral and organic matter composition, vegetation and climate, we found only two predominant species: Pentavalent Sb sorbed onto Fe or Mn oxide as polynuclear inner-sphere complex and a trivalent Sb hydroxide mineral.

Worldwide about 100,000 tons Sb are mined annually for use in alloys, as fining agent in glass and plastics, and as flame retardant in polymers, textiles and brake pads. In spite of its industrial importance, little is known on the environmental fate of Sb. The objective of our study was to investigate the predominant Sb species in shooting range soils by in-situ EXAFS spectroscopy.

We collected 9 topsoil samples in the target area of 6 shooting ranges in central, eastern and southern Switzerland, with Sb concentrations from 1300 to 17500 mg/kg, and pH from 3.1 to 7.5. Sb K-edge (30491 eV) EXAFS spectra were collected at the Rossendorf beamline (ESRF) in fluorescence mode using a 4-element Ge detector.

Due to the use of a cryostat for sample cooling to 20 K, high quality EXAFS spectra to ≥ 15 Å^{-1} could be collected (Fig. 1). The spectra were treated with iterative transformation factor analysis /2/. All spectra could be reconstructed with 2 factors, i.e. Sb speciation is dominated by 2 species (Fig.1). Their spectral components are represented in almost pure form by samples "Zuchwil Ah" (#1), collected near a corroding bullet in a circumneutral, sandy topsoil, and "Losone N4" (#2), collected from a very acidic, organic matter-rich topsoil (Fig. 2, Table 1). Their short range structure was determined by multi-shell fitting using paths calculated by FEFF7. In species #1, Sb is octahedrally coordinated to O, indicating pentavalent oxidation state. The small number of Fe and Sb neighbors and their distances suggest that Sb(V) is bound to the surface of Fe (or Mn) oxides as polynuclear inner-sphere surface complex (Table 1).
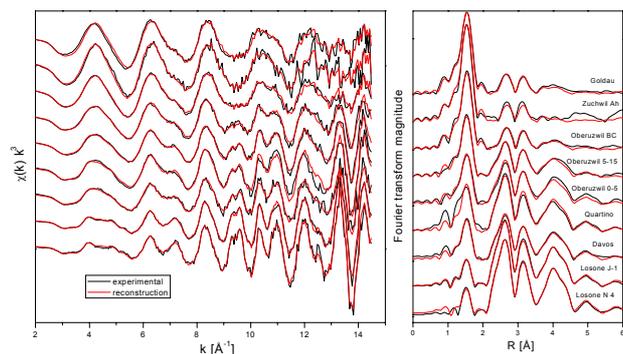
Fig. 1: Sb K-edge EXAFS spectra of soil samples from 6 different shooting ranges, and their reconstruction with 2 principal components.

In species #2, Sb is coordinated to 1.2 O atoms. Since Sb is coordinated to 2 or 3 O atoms in Sb(III) minerals, the low CN suggests an trivalent oxidation state for species #2. Seven Sb neighbors out to 6.73 Å could be fitted, suggesting that species #2 is a Sb(III) mineral. From the aqueous, low-temperature environment and from the low solubility of Sb(III) hydrox-ides, one can deduce that species 2 is in fact a Sb(III) hydroxide.

Tab. 1: Short-range structure of Sb species

Species 1			Species 2		
CN	R / Å	σ^2	CN	R / Å	σ^2
5.9 O	1.97	0.0030	1.2 O	1.98	0.0019
1.2 Fe	3.09	0.0024	2.1 Sb	2.91	0.0016
1.8 Sb	3.33	0.0056	2.7 Sb	3.35	0.0037
			7.5 Sb	4.30	0.0063
			4.2 Sb	4.52	0.0024
			3.5 Sb	5.45	0.0039
			5.8 Sb	6.33	0.0039
			5.1 Sb	6.73	0.0039

Samples from the vicinity of corroding bullets (Zuchwil Ah, Oberuzwil BC), where Fe corrosion products were visibly enriched, are dominated by the pentavalent sorption complex, in line with an accelerated Sb oxidation at the surface of Fe,Mn-oxides (Fig. 2). The very acidic Losone soil, where the absence of bullets suggests a very high corrosion rate, is dominated by Sb(III) hydroxide. The relatively low Sb concentration in this soil (1300-4000 mg/kg) confirms their low solubility. The other samples, which contain variable amounts of both species, are from calcareous soils.
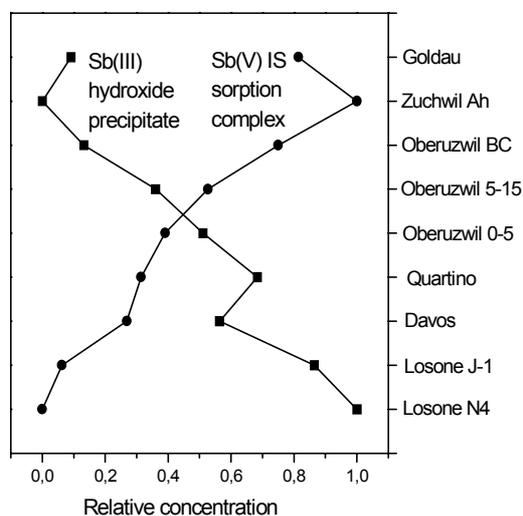
Fig. 2: Quantitative species distribution determined by iterative target test.

To the best of our knowledge, this is the first time that Sb species have been determined in situ in environmental samples. Since Sb(III) is mutagenic and more toxic than Sb(V), its immobilization in a relatively insoluble hydroxide mineral is of high environmental relevance.

References

/1/ Knechtenhofer, L.A. et al., J. Plant Nutr. Soil Sci. **166**, 84 (2003)

/2/ Roßberg, A., et al., Analytical and Bioanalytical Chemistry **376**, 631 (2003)

QUANTITATIVE ZINC SPECIATION IN SOIL BY SELECTIVE SEQUENTIAL EXTRACTIONS, EXAFS (MICRO-)SPECTROSCOPY AND ITERATIVE TRANSFORMATION FACTOR ANALYSIS

A.C. Scheinost, A. Roßberg, M. Marcus[1], S. Pfister[2], R. Kretzschmar[2]

[1]Advanced Light Source, Berkeley Lab, U.S.A.; [2]Institute of Terrestrial Ecology, ETH Zurich, Switzerland

Iterative transformation factor analysis (ITFA) was applied for the first time to a series of EXAFS spectra from soil samples to identify and quantify zinc species. In contrast to conventional statistical EXAFS analysis, the new method is less dependent on a complete set of reference spectra, and enabled us to identify a previously undetected Zn spinel mineral.

In our previous work /1/, we have investigated the Zn speciation in a soil profile contaminated by a nearby Zn smelter (Palmerton, PA, USA). EXAFS spectra have been collected after each step of a series of sequential chemical extractions, which removed increasingly recalcitrant zinc species. The set of EXAFS species was then evaluated by principal component analysis (PCA), which revealed three species in the topsoil. These three species were identified by target test and quantified by linear combination fit, using a spectral library of 30 zinc species.

An intrinsic property of this method is that it works only, if all species of the investigated sample are contained in the spectral library. While we achieved a satisfactory fit with 10 % Zn^{2+} aqua-ion, 30 % sphalerite and 60 % franklinite as Zn species, synchrotron μ-XRF elemental mapping and μ-XANES did not indicate such a high amount of sphalerite /2/. Therefore, we tested a new approach, iterative transform factor analysis (ITFA) /3/, to re-investigate the data published in /1/.

Experimental

PCA was used to derive Eigenvectors and number of species from k^3-weighted EXAFS spectra. With VARIMAX rotation, the qualitative species concentrations were determined. Finally, iterative target test was applied to derive spectral components and their fractional contribution /3/.

Results

When applied to the 7 spectra of the topsoil sample (untreated and after each of 6 sequential extraction steps), PCA revealed three components, equivalent to Zn^{2+}, sphalerite and franklinite reference phases.
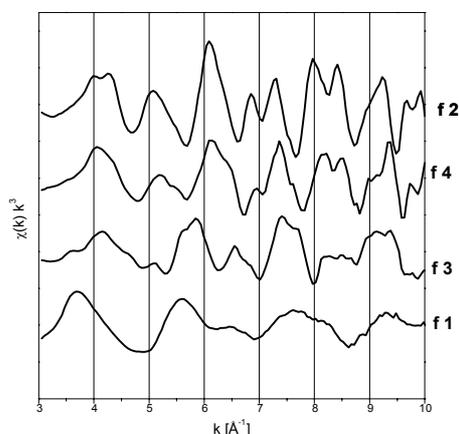
Fig. 1: Real spectral factors derived by ITFA, corresponding to the experimental XAFS spectra of franklinite (f 2), sphalerite (f 3) and Zn oxalate (f 1). Factor 4 corresponds to the XAFS spectrum of the previously undetected species, a Zn-Fe spinel (franklinite 2).

However, when these three references were included in PCA, a fourth component became statistically meaningful. Using iterative target test, the spectrum of this fourth component could be extracted (f 4, Fig. 1).The spectrum is similar to that of franklinite. A multishell fit based on FEFF7 gave the following short-range order: in component 4, Zn is octahedrally coordinated to O (5.4 O @ 1.99 Å) and surrounded by 12 Fe atoms at 3.48 Å. In component 2, Zn is tetrahedrally coordinated (3.5 O @ 1.96 Å) and surrounded by 13 Fe @ 3.53 Å. Both structures are consistent with an Fe-rich franklinite-like spinel phase, where Zn is hosted in both tetrahedral and octahedral sites.

The quantitative species distribution (Fig. 2) shows that 80 % of Zn occurs in these spinel phases, and only 10 % each as Zn^{2+} and in sphalerite, which is in good agreement with results from cation exchange and μ-XANES. Both spinel phases dissolve only partly during the acid-oxalate and ascorbic-acid dissolution steps (steps 4 and 5).
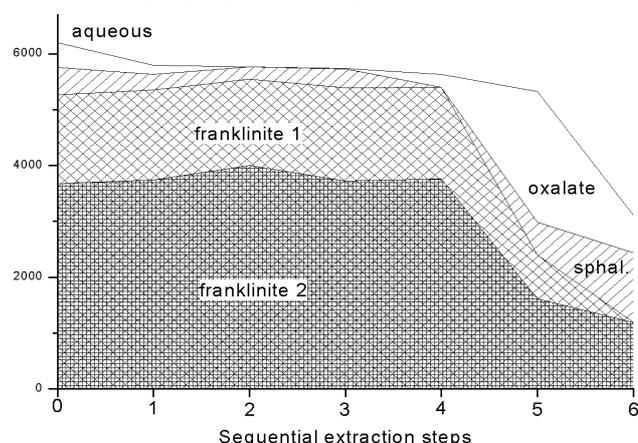
Fig. 2: Absolute species distribution (Zn in mg/kg, cumulative) of the untreated soil sample (step 0) and after each of the selective sequential extraction steps (1 to 6).

The results show that ITFA is able to derive meaningful spectral components of species not contained in reference data bases. Consequently, it also improves the quantitative speciation. ITFA is hence a valuable tool for speciation in complex systems like soils and sediments /4/.

References

/1/ Scheinost, A.C. et al., Environ. Sci. Technol. **36**, 5021 (2002)

/2/ Roberts, D.R. et al., Environ. Sci. Technol. **36**, 1742 (2002)

/3/ Roßberg, A. et al., Analytical and Bioanalytical Chemistry **376**, 631 (2003)

/4/ Scheinost, A.C. et al., Physica Acta, accepted

Interaction of Actinides / Radionuclides
with Solid Phases

SORPTION OF URANIUM(VI) ON PYROPHYLLITE – A COMBINED TRLFS AND EXAFS STUDY

M. Walter, T. Arnold, G. Geipel, G. Bernhard

The sorption of U(VI) on pyrophyllite was invesitgated by TRLFS and EXAFS spectroscopy. Three surface species were detected using TRLFS. The EXAFS spectrum represents the average of these species, which limits the infomation concerning the detailed surface complex structure.

Pyrophyllite, $Al_2[(OH)_2/Si_4O_{10}]$, is a 2:1 sheet silicate mineral, in which two sheets of silicate tetrahedra are linked by a gibbsite–like layer of aluminium octahedra. There is only a minimal substitution of both cationic positions. Consequently, pyrophyllite shows no permanent structural charge and and can be used as a reference compound for other sheet silicates.

Experimental

The sorption of uranium(VI) on pyrophyllite (grain size <2 μm, specific surface area BET: 15.7 m^2/g) was performed under ambient conditions. A suspension of 200 mg pyrophyllite, dispersed in 500 ml of 0.01 M $NaClO_4$ solution, was equalibrated for four weeks and the pH value was adjusted to 5.8. The initial U(VI) concentration was set to 2×10^{-6} M. For further experimental details see reference /1/.

Results

Approximately 20 % of the initial U(VI) in solution was sorbed onto pyrophyllite. This results in a surface loading of 469 mg/kg or 0.08 U–Atoms/nm^2.
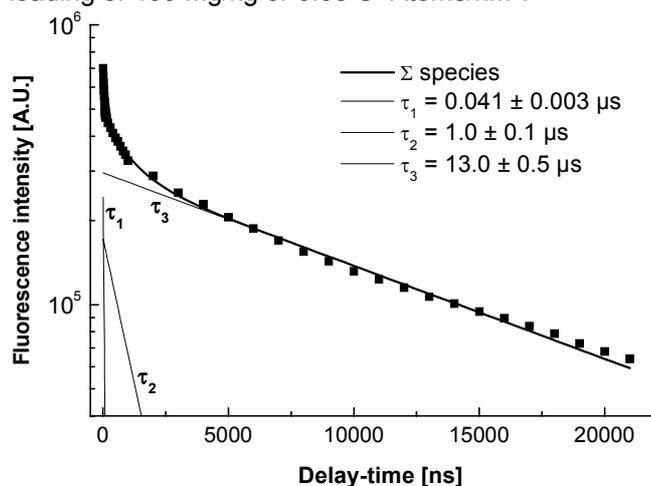
Fig. 1: Fluorescence decay of uranium(VI) sorbed on pyrophyllite at pH 5.8

Tab. 1: Fluorescence parameters of uranium(VI) sorbed on pyrophyllite at pH 5.8

	Lifetime [μs]	Peak maxima [nm]			
τ_1	0.041 (3)	499	521	544	570
τ_2	1.0 (1)	498	520	543	568
τ_3	13.1 (5)	498	520	543	569

standard deviations are given in parenthesis

The time-resolved fluorescence spectroscopy *TRLFS* indicates the presence of three different U(VI) surface species. Based on their lifetimes, the spectra of each species can be deconvoluted from the measured time-resolved fluorescence spectra /2/. As can be seen from Fig. 2, the spectra and the corresponding peak maxima (Tab. 1) of the three surface species are nearly identical.
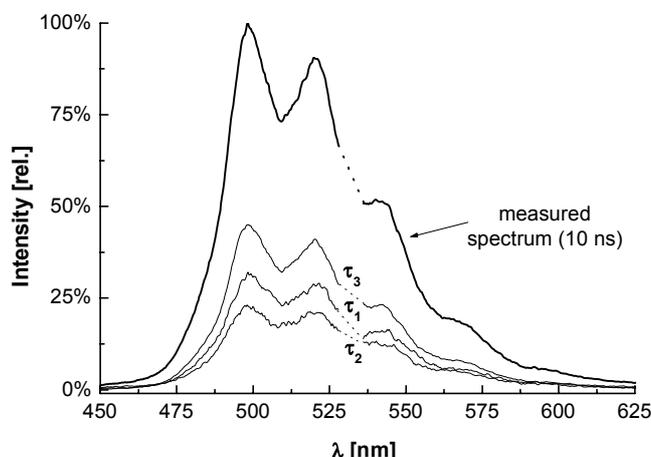
Fig. 2: Measured and deconvoluted fluorescence spectra of U(VI) sorbed on pyrophyllite

Figure 3 shows the k^3–weighted EXAFS spectrum and Fourier transform of U(VI) sorbed on pyrophyllite. The EXAFS spectrum was fitted with two axial oxygens at a distance of 1.77 Å and 4–5 equatorial oxygens (O_{eq}) at 2.36(2) Å. The Debye-Waller factor of the equatorial oxgyen shell was 0.015(4) $Å^2$. In combination with high disorder of the O_{eq} shell such short U–O_{eq} distances are typical for an inner sphere uranium(VI) surface complexation. However, it should be noted that these structural parameters represents the average of three uranium(VI) surface species.
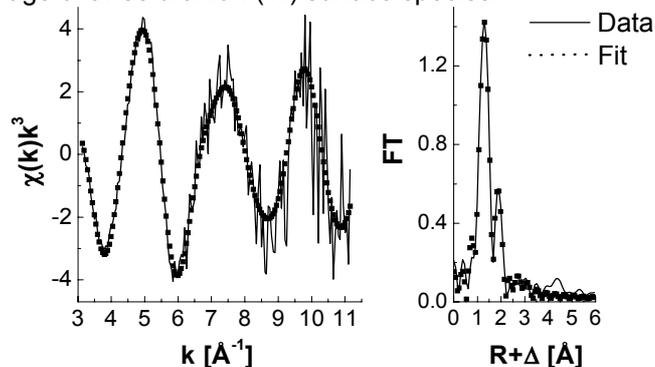
Fig. 3: U–L_{III} edge EXAFS spectrum and Fourier transform of the uranium(VI) sorption sample

Conclusion

The U(VI) sorption on the sheet silicate pyrophyllite occurs – even at low surface concentration – by the formation of three dominating surface complexes. Consequently, the EXAFS spectrum contains the average of the structural information. This may preclude the identification of the detailed surface complex structure by the EXAFS spectroscopy.

References

/1/ Walter, M., Dissertation, TU Dresden (submitted, 2003)
/2/ Moll, H., et al., J. Alloys Compound **271-273,** 765-768 (1998)

TRLFS SPECTRA OF URANYL SPECIES SORBED ON GIBBSITE AT VARIOUS PH VALUES

N. Baumann, V. Brendler, T. Arnold, G. Geipel

Based on fluorescence lifetime analysis, two uranyl surface species on gibbsite are postulated. Their emission bands do not differ significantly over the investigated pH range from 3.5 to 9.5 in steps of 0.5. We therefore assume, that these two surface species only differ in numbers of H_2O groups, but not in numbers of OH^- groups.

Batch experiments concerning the sorption behavior of uranyl on gibbsite as a powder of grain size < 45 μm were carried out at an ionic strength of 0.1 M (adjusted with $NaClO_4$) and in the pH range from 3.5 to 9.5. The gibbsite was separated by centrifugation after a contact time of 2 days in an overhead shaker. The concentration of adsorbed uranium on gibbsite was calculated by the following equation: $U_{ads} = U_{total} - U_{solution} - U_{wall}$.
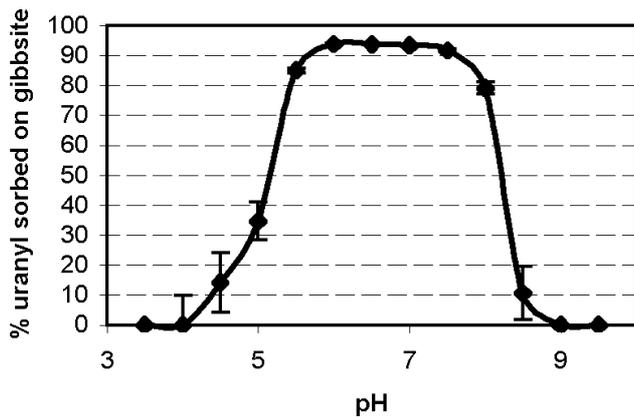
Fig. 1: Uranium sorbed on gibbsite in dependence on pH-value (Batch Experiments)

The gibbsite residue was suspended in a solution of the same pH and ionic strength. TRLFS spectra were recorded of these gibbsite suspensions. It was thus assured that the fluorescence signals were caused exclusively by adsorbed uranium(VI).

Based on the TRLFS spectra between 407 and 635 nm, the fluorescence decay function was determined. The wavelength range between 525 and 540 nm, which is dominated by the laser dispersion peak, was eliminated. The best approximation was a biexponential decay function

$$y = y_0 + A_1 e^{-(x-x_0)/t_1} + A_2 e^{-(x-x_0)/t_2}$$

yielding two decay lifetimes.

Tab. 1: Lifetimes from the fluorescence signals of the uranyl surface species on gibbsite

pH-value	t_1	t_2	r^2
5	210 ± 7	5200 ± 330	0.998
5.5	150 ± 6	3600 ± 400	0.995
6	370 ± 2	5700 ± 40	0.998
6.5	320 ± 12	5200 ± 220	0.998
7	300 ± 11	4600 ± 250	0.998
7.5	420 ± 15	5900 ± 280	0.999
8	380 ± 4	6500 ± 50	0.999
8.5	440 ± 7	7800 ± 100	0.998

Data processing was by the software Origin 6.01 (Origin Lab. Inc.).

The results are summarized in Tab. 1. t_1 and t_2 are the calculated lifetimes of the short-lived and long-lived adsorbed surface species with errors. r^2 is the correlation coefficient of the fluorescence lifetime fit. The intensities of the spectra are similar to the sorption curve: high intensities in the neutral range, lower intensities in more acid or base regions. But it is also obvious that there is no shift of the peak maxima at various pH values (Fig. 2).
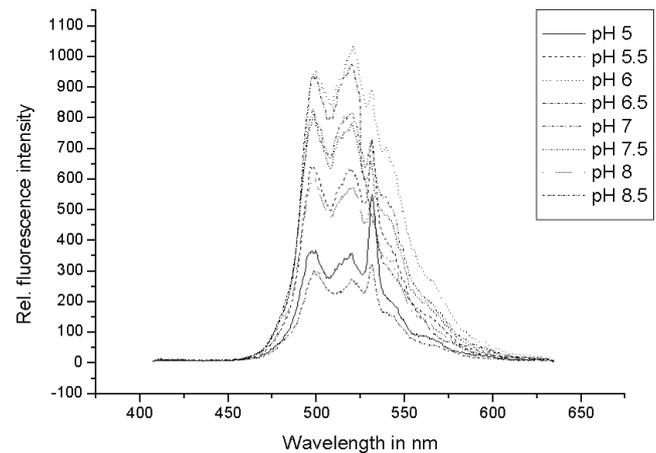
Fig. 2: Fluorescence spectra at shortest delay times

The uranium surface species are therefore assumed to be the same throughout the pH range studied.
This applies to both the short-lived and long-lived species, as indicated by a comparison of spectra at a delay time of 3,000 ns, at which the fluorescence of the short-lived species has disappeared (Fig. 3).
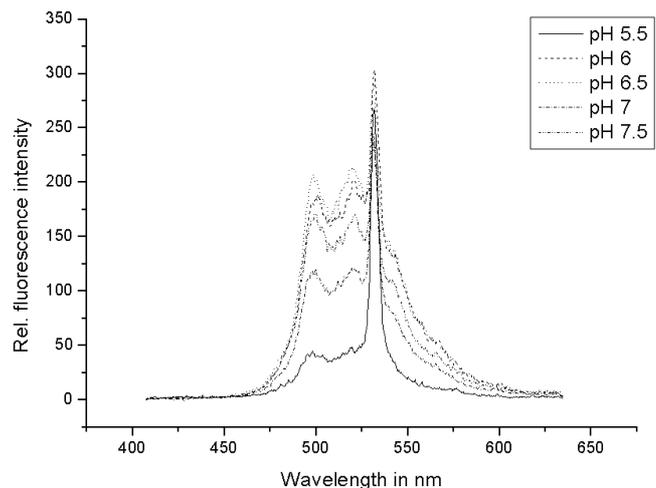
Fig. 3: Spectra recorded 3000 ns after excitation

At changed delay times the spectra do not differ in the position of their emission bands. In the batch sorption experiments two absorbed U(VI) species on gibbsite have to be formed and identified by two fluorescence lifetimes. Hence these species must have different numbers of H_2O molecules but equal numbers of OH^- groups in their coordination environment.

SPECTROSCOPIC CHARACTERIZATION OF SYNTHETIC SWARTZITE BY TRLFS

T. Arnold, S. Amayri[1], G. Geipel
[1]Institut für Kernchemie, Universität Mainz

Time Resolved Laser-induced Fluorescence Spectroscopy (TRLFS) was applied to obtain the characteristic positions of the fluorescence emission bands at 472.3, 488.9, 509.0, 531.1, 554.7, and 578.9 nm and the characteristic fluorescence lifetime of 178 ± 2 µs.

Introduction

Since natural uranium(VI) samples often exist as thin coatings on rock or mineral surfaces or as mixed component with other solids it is often difficult to identify small quantities of these secondary uranium(VI) phases with classical methods only. Spectroscopic methods like Time Resolved Laser-induced Fluorescence Spectroscopy (TRLFS) and Fourier-Transform Infrared Spectroscopy (FT-IR) however may provide an alternative in identifying such secondary U(VI) phases.

Experimental

The laser pulses from a Nd-YAG laser (SL 401-20, Spectron Laser Systems) were applied to the dry solid swartzite powder, which was synthesized following a procedure described in /1/. A SEM micrograph of the synthetic swartzite powder is shown in Fig. 1.
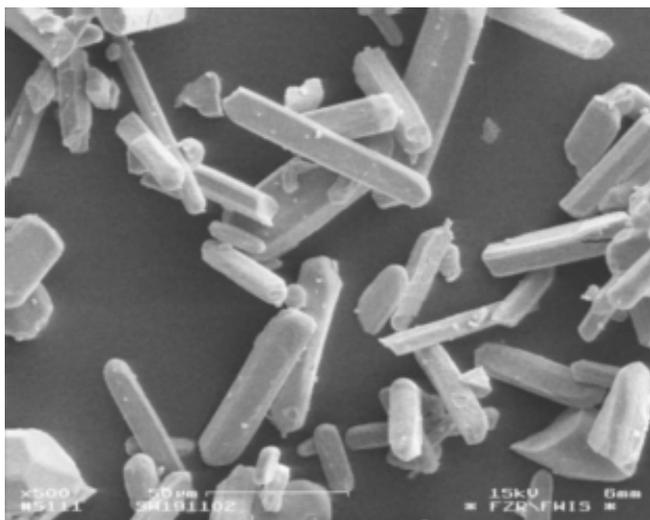
Fig. 1: SEM picture of a sample of synthetic swartzite

The fluorescence spectra are measured by a gate diode array (M 1475, EG&G). The spectra were collected with a controller (M 1471A, EG&G). A more detailed description of the experimental setup can be found in /2/]. In our study an excitation wavelength of 266 nm was used. The spectra were recorded in the range from 450 nm to 600 nm with delay times ranging from 0.1 ms to 100 ms after the application of the laser pulse. The gate time was 1 µs. The actual laser energy was 400 µJ.

Results

TRLFS was used to characterize the synthesized magnesium calcium uranyl carbonate swartzite (MgCa[$UO_2(CO_3)_3$]×12H_2O). TRLFS is a non-invasive method, i.e. no sample material is destroyed or consumed during the measurement.

Swartzite reveals six characteristic fluorescence emission bands at 472.3, 488.9, 509.0, 531.1, 554.7, and 578.9 nm and showed a fluorescence lifetime of 178 ± 2 µs. The positions of the emission peaks is similar to ones found in the free uranyl(VI) system. However, the fluorescence lifetime obtained for the swartzite system is significantly longer than the one obtained in the free uranyl(VI) system.
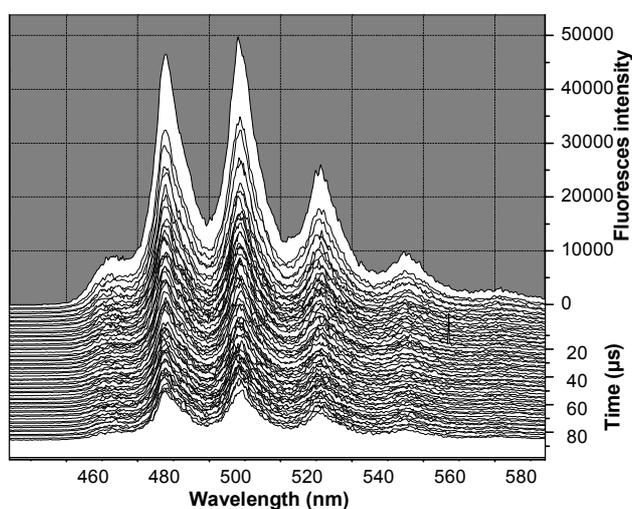
Fig. 2: Fluorescence spectra of synthetic swartzite as a function of delay time

Conclusions

The presented TRLFS method is a suitable method to identify in a fingerprinting procedure secondary U(VI) phases in mixtures with other phases or as thin coatings on mineral and rock surfaces.

The gained results are also of fundamental significance for uranyl(VI) adsorption studies. Since spectroscopic information obtained for well characterized uranium minerals by TRLFS are useful to identify the coordination environment and structure of unknown adsorbed uranium(VI) surface species on minerals surfaces.

Acknowledgments

References

/1/ Amayri, S. et al., submitted to Canadian Mineralogist.
/2/ Geipel, G. et al., Radiochimica Acta **75**, 199-204 (1996)

QUANTIFICATION OF FERRIHYDRITE IN WEATHERED CHLORITE BY MÖSSBAUER SPECTROSCOPY

T. Arnold, H. Reuther[1], E. Krawczyk-Bärsch
[1]Institute of Ion-beam Physics and Materials Research

By using moessbauer specroscopy we were able to identify and quantify a fraction of ferrihydrite of 5.0 ± 0.9 % which has formed during a mixed-flow reactor experiment with chlorite.

Introduction

During batch sorption experiments of heavy metals on chlorite not only sorption reactions take place, but also reactions of chemical weathering leading to mineral dissolution and the formation of secondary phases, in particular the Fe-oxy-hydroxide ferrihydrite. Despite of its minor mass, ferrihydrite plays a major role in removing aqueous uranium(VI) from solution. To accurately model the sorption and transport on or through geological materials it is necessary to precisely determine the mass of the newly-formed Fe-phase.

Approach

Spectra of pure chlorite and pure ferrihydrite, shown in Fig. 1, were recorded and used to simulate Mössbauer spectra of defined chlorite and ferrihydrite ratios. The simulated spectra were then used as calibration standards for chlorite samples, obtained from mixed-flow reactor experiments, to identify and to quantify minor amounts of newly-formed ferrihydrite within narrow analytical errors. According to /1-3/ the spectra were decomposed by several doublets The hyperfine parameters are given in the Table 1. The Mössbauer spectra of the mixed powders were fit with the above given hyperfine parameters by varying only the fractions of the two compounds and keeping fix all other parameters. For the mixture with a small amount of ferrihydrite it made sense to combine its three doublets to one with δ = 0.237 mm/s and Δ = 0.700 mm/s. The agreement between the origin fractions and those obtained by the fit was good.

For standard deviation ranges from 3 % for the high to 10 % for the low ferrihydrite content. Because of this good agreement the method was applied to a "real" sample. For this purpose a mixed-flow reactor experiment with 500 mg of chlorite was conducted through which for three weeks a 0.1 N NaClO4 solution at a flow rate of 19 mL/h was pumped. The pH value of the solution was monitored and pH values of around 7 were recorded.

Tab. 1: Hyperfine parameters and spectrum areas of ferrihydrite and chlorite.

	Doublet	Isomer shift δ in ref. to α-Fe (mm/s)	Quadrupole splitting Δ (mm/s)	Relative spectrum area (%)
Ferrihydrite	1 (Fe^{3+})	0.346	1.101	21.5
	2 (Fe^{3+})	0.350	0.744	41.7
	3 (Fe^{3+})	0.346	0.456	36.8
Chlorite	1 (Fe^{2+})	1.133	2.600	86.8
	2 (Fe^{3+})	0.425	0.603	10.1
	3 (Fe^{2+})	0.819	1.398	3.1

Results

In comparison to the spectrum of the untreated chlorite the formation of the secondary phase is obvious due to the pronounced grow of the shoulder at about 1.0 mm/s (Fig. 2). Applying the above described algorithm we obtain a fraction of ferrihydrite of 5.0 ± 0.9 %.
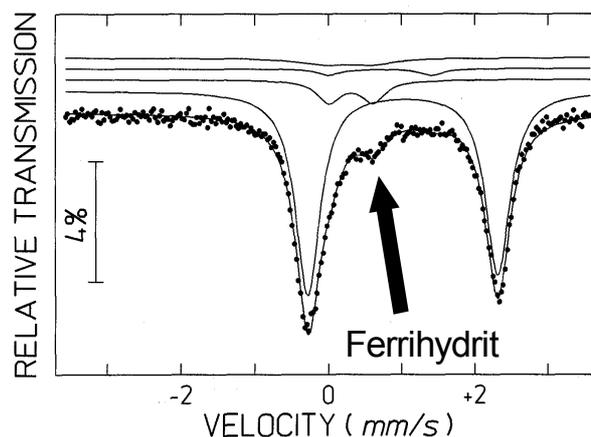
Fig. 2: Moessbauer spectrum of a chlrite sample obtained from a mixed-flow reactor experiment.

References

/1/ Murad, E., Schwertmann, U. Am. Mineral. **65**, 1044 (1980)

/2/ Arshed, M. et al., Phys. stat. sol. (a) 137 (1993) K33

/3/ Kodama, H. et al., Can. Mineral. **20**, 585 (1982)

Fig. 1: Moessbauer spectra of pure chlorite and pure ferrihydrite.

URANIUM SORPTION ONTO MUSCOVITE

V. Brendler, M. Swantusch[1]

[1] Hochschule für Wirtschaft und Technik, Dresden

Uranium sorption onto muscovite helped to improve the sorption database for clay compounds and to further gain insight into sorption processes on model substances for clays. The protolysis constants pK1 and pK2 were determined at 4.43 and 8.82, respectively. Log K for the formation of =XO-UO$_2$OH (proven by TRLFS) was determined at -5.56.

Several aluminum (hydr)oxides and mica have been investigated with regard to their sorption properties to obtain general conclusions of the influence of aluminol surface sites in clay minerals compared to silanol groups. Here, the work concerning uranium(VI) sorption onto muscovite ($KAl_3Si_3O_{10}(OH)_2$) is presented. The mineral sample was obtained from F.Krantz Rheinisches Mineralien-Kontor and originated from Iveland / Norway. Purity was checked through X-ray diffraction and X-ray fluorescence analysis. N_2-BET measurements gave a specific surface area of 4.61 m^2/g for the grain size fraction of 63 - 200 μm. Acid-base surface titrations (from pH 3.5 to 9.5 at ionic strengths of 0.1 / 0.05 / 0.01 M NaClO$_4$) and batch experiments (sorption edges, see Fig. 1, and sorption isotherms, all at 1 g solid per 20 mL solution) enabled the derivation of parameters for Surface Complexation Models (SCM), namely the Diffuse Double Layer Model (DDLM). The data processing was done by the FITEQL 3.2 software /1/. The protolysis constants pK$_1$ and pK$_2$ were determined at 4.43 and 8.82, respectively, at a surface site density (SSD) of 4.4 nm^{-2}. The surface site type is a generic one because the data did not allow distinguishing between silanol and aluminol groups.
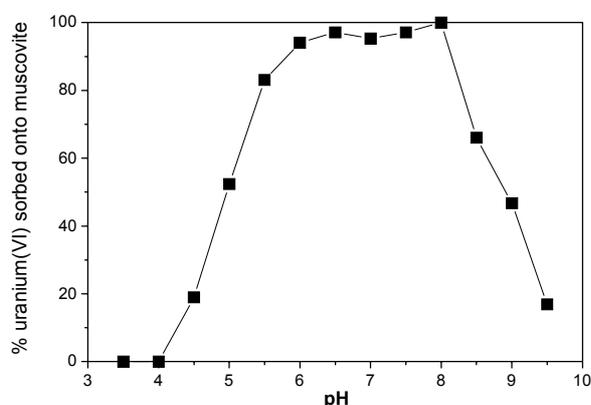
Fig.1: Sorption edge of uranium(VI) sorption onto muscovite at 10^{-7} M UO$_2^{2+}$ and I = 0.1 M NaClO$_4$

Assuming a surface complex formation according to:

$$=XOH + UO_2^{2+} + H_2O <=> =XO\text{-}UO_2OH + 2\,H^+,$$
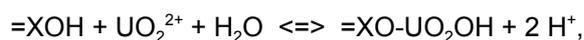
a log K = -5,56 was derived. Adding the reaction

$$=XOH + UO_2^{2+} <=> =XO\text{-}UO_2^+ + H^+$$
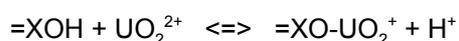
did not improve the fit of the sorption data. The surface species =XO-(UO$_2$)$_3$(OH)$_5$ reported by some authors can be excluded due to the low overall uranium concentration. The surface species =XO-UO$_2$OH was confirmed by independent time-resolved laser-induced fluorescence spectroscopy (TRLFS, Fig. 2) after comparison with literature values summarized in Tab. 1.
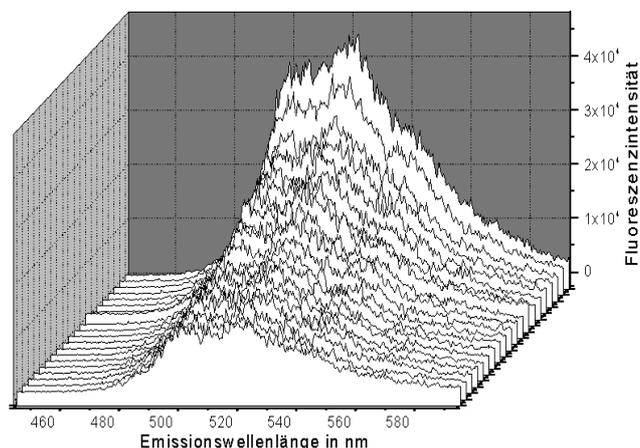
Fig. 2: TRLFS measurements of uranium(VI) sorbed onto muscovite crystals

Tab. 1: Comparison of fluorescence properties of uranium(VI) surface species

Species	Fluorescence Decay / ns	Main Peaks / nm
=XO-UO$_2$OH	3200±200	497.3; 518.4; 541.3
=XO-UO$_2^+$	1800±200	488.9; 519.5; 533.9; 559.4
this work	3560±435	499; 517; 543

The obtained SCM parameters fit well into the range of parameters obtained so far for other mica /2/ as can be seen from Tab. 2.

Tab. 2: Surface properties of mica

Mineral	SSD / nm^{-2}	pK$_1$	pK$_2$
Biotite	50	-	-
Muscovite	261	540	847
Glauconite	10	364	880
Phlogopite	100	522	978

References

/1/ Herbelin, A.L., Westall, J.C. (1996). *FITEQL -Version 3.2.* Report 96-01, Department of Chemistry, Oregon State University, Corvallis

/2/ Brendler, V. et al., J. Contam. Hydrol. **61**, 281 (2002)

THORIUM(IV) SORPTION ONTO QUARTZ SAND IN THE ABSENCE AND PRESENCE OF HA

A. Křepelová, S. Sachs, K.H. Heise, G. Bernhard

Recently, we have determined the influence of humic acid (HA) on Th(IV) sorption onto commercial quartz from Merck. In this work we investigated the Th(IV) sorption onto natural quartz sand in the absence and presence of HA as a function of the pH value. The results have been compared with those obtained in sorption experiments with Merck-quartz.

Introduction

Understanding the sorption behavior of tetravalent actinides on geological materials is essential for a reliable safety assessment of nuclear waste disposal sites. The sorption behavior of actinides may be strongly influenced by HA. We investigated the influence of HA on Th sorption onto quartz sand as a function of the pH.

Experimental

The sorption experiments were performed under conditions described in /1/. The final concentrations of Th and HA (^{14}C-M42) were 1.2×10^{-8}M and 20 mg/L, respectively. The solid solution ratio was 5 mg/L, ionic strength was 0.1M NaClO$_4$. The quartz sand (100–300 μm) was of marine origin (Netherlands). Prior to its use the sand was pre-treated with Milli-Q-water and it was annealed by 700°C for 4 hours. After purification, the chemical composition of the sand was 0.3 % of Al, 0.02 % Ti, 0.02 % Fe, and 99.66 % SiO$_2$.

Sorption of Th onto the vial walls and filters:
As in /1/ significant Th(IV) sorption onto vial walls was observed in the absence of HA. The sorption onto vial walls was suppressed in the presence of HA. In order to estimate the degree of Th(IV) sorption on filter materials, one series of direct measurements of Th(IV) in non-filtered supernatants was performed. The results were compared with those from experiments with filtration. It could be shown that there was no significant difference between the concentration determined from the supernatant and the 450 nm filtrate in the pH range between pH 4 and 7.5.

Results and discussion

Sorption of HA onto quartz sand:
The sorption of HA on quartz sand depends on pH. The HA sorption decreases with increasing pH value. The results show that about 70 % of HA are sorbed onto quartz sand at pH 3. However, there is a possibility that a part of HA is precipitated on the surface at pH 3. There could be an overlapping of both processes, HA sorption and precipitation. At pH values ≥ 7 no HA adsorption was detected. These results correspond to the properties of quartz sand and HA in solution. Quartz has a low point of zero charge (PEC: 2.0 /2/), which results in predominantly negatively charged surface species (> SiO$^-$) in the pH range studied. At pH values > pH 7 carboxyl groups of HA are deprotonated, resulting in a negative charge of the HA. Due to electrostatic repulsion no HA is sorbed onto the negatively charged surface of quartz sand, which explains the observed sorption behavior.

Sorption of Th onto quartz sand:
In the pH range > pH 5.5, the sorption of Th(IV) in the absence of HA is weak due to the high wall adsorption of Th(IV). Thus it is not comparable with the sorption in the presence of HA. In the pH range between pH 3
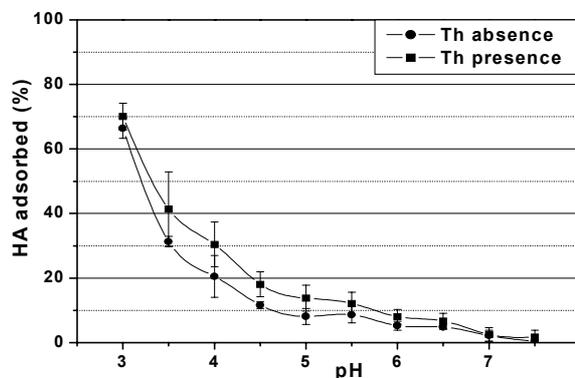
Fig.1: HA uptake by quartz sand

and pH 4, the sorption of Th(IV) on quartz sand in the presence of HA seems to be slightly higher compared to the HA free system. A possible reason for that are the additional binding sites from HA. From pH 4 to pH 5.5 dissolved HA leads to a decrease of Th(IV) uptake compared to the system free of HA due to formation of dissolved Th(IV)-humate complexes. Compared to the Th(IV) sorption onto Merck-quartz in the same pH range /1/, the sorption curve of Th(IV) in the absence of HA for the quartz sand is significantly different. There is only one difference between these two investigated solids. Both differ in trace amounts of Fe, Al, Ti in form of oxides. So it seems probable, that for quartz sand these minor components contribute to an enhancement of Th(IV) sorption by forming of additional binding sites in the absence of HA, whereas in its presence they show no influence.
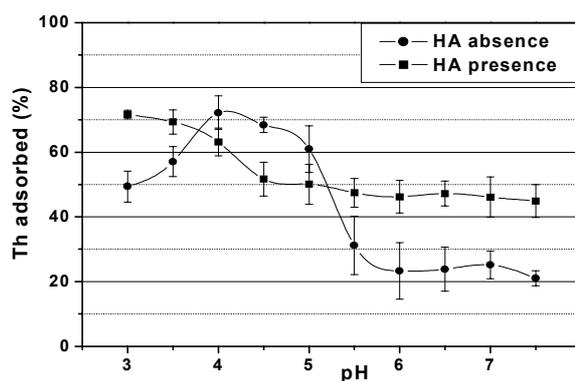
Fig.2: Th(IV) uptake by quartz sand

References

/1/ Křepelová, A. et al., Report FZR-373, p.19 (2003)
/2/ Schmeide, K. et al., Radiochim. Acta **88**, 273 (2000)

BLIND PREDICTIVE MODELING FOR SELENIUM SORPTION ONTO GOETHITE

V. Brendler

Making use of the RES³T mineral-specific sorption database, surface complexation parameter sets for the sorption of selenate and selenite onto goethite were derived. These sets allowed a blind predictive modeling for conditions taken from experimental work by Hayes. The prediction quality was in general satisfactory, with larger deviations for high pH ranges.

The paper presents an example illustrating the current blind predictive capabilities of surface complexation models (SCM) and respective databases.

Goethite as a well defined mineral often used as model substrate has been thoroughly characterized in previous studies. To keep the number of parameters at a minimum, the Diffuse Double Layer model (DDLM) was selected to account for electrostatics. There were 13 independent surface protolysis data records based on this model available in the RES³T database /1/. From that pool averages for the first and second surface site hydrolysis step were derived after normalization of the original values to a reference site density of 12.05 nm^{-2}, yielding $pK_1^n = 6.59\pm0.60$ and $pK_2^n = 10.41\pm0.80$.

The selection of species started from a survey over all iron (hydr)oxides. For the sake of simplicity, bi-dentate surface complexes were not considered. This led to the species listed below (in parentheses: number of publications):

a) Selenate: $=Fe\text{-}SeO_4^-$ (1), $=FeOH\text{-}SeO_4^{2-}$ (1), $=FeOH_2\text{-}SeO_4^-$ (3), and $=FeOH_2\text{-}HSeO_4$ (1)

b) Selenite: $=Fe\text{-}SeO_3^-$ (3), $=Fe\text{-}HSeO_3$ (1), and $=FeOH\text{-}SeO_3^{2-}$ (1)

The first and third selenate species are indistinguishable for FITEQL for reasons explained above. Furthermore, DDLM parameters were only available from /2/, so the species and SCM parameters listed below are all from the same source, at least guaranteeing a high degree of consistency.

$=Fe\text{-}SeO_4^-$	$\log K^n = 7.00$
$=FeOH\text{-}SeO_4^{2-}$	$\log K^n = 0.07$
$=Fe\text{-}SeO_3^-$	$\log K^n = 11.96$
$=FeOH\text{-}SeO_3^{2-}$	$\log K^n = 4.44$

The aqueous speciation of selenate and selenite (basically the hydrolysis steps of H_2SeO_4 and H_2SeO_3), as well as the respective data for the carbonate system, were based on the NEA TDB.

FITEQL version 3.2 /3/ was used as modeling software. High-quality experimental sorption data sets as provided by Phase II of the NEA Sorption Project for its fitting assessment efforts were used. The experimental data stem from work by Hayes /4/. 70 data points for selenate sorption and 22 data points for selenite sorption were used for the prediction test. This system is especially challenging due to a very sparse parameter matrix and really high pH values for some data points. Further experimental data at an ionic strength of 1 molar were not used because FITEQL can not handle such solutions properly. Ionic strength, solid/liquid ratio and pH were varied. The experiments were carried out under air atmosphere. The only system-specific parameters directly going into the computations were the solid-liquid ratios and the specific surface area (52 m²/g).

The quality of the blind prediction is based on the difference between the logarithms of experimental and predicted K_d. Following the recommendations of the NEA sorption project, deviations smaller than one order of magnitude are considered satisfactory for performance assessment applications. The results for the Se(IV)/Se(VI) sorption onto goethite are illustrated by Fig. 1.
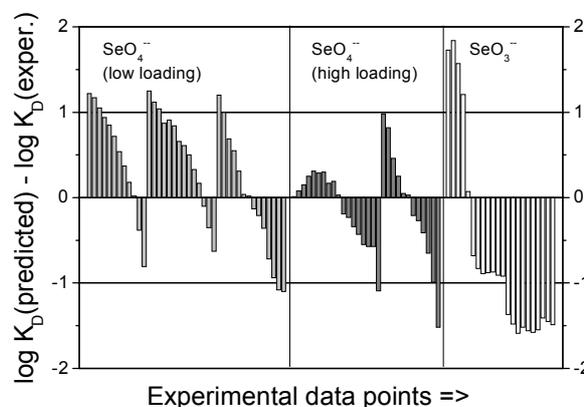
Fig. 1: Comparision of predicted and published experimental distribution coefficients for SeO_4^{2-} and SeO_3^{2-} with goethite

For the selenate sorption, there are larger differences in the acidic range at very high loadings. This is not really worrying because also the experimental error expressed in K_d is highest there, when more than 99% of the selenium is bound to the surface. More serious are the underestimations in the basic region beyond pH 9 (and thus above the PZC of goethite) indicating the possible existence of another surface species. There are general difficulties with the selenite sorption, the supporting reaction constants are based on too few experiments probably.

References
/1/ Brendler, V. et al., J. Contaminant Hydrology **61**, 281-291 (2002)
/2/ Dzombak D.A., Morel F.M.M. *Surface complexation modeling. Hydrous ferric oxide*, Wiley. New York (1990)
/3/ Herbelin, A.L., Westall, J.C.. *FITEQL -Version 3.2.* Report 96-01, Department of Chemistry, Oregon State University, Corvallis (1996)
/4/ Hayes, K.F. PhD Thesis. Stanford University. (1987)

BLIND PREDICTION OF COPPER(II) SORPTION ONTO GOETHITE

A. Richter, V. Brendler

A system for illustrating the current blind predictive capability of Surface Complexation Models using the RES³T database is the Cu^{2+} sorption onto goethite. The model prediction always represented the experimental values for the sorbed amount of Cu^{2+}, expressed as conventional distribution coefficients K_D inside one order of magnitude.

RES³T – the Rossendorf Expert System for Surface and Sorption Thermodynamics – is a digitized thermodynamic sorption database utilizing surface complexation models (SCM) /1/. The Cu^{2+} sorption onto goethite is an example for illustrating the current blind predictive capability of SCM using the RES³T database

The model independent surface species =FeO-Cu⁺ and =FeO-CuOH have been reported in RES³T. The SCM parameters from the literature survey in RES³T were the surface protolysis constants and the stability constants of the relevant surface complexes. No distinction between strong and weak surface sites was undertaken. The reported data are related to different surface site densities. So it was necessary to normalize the values to a reference state. Here the procedure according to Kulik /2/ was followed based on a reference state of 12.05 sites/nm² All reaction constants were converted to infinite dilution by determination of the activity coefficients with the Davies equation.

The selected species with their averaged surface reaction constants are given in table 1. The experimental data sets used for the quality assessment of the prediction comprised of 30 data points for the Cu(II) sorption under inert gas atmosphere /3/. The parameters derived from these data were excluded to assure a proper blind prediction.

Tab. 1: Selected surface reaction constants

Surface species	log K (I=0)
=FeOH₂⁺	6.49 +/- 0.59
=FeO⁻	-10.41 +/- 0.72
=FeO-Cu⁺	1.28 +/- 0.81
=FeO-CuOH	-7.22

To keep the number of parameters at a minimum, the Diffuse Double Layer model was selected. The calculation was performed with the FITEQL code, version 3.2 /4/.

The value for specific surface area strongly depends on the sample history and can not be generalized, so the respective experimentally determined value for goethite of 79.4 m²/g from Ali and Dzombak /3/ was used for computations.

In figure 1 the predicted trend of Cu(II) sorption onto goethite is compared with the experimental values for two total Cu concentrations. The trend line is outside of error margin, but inside the usual limit of such blind predictions.

Figure 2 shows the difference between predicted and experimental distribution coefficients K_D. This clearly illustrates the good prediction quality for the copper sorption onto goethite. The accordance for all data points is within one order of magnitude. This spread-

ing is considerd to be reasonable for performance assessment software.

It is obvious that the SCM concept with a suitable database can complement the classical K_D approach in reactive transport modelling.
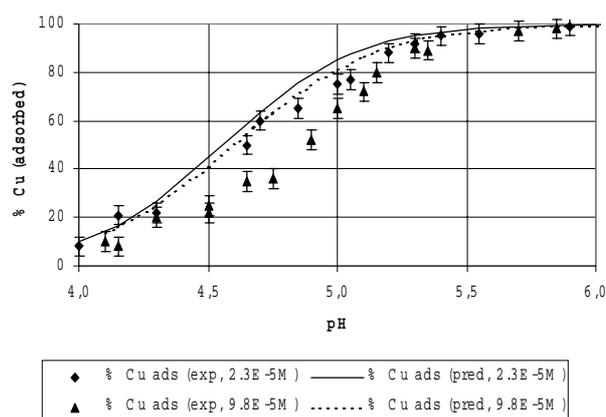
Fig. 1: Predicted percentages of Cu(II) sorbed onto goethite compared with experimental values from /3/
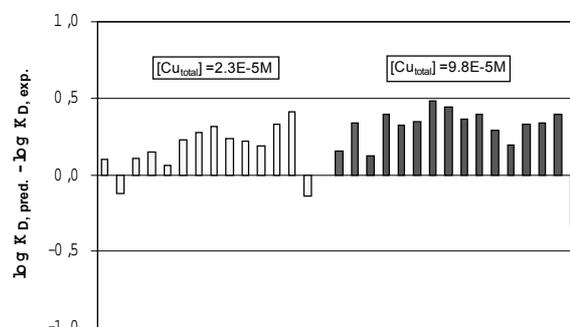
Fig. 2: Difference between predicted K_D and experimental values

References

/1/ Brendler, V. et al., J.Contam. Hydrol. **61**, 281-291 (2002)
/2/ Kulik, D.A., Am. J. Sc. **302**, 227-279 (2002)
/3/ Ali, M.A. and Dzombak, D.A., Geochim. Cosmochim. Acta **60**, 291-304 (1996)
/4/ Herbelin, A.L., Westall, J.C., *FITEQL-Version 3.2.* Report 96-01, Department of Chemistry, Oregon State University, Corvallis (1996)

INVESTIGATION OF PARTICLE FORMATION IN AN ACID ROCK DRAINAGE (ARD) SOLUTION AFTER ULTRAFILTRATION

W. Richter, H. Zänker

The formation of colloidal particles in acid rock drainage after filtration through 100-nm filters and ultrafiltration through 1-kD filters was studied. The two filter pore sizes were found to be associated with different particle growth rates. Two hypotheses suggesting possible reasons for these differences are discussed.

Samples of acid rock drainage waters from the abandoned "Himmelfahrt Fundgrube" Zn-Pb-Ag Mine at Freiberg (Saxony) were used for colloid-chemical investigations. According to former studies /1/ the colloidal particles in the ARD water with a pH of 2.4 and an SO_4^{2-} concentration of 52.6 g/L were composed of hydronium jarosite and schwertmannite. The Fe(II)/Fe(III) ratio of the solution was 6.1×10^{-4}. Arsenic was bound to the colloids by formation of a bidentate binuclear inner-sphere surface complex. After a prefiltration through a 100-nm syringe filter (Minisart, Sartorius AG, Göttingen) we filtered the filtrate with the help of a stirred ultrafiltration cell 8200 from Amicon with a 1-kD (about 1.2 nm) YM membrane. The filtrates were analysed by ion chromatography (Jasco) and ICP-MS (Elan 5000, Perkin Elmer). The size of the colloidal particles was measured by PCS (BI-90, Brookhaven Instruments). The PCS measurements began immediately after filtration. This filtration process was repeated.

Tab. 1 lists selected element concentrations of the raw water and the filtrates (100 nm and 1 kD) and the scattered light intensity (photomultiplier count rate of the PCS device). In spite of the relatively high scattered light intensity the particles >100 nm form only a minority fraction of the colloids. According to the PCS measurements the major colloidal fraction has a particle diameter of < 5 nm (Fig. 1b). From the filtrate-to-raw-sample concentration ratios in Tab. 1 we conclude that 24 % of Fe, 83 % of As and a trace of Pb occur as particles of 1.2 to 100 nm diameter.

Tab. 1: Chemical analysis of the ARD solution by ICP-MS and count rate (scattered light intensity) of the PCS-measurements

	Raw water	Filtration 100 nm	Filtration 1 kD-1	Filtration 1 kD-2
	Mol/L			
Mg	$7,70 \times 10^{-2}$	$7,55 \times 10^{-2}$	$7,31 \times 10^{-2}$	$6,96 \times 10^{-2}$
Al	$4,61 \times 10^{-2}$	$4,41 \times 10^{-2}$	$4,04 \times 10^{-2}$	$3,71 \times 10^{-2}$
Si	$1,38 \times 10^{-3}$	$1,25 \times 10^{-3}$	$1,17 \times 10^{-3}$	$1,10 \times 10^{-3}$
Ca	$1,14 \times 10^{-2}$	$1,12 \times 10^{-2}$	$1,12 \times 10^{-2}$	$1,12 \times 10^{-2}$
Fe	$7,30 \times 10^{-2}$	$7,11 \times 10^{-2}$	$4,82 \times 10^{-2}$	$4,21 \times 10^{-2}$
Mn	$1,97 \times 10^{-2}$	$1,91 \times 10^{-2}$	$1,84 \times 10^{-2}$	$1,78 \times 10^{-2}$
Cu	$1,42 \times 10^{-3}$	$1,36 \times 10^{-3}$	$1,37 \times 10^{-3}$	$1,31 \times 10^{-3}$
Zn	$6,14 \times 10^{-2}$	$6,12 \times 10^{-2}$	$6,40 \times 10^{-2}$	$6,09 \times 10^{-2}$
As	$6,19 \times 10^{-3}$	$6,03 \times 10^{-3}$	$1,05 \times 10^{-3}$	$5,22 \times 10^{-4}$
Pb	$7,00 \times 10^{-5}$	$1,01 \times 10^{-5}$	$6,80 \times 10^{-6}$	$6,47 \times 10^{-6}$

The time dependence of the PCS results is indicated in Fig. 1. Fig. 1a shows the course of the scattered light intensity in the filtrate after the filtration process, Fig 1b the development of the size of the freshly generated particles in the filtrates. We can see that the particle growth depends on the kind of filtration. Both the rise of scattered light intensity and the increase in particle diameter demonstrate that there are differences between the filtrates. Whereas in the 100-nm filtrate the scattered light intensity remains at a very low level over a long time span, in the 1-kD filtrates it starts to increase immediately after filtration.
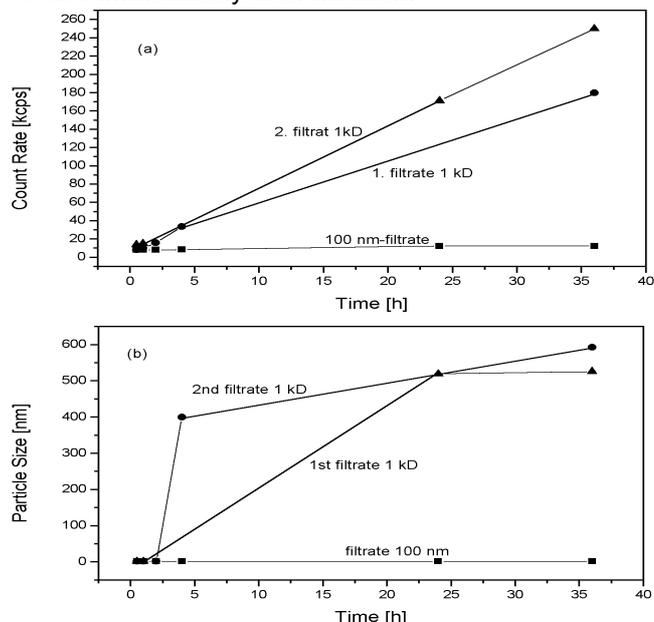
Fig. 1: Results of the PCS-measurements on the filtrates of the ARD-water, (a) the scattered light intensity (count rate) and (b) the particles size according to the deconvolution of the autocorrelation functions which was done with the CONTIN procedure.

Furthermore, the colloidal particles in the raw water and the 100-nm filtrate are <300 nm, while they grow up to 500-600 nm in the 1-kD filtrates. One explanation of these differences is that the formation and growth of the particles is governed by the concentration of As in the filtrate. In the raw water and the 100-nm filtrate the As/Fe ratio is 0.085, in the 1-kD filtrates it is <0.021. This influence of As on particle growth is in accordance with the results obtained by Waychunas et al. /2,3/ and Sherman and Randall /4/. They analysed arsenate sorption onto Fe oxyhydroxides (ferrihydrite, goethite, hematite) and onto schwertmannite and found that As affects the rate of generation and the size of the colloidal particles by "poisoning" crystal growth. A second hypothesis suggests that after filtration the mechanical strain exerted on the ultrafine iron polymers by the 1-kD filter pores triggers enhanced growth processes in the filtrate.

References
/1/ Zänker, H. et al., Appl. Geochem. **17**, 633-648 (2002)
/2/ Waychunas, G.A. et al., 11th Annual V.M. Goldschmidt Conference (2001)
/3/ Waychunas, G.A. et al., Geochim. Cosmochim. Acta **60**, 1765-1781 (1996)
/4/ Sherman, D.M. Randall, S.R., Geochim. Cosmochim. Acta **67**, 4223-4230 (2003)

INVESTIGATION OF COLLOIDS IN THE KAITZBACH STREAM

S. Weiss, K.-U. Ulrich, H. Zänker

Water of the Kaitzbach stream was investigated by centrifugation, filtration, ICP-MS, AAS, SEM/EDXS, TOC, UV/VIS-spectroscopy and photon correlation spectroscopy (PCS). The colloidal material was found to consist mainly of iron and aluminium but not of uranium.

Introduction

Colloids play an important part in the mobilization and immobilization of contaminants by adsorption and sedimentation in surface waters [1]. The Kaitzbach stream arises near Freital, passes along the edge of a waste dump of an abandoned uranium mine at Dresden-Gittersee and flows into the Carolasee lake at the centre of the city of Dresden. In April and June 2003 samples were taken from the spring and from the stream after it had passed the dump. Techniques developed and successfully used for colloid investigations in waters of abandoned mines [2] were applied for colloid characterization.

Experimental

Aliquotes of the raw samples, of the centrifugates (supernatants) after several parallel centrifugations and of the filtrates after several parallel filtrations were analysed by the methods mentioned above. In addition, colloids were concentrated on filter membranes, dried, coated with Au or C, and visualized by SEM, analysed for their major elements by EDXS.

Results

Water samples taken from the spring and the stream showed different concentrations of cations and colloids. Water from the source was almost free of particles. Due to the low scattered light intensities, particle sizing by PCS was not possible for these samples. However, LIBD measurements, which are much more sensitive for particles < 50 nm, revealed the presence of colloids < 30 nm at a concentration level of 50-100 ppt [3]. The concentrations of elements such as iron, aluminium and uranium were higher after passing the dump than they were at the spring (Tab. 1). Samples taken from the stream contained enough particles of the submicron range (< 1 μm) for successful particle sizing after performing certain separation steps. Colloids in the range from 150 to 300 nm in diameter were found in these samples, which correlates well with the SEM pictures.

The metal concentrations in the centrifugates and filtrates showed that approximately 70% of the iron and aluminium and 20% of the manganese concentrations existed as colloidal material (Fig. 1). Elements such as uranium and silicon were truly dissolved under the given conditions (pH, carbonate concentration). Filtration combined with UV/VIS and TOC measurements revealed that about 75% of the organic carbon is present either truly dissolved or as colloids < 50 nm in diameter.

Due to the high TOC value compared with the concentrations of the colloid-borne metals, a reliable identification of the nature of the colloids was not possible. They may consist of Fe, Al and Mn oxyhydroxides or of inorganic salts such as calcium carbonate or of organic material. Further investigations by TEM/EDXS and ultrafiltration may help to characterize these associations in more detail. Uranium probably occurs in the shape of uranyl carbonate complexes, which prevents it from being adsorbed onto the colloids.

Parameter	Spring	Stream
pH	7.4	7.6
Carbonate [mg/L]	83	125
TOC [mg/L]	2.05	2.45
Iron [μg/L]	15.4	95.9
Aluminium [μg/L]	15.3	37
Manganese [μg/L]	6.2	32.9
Uranium [μg/L]	3.2	19.7
Calcium [mg/L]	85.2	94.4
Silicon [mg/L]	5.74	4.16

Tab. 1: Characterization of the samples (April 2003)
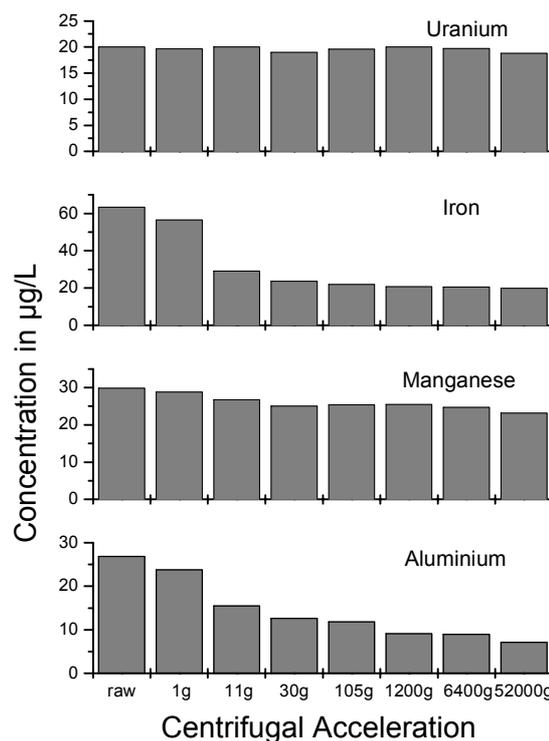
Fig. 1: Concentration of the key elements (stream, April 2003) in various centrifugates (centrifugation time: 1h)

References

/1/ Buffle, J. et al. Env. Sci. Technol. **29**, 2169 (1995)

/2/ Zänker, H. et al., Coll. Surf. A: Physicochem. Eng. Aspects **217**, 21 (2003)

/3/ Opel, K. et al., this report p.47

INTERACTION OF URANIUM WITH NATURAL COLLOIDS FORMED BY MIXING OF ACID MINE WATER WITH OXIC GROUNDWATER

K.-U. Ulrich, S. Weiß, H. Zänker

Mixing of acid flood water from the abandoned Königstein uranium mine with oxic groundwater generated colloidal particles of ferrihydrite and Al compounds due to Fe(II) oxidation and pH increase. Adsorption of uranyl started at pH >4.5 and reached up to 98% of total uranium at pH 6.0.

Introduction

The mixing of acid rock drainage or mining leachate with near-neutral bulk water is crucial for the speciation and partitioning of actinides in the mixed effluents of (abandoned) uranium mines. During the neutralization process colloids are formed mainly consisting of Fe and Al compounds known to bind trace metals and to remove them by adsorption and/or coprecipitation [1-3]. Our study simulated the end phase of mine flooding by mixing acid floodwater (pH 3) from the Königstein mine with oxic groundwater (pH 6.5) in a 100 L scale (two batches). The freshly generated colloids were characterized by REM, EDXS, ICP-MS, AAS, XRD, PCS, and laser Doppler electrophoresis.

Results

The main constituents of the colloids were, besides oxygen, Fe (37%), Al (7%), and U (up to 2%). Trace components were S, Si, Pb, As, Zn, and further elements not yet quantified. XRD spectra of the samples resembled those of "two-line ferrihydrite" (cf. [4]). The proportion of colloidal Fe rose with progressive Fe(II) oxidation and pH increase and was a function of both mixing ratio and time. At pH >4.5 colloidal Al and U emerged, reaching a proportion of about 60% at pH 5 and about 100% at pH 6 (Fig. 1). The colloid particles with a size of 75-100 nm had zero points of charge of pH 6 and pH 6.5 in the two batches. This explains their tendency of rapid aggregation at the final pH due to low electrostatic stability (Fig. 2).

By use of tangential flow 30 kD ultrafiltration followed by centrifugation we compacted several grams of colloids as a wet paste to investigate the atomic short-range order with $U-L_{III}$ and Fe-K EXAFS at ROBL. We intend to detect the uranyl adsorption partners and the molecular structures of the adsorbent (inner-sphere or outer-sphere complexes) as well as the mineral phases.

Though the experiments are still in progress, they already showed that colloids may scavenge and immobilize uranium in oxic mine waters. Detailed studies on the long-term effects of uranium immobilization are under way.

References

/1/ Webster, J.G., Swelund, P.J., Webster, K.S., Environ. Sci. Technol. **32**, 1361-1368 (1998)
/2/ Lee, G., Bigham, J.M., Faure, G., Applied Geochem **17**, 569-581 (2002)
/3/ Tonkin, J.W., Balistrieri, L.S., Murray, J.W., Environ. Sci. Technol. **36**, 484-492 (2002)
/4/ Schwertmann, U., Friedl, J., Stanjek, H., J. Colloid and Interface Science **209**, 215-223 (1999)
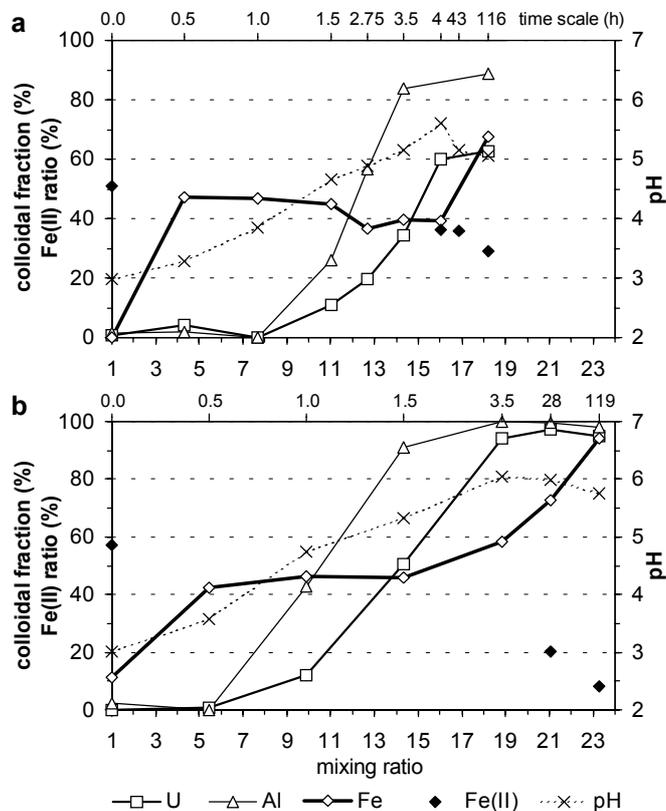
Fig. 1: Percentages of colloidal U, Al, Fe, and Fe(II) fraction (left ordinate) and pH (right ordinate) depending on mixing ratio (lower abscissa) and course of time (upper nonlinear abscissa) in the two batches of acid floodwater mixed by oxic groundwater up to a final pH 5.0-5.5 (a) and 5.5-6.0 (b). The colloidal metals were identified by 3 kD ultrafiltration.
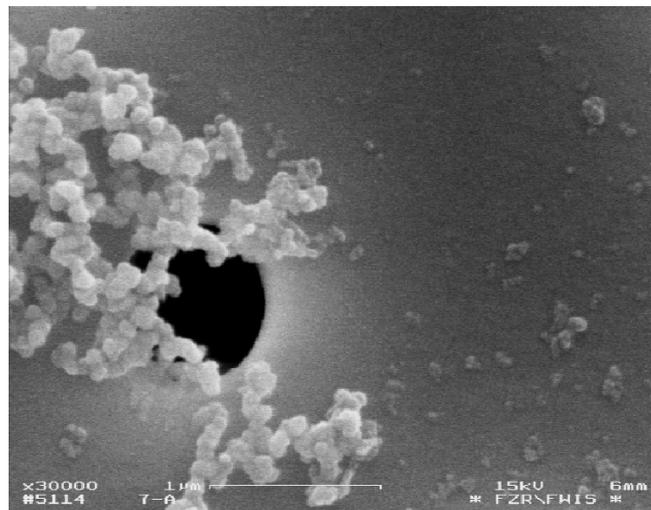
Fig. 2: SEM image (30000 x) of colloid particles and aggregates in the first batch, and pore of 1 µm filter membrane (Shot: E. Christalle).

LASER-INDUCED BREAKDOWN DETECTION (LIBD) OF AQUATIC COLLOIDS – THE APPARATUS

S. Hübener, K. Opel

An experimental set-up for laser-induced breakdown detection (LIBD) of aquatic colloids has been established.

Laser-induced breakdown detection (LIBD) is a detection method for aquatic colloids based on the generation of dielectric breakdown events on individual colloidal particles by focused laser pulses. The plasma plumes generated are observed by CCD cameras and/or photoacoustic detectors. LIBD is a very sensitive in-situ method providing information on the particle size down to about 10 nm and the particle concentration down to a few ppt /1/. The method was created several years ago but a manufacturer for LIBD instruments has not been found up to now. Here we describe the experimental set-up for laser-induced breakdown detection of aquatic colloids established at the Institute of Radiochemistry. The optical set-up is shown schematically in Fig.1.
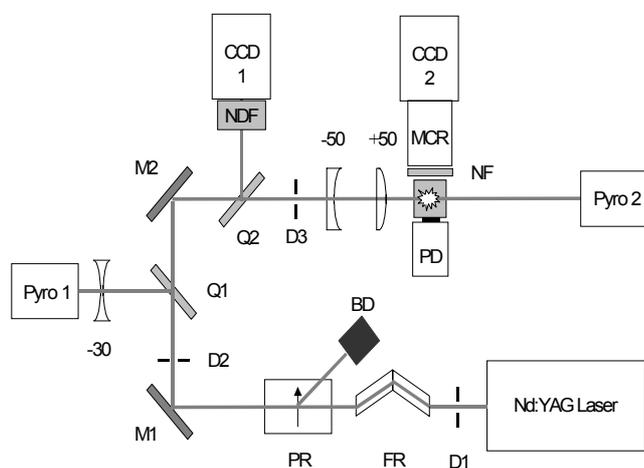
Fig. 1: Optics system of the experimental set-up. For details see text.

A diode pumped Nd:YAG laser (Thales DIVA II 532 HP, pulse energy 10 mJ, repetition rate 0 – 20 Hz, pulse duration 8 – 12 ns, beam diameter ~ 1.5 mm, beam profile TEM 00) is used as the light source. For stability reasons the laser is operated at maximum power. The pulse energy is controlled by a combination of two Fresnel rhombs (Newport broadband polarization rotator, FR) and a Glan-Laser calcite polarizer (PR). The Fresnel rhombs are manually rotated. The beam component to be rejected is guided into a beam dump (BD), while the main beam transmitting the polarizer is deflected by 90° by a dielectric mirror (M1; Newport high-energy Nd:YAG laser mirror). On its way to the second mirror (M2) the beam passes through a parallel quartz plate (Q1), which deflects about 5 % of the light into a pyroelectric detector (Pyro 1; Scientech P09). Prior to entering the detector, the beam is expanded by an f = -30 mm lens. By the use of the quartz plate Q2 some 5 % of the light are deflected through an attenuator into the camera CCD1 (Laser 2000 WinCamD) for beam diagnostics. The

main beam passes through the diaphragm D3, an f = -50 mm planoconcave lens which expands the beam, and an f = + 50 mm planoconvex lens for beam focusing. The beam is focused into a quartz cell containing the particle suspension to be analyzed. Static cells as well as flow-through cells in two different sizes are in use: $10x10x34$ mm^3 and $20x20x34$ mm^3. The cells are inserted into home-built mounts to ensure precise centering perpendicular to the laser beam. Behind the cell the pulse energy can be measured by a pyroelectric detector (Pyro2; Scientech P25) for energy calibration. For adjustment and control of the beam alignment the camera CCD1 or other optical elements can be placed there, too.

The breakdown events are observed by either photoacoustic detection with a piezoelectric detector (PD) or by optical monitoring with the camera CCD2 (Pulnix TM-1040) or by both detection units simultaneously. The piezoelectric detector, home-built using piezoelectric ceramic plates ($10x10x1$ mm^3; PI ceramic), is in direct contact with the quartz cell perpendicular to the laser beam axis. Through the opposite cell window the plasma plumes are observed by the monochrome camera CCD2 in combination with the macroscope MCR (Askania MZM 1). The notch filter NF placed in front of the camera system suppresses the 532 nm straylight by more than six orders of magnitude.

The pulse energy and all other beam parameters are manually adjusted. The WinCamD system (CCD, PCI card, PC with profiler software), which displays and evaluates the actual beam, is used for beam control. The data acquisition system comprises another PC, which runs a home-built LabView program controlling a digital oscilloscope (LeCroy LT 584 L, 1 GHz, 1 GS/s, 4 channels) for data acquisition, a delay generator (BME_SG02p) for time control and a frame grabber (Matrox Meteor II Digital) for recording the plasma plume picture. The signals of the piezoelectric detector are directly recorded by the oscilloscope, the energy detector signals via two power meters (Scientech SCI-S310).

Some first results of acoustic detection of breakdown events on colloids in almost particle-free waters are presented in /2/.

References

/1/ Walther, C., Colloid Surf. A **217**, 81 (2003)
/2/ Opel, K. et al., this report p.47

LASER-INDUCED BREAKDOWN DETECTION OF AQUATIC COLLOIDS – MEASUREMENT BY ACOUSTIC DETECTION OF PLASMA EVENTS

K. Opel, S. Hübener

A modular system for laser-induced breakdown detection (LIBD) of aquatic colloids was set up. The calibration of the system with solutions of polymer standards is presented. Some first measurements of the filtrate of an almost particle-free environmental water demonstrate the ability to detect particles significantly smaller than 30 nm in concentrations of less than 50 ppt.

Introduction

The determination of the concentration, size distribution and composition of colloids in natural waters is of interest due to their impact on the migration of contaminants. In contrast to other methods, laser-induced breakdown detection is capable of detecting small colloids (a few nm) even in concentrations in the ppt range. An LIBD-system similar to the systems developed by Walther et al. at FZK-INE /1/ was recently set up at the IRC. The basics of LIBD are also described in /1/.

Experimental

Polymer standards of various sizes were diluted with deionized water (Membrapure) to a particle number concentration of $2 \cdot 10^{-7}$ cm^{-3}. These solutions were used for calibration of the LIBD system described in detail in /2/. The breakdown probability was calculated on the basis of 1,000 pulses for each data point.

As an example of an almost particle-free water, source water from the Kaitzbach stream was centrifuged at various accelerations and filtered through Nucleopore filters of various pore sizes. The filtrates and the centrifugates were analysed by LIBD, as in the calibration with 1,000 pulses for each data point.

Results

The background level was determined by examination of deionized water of two commercially available systems (MilliQ and Membrapure). The Membrapure water was found to be better suited to preparation of calibration solutions than MilliQ water because of its reproducibly higher breakdown threshold (energy required for 1% breakdown probability, Fig. 1).

The breakdown threshold is an indicator of the average particle size. With decreasing particle size it shifts to higher pulse energies. Conclusions as to particle concentration can be drawn from the slope of the curves. It is obvious that the probability of the presence of a particle in the laser focus increases with increasing concentration.
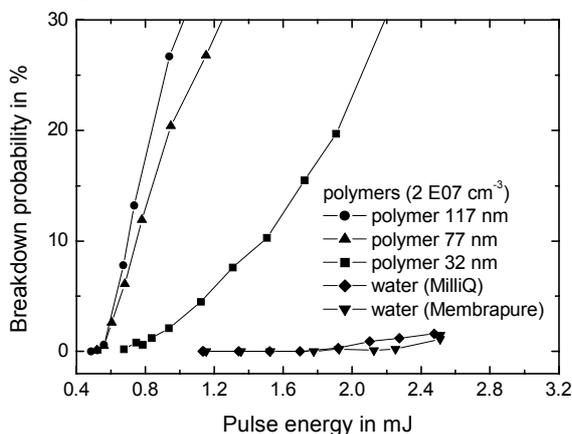
Fig. 1: Calibration using various polymer standards, background of two deionized waters

The measurement of fractions of Kaitzbach source water produces the curves shown in Fig. 2. As expected, the breakdown threshold increases and the slope of the curves decreases with increasing speed of centrifugation and decreasing filter pore size due to gradual separation of particles. Centrifugation at 7 krpm corresponds to filtration with a filter pore size of 400 nm.

Whereas photon correlation spectroscopy (PCS) is too insensitive to allow particle sizing even in untreated water /3/, LIBD is capable of estimating particle size and concentration in samples filtered by a membrane of 50 nm pore size. The breakdown treshold of this filtrate was determined to be equal to a laser pulse energy of about 1.5 mJ. The corresponding particle size is thus significantly smaller than the smallest particles in calibration (32 nm). The slope of the curve, which is less steep than in calibration, reveals a particle concentration of about 50 ppt in the 50-nm filtrate.
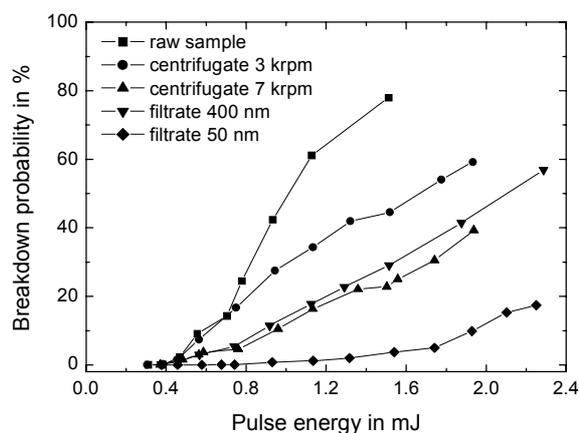
Fig. 2: Breakdown probability vs. pulse energy for various fractions of Kaitzbach source water

The figures are rough estimates due to problems caused by instability of the laser system. Changes in the setup, especially in focusing the laser beam, require the calibration to be verified. We hope to achieve better results by including the optical detection of plasma events. This will make it possible to verify the two detection methods by comparing them with each other and to improve the accuracy of measurements. The instrumental setup has been implemented, experiments are in progress.

References

/1/ Walther, C. et al., Nucl. Instr. and Meth. In Phys. Res. B **195**, 374 (2002)

/2/ Hübener, S. et al., this report, p.46

/3/ Weiss, S. et al., this report, p.44

ANALYTICAL CENTRIFUGATION WITH PREPARATIVE CENTRIFUGES

H.Zänker

A method to do analytical centrifugation with preparative centrifuges is described. It allows particle sizing on colloidal solutions in a colloid concentration range by several orders of magnitude lower than the concentration range of traditional analytical centrifugation.

Centrifuges are not only a means of colloid (particles of 1 nm to 1 µm) fractionation. They also serve well in the determination of particle sizes. Particle sizing by centrifugation is much less troubled by artifacts than, for instance, particle sizing by filtration (even though centrifugation is not free of artifacts, cf. /1/).

The centrifugal force builds up a particle concentration gradient which is, however, reduced again by the diffusion of the particles. If transparent disc rotors are used or if the centrifugal tubes are designed as transparent cuvettes (analytical centrifuges), the spatial and temporal concentration distribution of the colloid particles can be followed in situ by measuring light extinction or refractive index (instead of light extinction the absorption of X-rays can also be measured). This enables a very detailed description of the sedimentation process of the particles and, if enough information about the density of the particles is given, a calculation of the hydrodynamic particle size distribution. The disadvantage of analytical centrifugation and analytical ultracentrifugation is that the required colloid concentrations are significantly higher than those of most environmental samples (range of g/L).

We developed a method with the help of which one can do analytical centrifugation and ultracentrifugation even if the particle concentration is in the "environmental" concentration range (mg/L to µg/L). This can even be accomplished by using a preparative instead of an analytical centrifuge/ultracentrifuge. A disadvantage, however, is that our method is significantly more time-consuming than traditional analytical centrifugation.

In the case of centrifugation which is capable of analyzing particles down to about 30 nm the sedimentation of the particles can be described by (cf. /2/)

$$d = \sqrt{\frac{18\eta \ln(r_1 / r_0)}{(\rho_2 - \rho_1)\omega^2 t}} \quad (1)$$

with d = particle diameter, η = viscosity of the solvent, r = distance of the particle from the center of rotation, ρ_1 = density of the solvent, ρ_2 = density of the particle, ω = angular rate, and t = time. (This equation does not hold for the case of ultracentrifugation where centrifugal accelerations of up to 1 Mio x g are applied and particles down to 1 nm can be analyzed. Here particle diffusion against the gravitational field needs to be taken into consideration /3/).

In our method the in-situ observation of the particle sedimentation behavior applied in analytical centrifugation is replaced by the following: Five to ten aliquotes of the sample are centrifuged for 1 h at different revolutions per minute, the supernatant half of the centrifuged samples is sucked off and the supernatants are analyzed by ICP-MS or AAS. Normally,

the behavior of the chemical elements follows two different patterns. Elements whose concentration is decreased by the centrifugation (typically Fe(III), Al, Pb, As, Cu etc.) are regarded as colloidal. Elements not significantly influenced by centrifugation (e.g. Mg, Ca, Na, Fe(II)) are taken as truly dissolved or as forming colloids fine enough not to be influenced by the centrifugal force applied. Tab.1 gives the maximum conceivable hydrodynamic diameter of particles of two typical materials (gibbsite and ferrihydrite) still present in the supernatant after centrifugation at different rpms (high speed centrifuge Kontron T-124, swing-out rotor AS 4.7, centrifuged aliquote volumes 25 ml, volume of supernatants 12.5 ml, maximum distance of particle movement: from r_0 = 10.4 cm to r_1 = 12.8 cm). The comparison of the experimental results for the disappearance of the colloid-borne chemical elements from the supernatant at increasing centrifuge speed with the data of Tab. 1 provides information on the hydrodynamic diameter of the particles (cf. /4/).

Revolutions per Minute [rpm]	Centrifugal Acceleration	d_{max} Ferrihydrite [nm]	d_{max} Gibbsite [nm]
300	13	563	813
500	40	338	488
700	70	242	349
1000	145	169	244
2000	570	85	122
4000	2300	44	61
5000	3600	35	49
7000	7000	25	35

Tab.1: Maximum hydrodynamic diameter of ferrihydrite (ρ = 3.96 g/cm^3) and gibbsite (ρ = 2.42 g/cm^3) particles in the supernatant (centrifugation time: 1 h)

References

/1/ Salim, R., Cooksey, B.G., Wat. Res. **15**, 835 (1981)
/2/ McFadyen, P., Fairhurst, D., Clay Minerals **28**, 531 (1993)
/3/ Williams, J.W. et al., Chem. Rev. **58**, 715 (1958)
/4/ Zänker, H. et al., this report, p.49

PARTICLE SIZING ON TYPICAL ENVIRONMENTAL WATERS WITH A PREPARATIVE CENTRIFUGE

H. Zänker, S. Weiß, G. Hüttig, K. Opel

Three typical oxic waters were analyzed for the size of their colloids using a preparative centrifuge as an analytical centrifuge.

First, water of the main drainage gallery of the Freiberg mining area, the "Rothschönberger Stolln" adit (pH 7.2), was investigated according to the method described in /1/. About 25 elements were analyzed; Fig. 1A gives the centrifugation behavior of Al and Fe. It follows from the amounts of metals removable by centrifugation that the matrix of the colloids in the adit consists of Al and Fe. For Al, the successive increase of the centrifugal acceleration from 13 x g to 2300 x g results in a continuously decreasing concentration in the supernatant. From Tab.1 in /1/ can be concluded that a broad particle size distribution from >1 µm down to about 60 nm exists. An increase of the centrifugal force beyond 2300 x g does not induce a further increase of the centrifugable amount of Al. The Al still detectable in the supernatants after the $\geq$ 2300 x g centrifugations is probably truly dissolved. The behavior of Fe indicates a relatively broad particle size distribution down to about 350 nm (relative centrifugal acceleration of 40 x g). First, a further rise in centrifugal acceleration does not increase the removal of the Fe. However, at centrifugal accelerations of more than 150 x g a second Fe component is removed. Thus the Fe particles seems to have a bimodal particle size distribution. According to Tab. 1 in /1/ the particle size of the second Fe component is < 170 nm (centrifugal acceleration 150 x g), but > 40 nm (2300 x g). Not much can be said about the tiny trace of iron that is not even removed by centrifugal accelerations of $\geq$ 2300 x g (extremely fine colloids, polymers or monomeric ions). The colloid-borne trace components Pb, Cu and As of the "Rothschönberger Stolln" adit (results not given here) follow the bimodal pattern of the Fe particles.

In a second experiment, the colloidal particles of the Kaitzbach, a small creek (pH 7.6) receiving seepage water from uranium mine tailings, were studied. The sedimentation behavior of the two elements Al and Fe (examples out of a whole of ca. 25 elements again) during centrifugation is given in Fig. 1B. The Al-containing particles show a broad monomodal particle size distribution from >1 µm down to $\leq$ 35 nm according to a comparison of Fig. 1B with Tab. 1 in /1/. The Fe-rich particles, too, have a monomodal particle size distribution. However, their size range lies between 1 µm and about 200 nm. The relatively high iron concentration of 20 µg/L remaining in the solution after centrifugations at $\geq$ 1200 x g cannot be explained by the presence of ionogenic iron alone since Fe^{3+} is highly oversaturated at the given pH. We suppose that this iron fraction is stabilized in solution by complexation with organic ligands; it might occur as humic complexes of only few nanometers in size. In contrast to the "Rothschönberger Stolln" adit water, not only Al and Fe play a role as matrix elements of the colloids in the Kaitzbach creek. Also Ca and organic substances seem to contribute to the colloid matrix (results not given here).

In a third experiment water of the river Elbe (pH 8.4) was studied. Fig. 1C shows the behavior of the two elements Fe and Al again. In the case of the Elbe the colloid matrix contains also Mn, Zn and in particular Si, besides Fe and Al. A comparison with Tab. 1 in /1/ reveals that the size distribution of the Fe- and Al-containing colloids is monomodal and covers a range from >1 µm down to about 30 nm. This particle size distribution is also representative of the colloid-borne elements Si, Mn and Zn (not given here).

The three examples show that studies with a preparative centrifuge can provide valuable information on the ratio between truly dissolved and colloid-borne components of an environmental water, on the absolute colloid inventories, on the composition of the colloid matrices, on colloid-borne trace elements and on the in-situ particle size distribution of the colloids. Thus they can be a substitute for classic analytical centrifugation that even works at concentration levels down to the µg/L range.
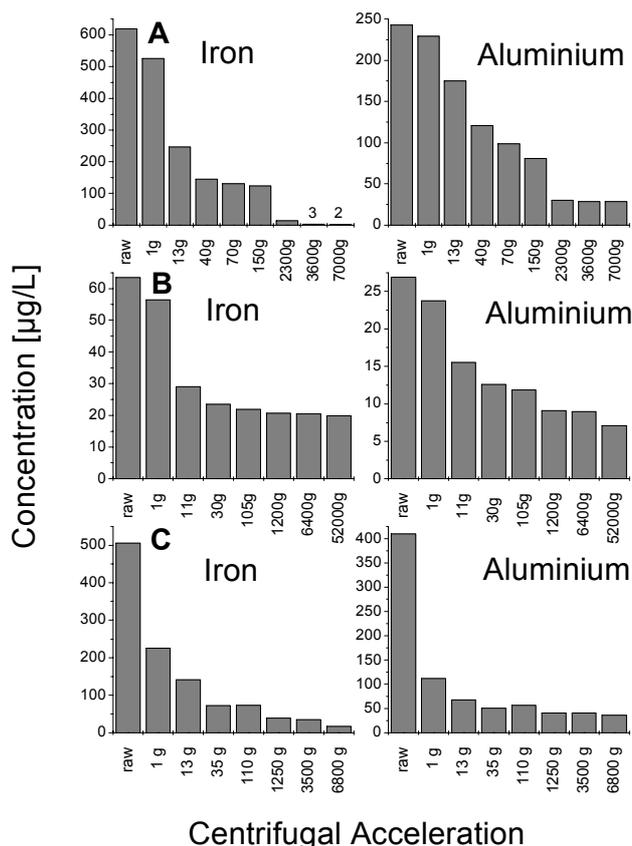
Fig.1: Al and Fe concentration after 1-hour centrifugations at various centrifugal accelerations in the water of the "Rothschönberger Stolln" adit (**A**), the Kaitzbach creek (**B**) and the river Elbe (**C**)

References

/1/ Zänker, H., this report, p.48

EXPLORING THE SPATIAL RESOLUTION OF THE PHOTOTHERMAL BEAM DEFLECTION TECHNIQUE IN THE INFRARED REGION

H. Foerstendorf, W. Seidel[1], J.M. Ortega[2], F. Glotin[2], R. Prazeres[2]

[1]Institute of Nuclear and Hadron Physics; [2]LURE, Université de Paris-Sud, Orsay, France

Photothermal spectroscopy using an infrared pulsed pump source provides spatial information of a sample surface. In this model investigation we obtained a spatial resolution of approximately 25 µm using a strongly focused probe beam in a reflecting scheme.

In photothermal beam deflection spectroscopy (PTBD) generating and detection of a thermal wave occur normally in the sub-millimeter length scale. Therefore, PTBD can potentially provide spatial information about the surface of the sample and permits imaging and/or microspectrometry. This will possibly lead to a useful tool for investigation of sorbed species on mineral surfaces.

Experimental

In PTBD the thermal wave is generated by intermittent laser heating and is detected by a probe laser beam (*e.g.* a HeNe laser) which is reflected from the surface of the sample next to the spot of the incident pump beam (FEL). Depending on the modulated intensity of the FEL a thermoelastic deformation of the surface is induced which results in periodically, photoinduced displacement of the probe beam /1/. Thus, a different reflection angle is observed which is monitored by the use of a high resolution position detector placed at a suitable distance from the illuminated sample (Fig. 1).

Results and Discussion

As a model compound we investigated the border range between an O^+-implanted and an untreated region of a Ge-substrate by recording time curves of the deflection signal at distinct positions of the surface of the substrate using a constant FEL wavelength (11.6 µm). The recording of the time curves is synchronized to the FEL pulses. The deflection signal shows up after a short delay time (~7 µs) while the thermal wave propagates from the incident FEL beam to the probe beam spot. Due to the different absorption coefficients the deflection signal decreases from the O^+-doped region to the nearly transparent pure germanium. Synchronization of sample micropositioning and data acquisition provides the recording of mapping plots of the sample's surface (Fig. 2, inset).
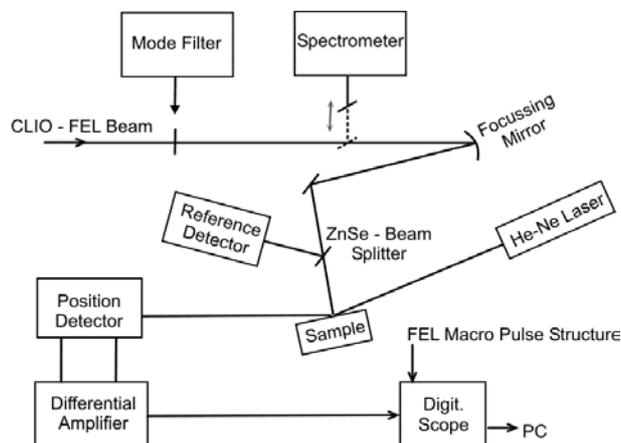
Fig. 1: Schematic diagram of the thermal deflection experiment setup.
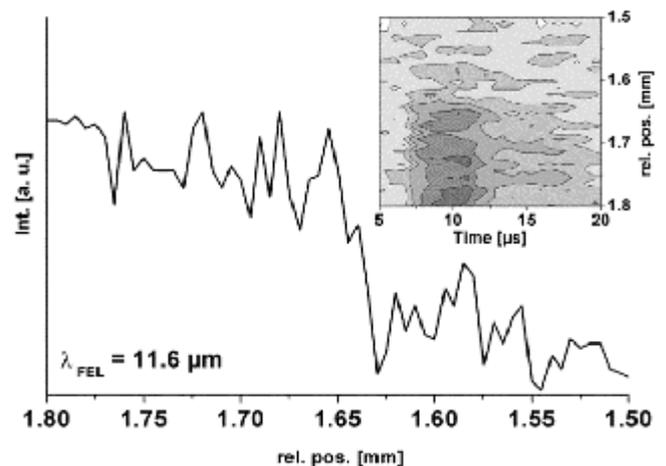
Fig. 2: Absorption profile of the border range between O^+-doped and pure germanium (extracted from inset; t = 10.6 µs). Inset: mapping plot of the set of time curves of the deflection signal.

In a first approach the spatial resolution obtained was about 50 µm /2/. In the present study we improved the spatial resolution by focusing the HeNe laser probe beam in front of the surface of the sample extensively. The diameter of the laser spot was about 15 µm at the surface of the sample. It was found that the spatial resolution of the profile is very sensitive to the focusing of the probe beam. The deflection signal can also be increased by focusing the pump beam which, however, becomes crucial with respect to the high laser power.

The set of the recorded time curves of the deflection signal at distinct sample positions is shown in the inset of Fig. 2. The step width between the distinct sample position was 5 µm. The absorption profile in Fig. 2 was extracted from the set of the time curves near the maximum of the amplitude at 10.6 µs. The transition between the O^+-doped and the untreated region of the substrate can be seen around 1.65 mm rel. pos. within a range of about 25 µm.

In the next series of experiments we will continue to enhance the spatial resolution to a few microns by utilizing more sophisticated focusing components. Simultaneously, this requires more complex samples showing well-defined patterns of doped regions on the germanium substrates.

Acknowledgements

References

/1/ Olmstead, M.A. et al., Appl. Phys. A **32**, 141-154 (1983)

/2/ Seidel, W. et al., Report FZR-373, p. 51 (2003)

LINKING MONTE-CARLO SIMULATION AND TARGET TRANSFORMATION FACTOR ANALYSIS: A NOVEL TOOL FOR THE EXAFS ANALYSIS OF MIXTURES

A. Roßberg, A.C. Scheinost

We have developed a new algorithm to determine the spectra of species in mixtures, based on a combination of Monte-Carlo Simulation and Target Transformation Factor Analysis (MCTFA). This novel approach requires solely the structure of the ligand as input data, enabling the determination of organic complexes even in "messy" environmental samples.

MCTFA combines the advantages of modeling and statistics. The MC simulation allows to model the three dimensional structure of the complexes by using the experimental XAS spectra and the structure of the interacting ligand as constraints /1/. TFA allows to check whether the resulting EXAFS spectrum of the calculated complex is a component of the series of measured EXAFS spectra /2/.

Eight samples were prepared in the pH range 0.1-4.5 at an ionic strength of 1.2 mol/L. For all samples [U(VI)] was 0.05 mol/L and the acetic acid concentration [ac] was 1 mol/L except for the sample at pH 4.5, where [U(VI)] = 0.025 mol/L and [ac] = 0.5 M. The U L_{III}-edge EXAFS spectra of the pH series were measured at the Rossendorf Beamline (ROBL) at the ESRF in transmission mode at room temperature. Crystallographic data of sodium tris(acetato)dioxouranate /3/ were used to create the ligand structure for the MCTFA and to calculate the theoretical phase and amplitude functions for EXAFS data analysis (FEFF6).

A simplified description of the MCTFA procedure follows: Theoretical $EXAFS_{theo}$ spectra are calculated for random positions of the uranium atom around the ac molecule using bond distance of $U-O_{ax}$, Debye-Waller factor (DW) of O_{ax}, O_{eq}, C, and the energy shift ΔE_0. For the estimation of these parameters we used the EXAFS spectrum at pH 2.69 and the EXAFSPAK software. The $EXAFS_{theo}$ is subjected as a test vector $\mathbf{x}_{test}$ to the TFA procedure to yield the predicted vector $\mathbf{x}_{pred}$. $\mathbf{x}_{test}$ is a component of the spectra of the complex mixtures, if it is in agreement with $\mathbf{x}_{pred}$ /5/. This is the case, when the random position of U is in agreement with the real position of U at the ligand.

Fig. 1: (a) Speciation for [U(VI)] = 0.05 mol/L, [ac] = 1.0 mol/L, I = 1 mol/L (complex stability constants from /4/); (b) experimental data and their abstract reproduction using abstract spectra, (c) eigenvectors and (d) abstract concentrations.

Fig. 1 (a) and (b) shows the pH speciation of the U(VI)/ac system and the experimental EXAFS spectra.

All spectra can be reproduced with two components, consisting of two structurally different fragments: coordinated water and ac molecules. Only the ratio between the two fragments varies as a function of pH.

Fig. 2: MCTFA result. Brighter balls indicate U positions with the highest likelihood (good fits), darker balls indicate positions resulting in poorer fits. U-atom bond distances are given for the optimum position (black dots).

The MCTFA result (Fig. 2) is in good agreement with the U-atom bond distances found for the pure 1:3 U(VI)/ac complex at pH 4.5 /6/. Note that according to the calculated speciation (Fig. 1a) a maximum of 34% of the UO_2-ac structural unit is present in the investigated spectra (remainder: coordinated water molecules with radial $U-O_{eq}$ bond distance of 2.41 Å). The influence of the DWs, which are necessary to calculate the $EXAFS_{theo}$, on the MCTFA result is small. Hence estimates of DW can be used.

The results demonstrate that MCTFA is a powerful tool for the determination of the structure of pure complexes in mixtures, even when spectra and information about concentrations of pure complexes are not available. Thus, the newly developed method may be extremely useful to decipher the structure of metal complexes in environmental samples where a wide range of organic ligands, from simple organic acids to large biopolymers may be present.

References

/1/ McGreevy, R.L., J. Phys. Cond. Matt. **13**, 877 (2001)
/2/ Wasserman, S.R., J. Phys. IV France **7**, 203 (1997)
/3/ Templeton, D.H. et al., Act. Cryst. **C41**, 1439 (1985)
/4/ Ahrland, S. et al., Acta Chem. Scand. **5**, 199 (1951)
/5/ Malinowski, E.R., *Factor Analysis in Chemistry*, John Wiley & Sons, New York (1991)
/6/ Roßberg, A., Doctoral Thesis, Technical University Dresden (2002)

THE PRECISION OF QUANTITATIVE SPECIATION BY ITERATIVE TRANSFORMATION FACTOR ANALYSIS OF EXAFS SPECTRA

A. Roßberg, A.C. Scheinost

Evaluating U-LIII EXAFS spectra of U(VI) species mixtures with known composition by iterative transformation factor analysis (ITFA), we found an error of less than 2 % for reconstructed concentrations. The precision strongly depends on k-range and k-weighting.

ITFA has been used for quantitative speciation of U species in aqueous solutions and of Zn species in soil samples /1,2/. However, the precision of this method is unknown. Furthermore, a systematic investigation of the influence of k-range, k-weighting and noise level on the result of ITFA is lacking. Therefore, we investigated the EXAFS spectra of species mixtures with known composition.

We prepared 4 mixtures of 3 uranyl solids, oxalate trihydrate (ox), uranyl acetate dihydrate (ac), and m-autunite (au). Their known relative concentrations are given in table 1. The U L_{III}-edge EXAFS spectra (Fig. 1a) of the pure compounds and their mixtures were measured at the Rossendorf Beamline (ROBL) at the ESRF at room temperature in transmission mode. ITFA was performed as given /1/.

The EXAFS spectra of the pure compounds and their mixtures are shown in Figure 1a. Figure 1b gives the error of the relative concentrations as a function of the k-range and k-weighting. Three main features are visible: (I) For all k-weightings the error reaches a minimum, when a k-range of 2 to 6 Å^{-1} is used. (II) For k-ranges > 6 Å^{-1} the error increases. (III) The error increase is more pronounced for higher k-weighting.

Tab. 1: Known and estimated (ITFA) relative concentrations of the U(VI) compounds.

Sample	Known			Estimated		
	Ox	ac	Au	Ox	ac	Au
1	100	0	0	100^f	0	0
2	0	100	0	0	100^f	0
3	0	0	100	0	0	100^f
4	7.9	46.2	45.9	7.5	48.4	45.6
5	54.2	27.7	18.1	55.8	27.4	17.7
6	53.5	19.5	26.9	54.2	17.2	27.8
7	25.4	25.3	49.4	25.2	26.0	49.9

^{f}) fixed; investigated k-range: 2-6 Å^{-1}; weighting: k^1

Using the optimized conditions (k-range 2 to 6 Å^{-1}, k^1-weighting), the relative concentrations can be derived with a very low error of 1.1 %, demonstrating the reliability of the ITFA method (Table 1). However, it is evident that the choice of k-range and k-weighting is critical. When the k-range is extended above the threshold value, the increase of the signal-to-noise ratio reduces the quality of the prediction. While this error increase is negligible for unweighted data, it is pronounced when the experimental noise is enhanced by the k-weighting. The minimum of the error at 6 Å^{-1} corresponds to amplitude function of the coordinated oxygen atoms, which has a maximum between 2 and 6 Å^{-1}. Hence the minimum position depends on the type of structure, and may be at higher k values (or higher k-weighting), if backscattering atoms heavier than O or C are present in the next-nearest shells.
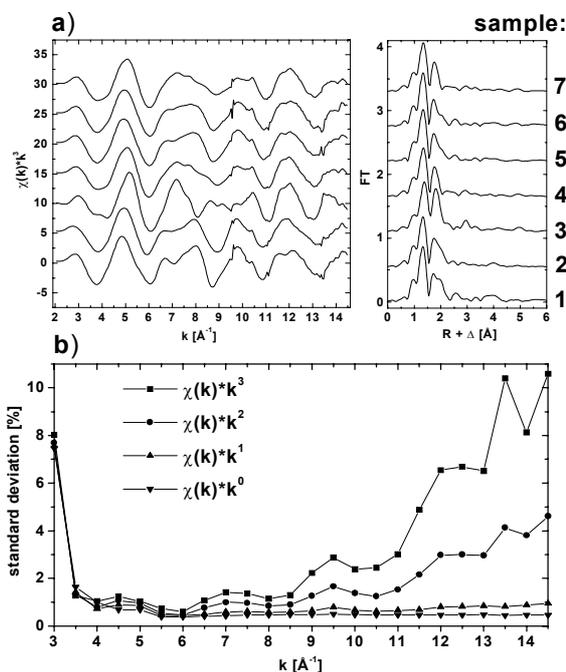
Fig. 1: a) EXAFS spectra and Fourier transforms of model compounds (1-3) and their mixtures (4-7).
b) Error of relative concentrations as a function of k-ranges and k-weightings.
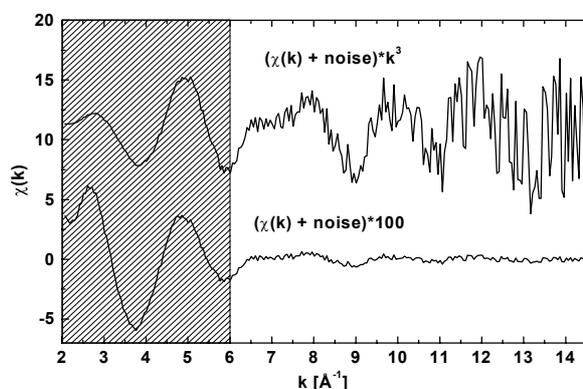
Fig. 2: k^3- and k^0-weighted EXAFS spectra of ac with artificial noise. Dashed – the optimum k-range for analysis.

If artificial noise is added to the samples, as is demonstrated for sample ac in Figure 2, the error of relative concentration increases to 2.6% only by using the optimum analysis conditions.

Even for unknown species mixtures, optimized parameters may be derived from the spectra of the spectral components. Hence even at elevated noise levels, relatively low error levels (< 3 %) can be achieved for the quantitative speciation by ITFA.

References

/1/ Roßberg, A. et.al, Analyt. and Bioanalyt. Chem. **376**, 631(2003)

/2/ Scheinost, A.C.*, et al.*, Physica Acta, accepted (2004) and this issue

POLARIZATION DEPENDENT EXAFS. PART 1: URANIUM L_1 EDGE

C. Hennig, A. Scheinost

We determined the polarization dependence of the U L_1 edge EXAFS using $Ca[UO_2PO_4]_2 \cdot 6H_2O$.

X-ray synchrotron radiation created by a bending magnet is to approximately 95% linearly polarized. In anisotropic materials the amplitude of the EXAFS spectrum and thus the coordination number N depends on the angle θ between the polarization vector $\vec{\varepsilon}$ and the vector $\vec{r}$ connecting the absorbing and backscattering atoms /1/. As result, the real or crystallographic coordination number N_{cryst} is detected as a function of θ and appears as effective coordination number N_{eff}. For a single-scattering process and in plane–wave approximation the angular dependence can be written for both L_1 and K edges as:

$$N_{eff}(\theta) = \sum_{n=1}^{N} 3 \left| \vec{\varepsilon} \cdot \vec{r} \right|^2 \qquad (1)$$

The curved-wave approximation of the photoelectron scattering includes a second order term /2/, which is negligible. In most cases $\vec{r}$ is unknown. In order to relate $\vec{\varepsilon}$ and $\vec{r}$ to morphological parameters of the sample, θ is divided into two angles, where α is the angle between $\vec{\varepsilon}$ and a morphological plane of the sample and β is the angle between $\vec{r}$ and the normal vector $\vec{n}$ of the morphological plane /3/:

$$\left| \vec{\varepsilon} \cdot \vec{r} \right|^2 = \cos^2 \theta = \cos^2 \beta \sin^2 \alpha + (\sin^2 \beta \cos^2 \alpha)/2 \qquad (2)$$

The effective coordination number N_{eff} is then related to the real crystallographic coordination N_{cryst} by:

$$N_{eff}(\theta) = N_{cryst} 3 \left(\cos^2 \beta \sin^2 \alpha + (\sin^2 \beta \cos^2 \alpha)/2 \right) \qquad (3)$$

A special case happens if $\left| \vec{n} \cdot \vec{r} \right|^2 = 1/3$ /4/. At this so-called magic angle, the value N_{eff} is independent of β for an angle of $\alpha = 35.3°$, and inversely, N_{eff} is independent of α at $\beta = 54.7°$ /4,5/.

We investigated the polarization effect on the coordination number using a single crystal of $Ca[UO_2PO_4]_2 \cdot 6H_2O$, measured in transmission mode and at ambient temperature. In this structure, the uranium atom is coordinated to two opposing axial oxygen atoms and to four equatorial atoms in a tetragonal bipyramidal arrangement.

In order to tilt the sample along α, an uniaxial goniometer was used. EXAFS measurements were taken at $\alpha = 0°$, 15°, 35° 55° and 75° (Fig.1). For the first fit the spectrum collected at the magic angle (35°) was chosen. The coordination numbers were fixed to the crystallographic values ($N_{eff} = N_{cryst}$) and S_0^2 was fixed to 1. Free fit parameters were the distances U-O_{ax} and U-O_{eq}, the associated Debye-Waller factors σ^2 and ΔE. For all other angles N_{eff} was fitted, while σ^2 were fixed at the values determined for the magic angle. The fit results for the coordination numbers N_{eff} in comparison to the theoretical values according equation (3) are shown in Fig. 2. The figure shows an agreement between experimental data and theory besides a small systematic deviation resulting proba-

bly from fixed Debye-Waller factors. The polarization dependence at the U L_1 edge is significant stronger than that observed at the U L_3 edge (see part 2).
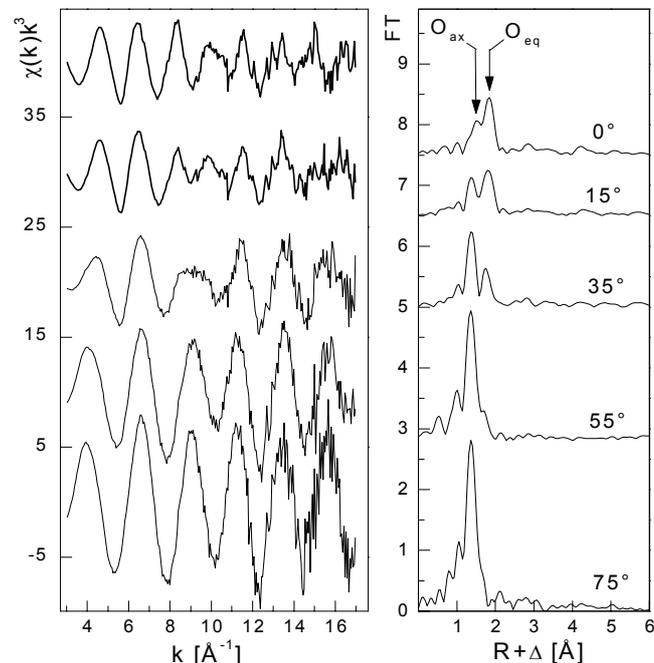
Fig. 1: U L_1-edge EXAFS spectra and their Fourier transforms at different angles α.
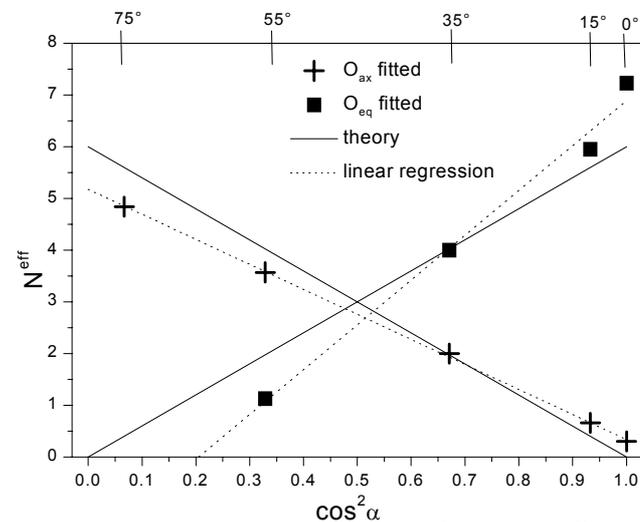
Fig. 2: Angular dependence of N_{eff}^{Oax} and N_{eff}^{Oeq} determined at the U L_1-edge in comparison with the theory.

References
/1/ Stöhr, J. et al., Phys. Rev. B **27** 5146 (1983)
/2/ Benfatto, M. et al., Phys.Rev. B **39** 1936 (1989)
/3/ Citrin, P.H., Phys. Rev. B **31** 700 (1985)
/4/ Pettifer, R.F. et al. Phys. Rev. B **42** 37 (1990)
/5/ Manceau, A. et al. Phys. Chem. Min. 347 (1998)

POLARIZATION DEPENDENT EXAFS. PART 2: URANIUM L_3 EDGE

C. Hennig, A. Scheinost

The polarization dependence of the U L_3 edge EXAFS was investigated using $Ca[UO_2PO_4]_2 \cdot 6H_2O$.

The polarization dependence of U L_1 edge EXAFS spectra is relatively simple, since the photoelectron is excited from a ground state s (l = 0) to one excited state (l = 1). By contrast, the polarization dependence is more complicated at the L_2 and L_3 edges, where the photoelectron is excited from p ground state to the final states s (l = 0) and d (l = 2). The EXAFS expression of L_2 and L_3 edges comprises here pure s, pure d and coupled s-d states /1/. Defining c as the ratio between the radial dipole matrix elements M_{01} and M_{21} coupling the initial $2p$ wave function with the $l = 0$ and $l = 2$ final states, the coordination number can be expressed as a sum of three effective partial coordination numbers /2/:

$$N_{eff}^d(\theta) = 0.5 \left[\frac{2}{2+c^2} \right] \sum_{i=1}^N (1 + 3|\vec{\varepsilon} \cdot \vec{r}|^2) \qquad (1)$$

$$N_{eff}^s = 0.5 \left[\frac{c^2}{2+c^2} \right] \qquad (2)$$

$$N_{eff}^{sd}(\theta) = \left[\frac{2c}{2+c^2} \right] \sum_{i=1}^N (1 - 3|\vec{\varepsilon} \cdot \vec{r}|^2) \qquad (3)$$

The value c is relatively independent of k and has been approximated to 0.2 for elements with $Z > 20$ /3/. Using c = 0.2 in eq. 1-3 and neglecting the N_{eff}^s term the expression can be approximated according /2/ by:

$$N_{eff}(\theta) = \sum_{i=1}^N (0.7 + 0.9|\vec{\varepsilon} \cdot \vec{r}|^2) \qquad (4)$$

Measurements at the U L_3 edge (Figure 1) were taken under the same conditions as at the U L_1 edge (see part 1). The spectra were fitted using the main N^d part only, whereas the N^s and N^{sd} terms were considered negligible. Phase and amplitude functions were calculated using FEFF 8.20. The spectrum at the magic angle was fitted with fixed coordination numbers and S_0^2, the fits at the other angles α were performed by fixing σ^2 to the values obtained at the magic angle.

The distances (Table 1) show a polarization dependence indicating that the phase function has also to be considered as a function of θ.

Tab. 1: Fit results for the U-O distances at the L_3 edge

α [°]	0	15	35	55	75
O_{ax} [Å]	1.75	1.77	1.79	1.80	1.80
O_{eq} [Å]	2.29	2.29	2.28	2.26	2.24

Figure 2 shows the fit results for the coordination numbers N_{eff} in comparison to the theoretical values according eq. 4. It is clearly visible, that the polarization dependency at the L_3 edge is less pronounced than that of the L_1 edge. The dominant contribution at the L_3 edge, N_{eff}^d, running with $1 + 3cos^2\theta$, has a similar angle dependence as N_{eff} at the L_1 edge but its

influence is attenuated by the N_{eff}^{sd} cross term running with $1 - 3cos^2\theta$ in the opposite direction. Consequently for studies of polarization dependence one should favor measurements at the U L_1 edge. Otherwise, the use of the L_3 edge seems to be more preferable for diluted samples due to the higher signal intensity /4/.
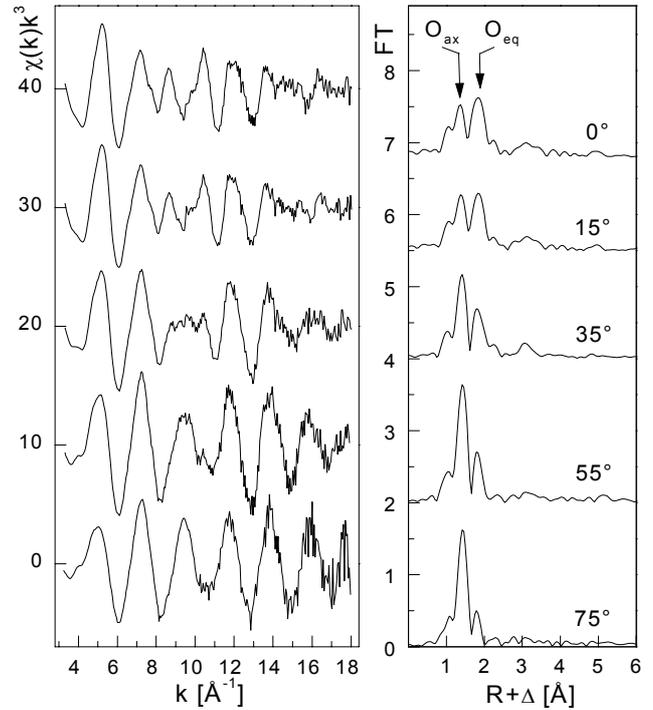
Fig. 1: U L_3-edge EXAFS spectra and their Fourier transforms at different angles α.
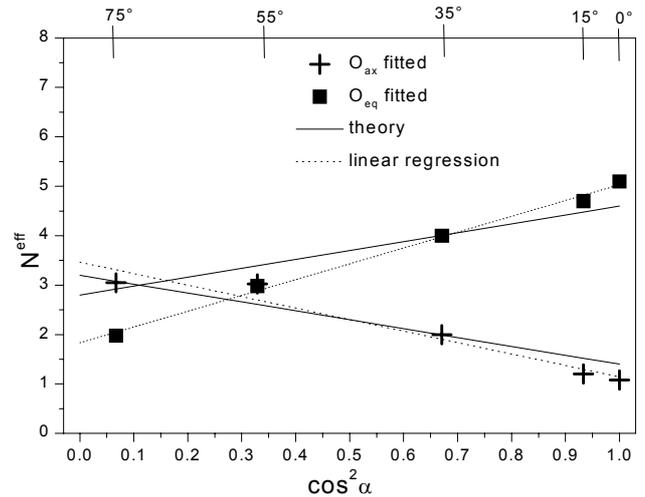
Fig. 2: Angular dependence of N_{eff}^{Oax} and N_{eff}^{Oeq} determined at the U L_3-edge in comparison with the theory.

References
/1/ Stöhr, J. et al., Phys. Rev. B **27,** 5146 (1983)
/2/ Citrin, P.H., Phys. Rev. B **31,** 700 (1985)
/3/ Teo, B.K., J. Am. Chem. Soc. **101,** 2815 (1979)
/4/ Hudson, E.A., Clay & Clay Min. **47,** 439 (1999)

WAVELET ANALYSIS OF EXAFS DATA – RESOLUTION PROPERTIES OF THE MORLET WAVELET

H. Funke, M. Chukalina[1]

[1]Institute of Microelectronics Technology RAS, Chernogolovka, Russia

The Morlet wavelet (MW) is a mother wavelet very suited for the analysis of Extended X-Ray Absorption Fine Structure (EXAFS) data. We determined some relevant resolution properties of the MW.

The choice of the mother wavelet is the first crucial point for any application of wavelets. This difficulty (and at the same time the richness of the method) arises, because wavelets are built from a wide and flexible class (the function class I²) of window functions $\psi(k)$ with zero mean: $\int \psi(k)dk = 0$.

For EXAFS data analysis we have chosen the complex MW /1/, see figure 1. The selection of the MW has two reasons. First, its structure is similar to an EXAFS signal, since the wavelet consists of a slowly varying amplitude term and a rapidly oscillating phase term. Second, the formal mathematical description of the wavelet analysis can be treated in analogy to the Fourier analysis.

The MW is obtained by taking a complex sine wave (like in the Fourier transform (FT)), and by confining it with a Gaussian (bell-shaped) envelope.

$$\psi(k) = e^{i\eta k} \cdot \frac{e^{-k^2/2\sigma^2}}{\sqrt{2\pi\sigma}}. \tag{1}$$

The parameter η is the frequency of the sine and cosine functions, determining how many oscillations of the sine wave are covered by a Gaussian envelope with the half width σ=1.
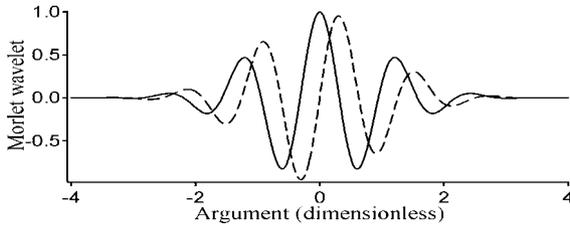
Fig. 1: Real (full line) and imaginary (dashed line) part of the MW for η=5 and σ=1.

Similar to a Gaussian normal distribution, where the information uncertainty is described by the half-width σ², the WT distributes the information of the signal over some r-k cells, often called Heisenberg box /2,3/. The width of this cells is defined by the 2nd moments of the wavelet, par example in reference to k:

$$\Delta_\psi^2 = \frac{1}{\|\psi\|^2} \int_{-\infty}^{+\infty} k^2 |\psi(k)|^2 \, dk, \; with$$

$$\|\psi\|^2 = \int_{-\infty}^{+\infty} |\psi(k)|^2 \, dk \tag{2}$$

Both widths (r and k) of the cells depend on the chosen wavelet. The resolution properties of the WT are determined by the size of the corresponding uncertainty cell.

For the MW (1) the Heisenberg box has the form:

$$\left[k - \frac{\eta\sigma}{\sqrt{2}r}, k + \frac{\eta\sigma}{\sqrt{2}r}\right] \times \left[r - \frac{r}{\sqrt{2}\eta\sigma}, r + \frac{r}{\sqrt{2}\eta\sigma}\right] \tag{3}$$

From relation (3) follows that the $k - r$ window is narrowed in the k space for large values of r and is expanded for small r. The resolution in the r space decreases with increasing r. The Heisenberg uncertainty condition $\Delta_k \Delta_r \geq 1/2$ (see formula 3.2.17 /2/) is fulfilled by $\Delta_k \Delta_r = 1/2$. Therefore, the Morlet parameters η and σ determine the resolution in k and r. Figure 2 shows two typical uncertainty cells with the centers (k=2.5, r=4) and (k=8, r=1.3). The surface of both cells is equal.
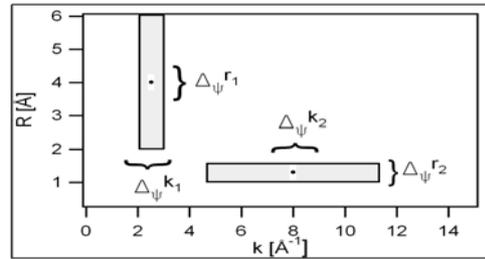
Fig. 2: Two typical uncertainty cells (schematic).

To demonstrate qualitatively the effect of the described resolution properties to WT plots, the corresponding model function and their WT are plotted in figure 3. The MW parameters are η=7.5 and σ=0.5.
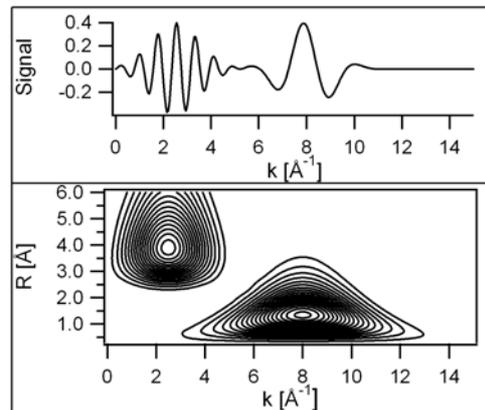
Fig. 3: Model function with distances r_1=4.0 and r_2=1.3 centered at k=2.5, k=8.0 and the WT.

The qualitative knowledge about the behavior of the uncertainty boxes is indispensable for a deeper understanding of the WT.

References

/1/ Funke, H. et al., *Physica Scripta*, accepted

/2/ Chui, C.K., *An Introduction to Wavelets*, Academic Press, San Diego, London (1992)

/3/ Louis, A.K., Maas, P., Rieder, A., *Wavelets: Theory and Applications*, Wiley, New York (1997)

APPLICATION OF THE WAVELET TRANSFORM TO THE ANALYSIS OF Zn-Al LAYERED DOUBLE HYDROXIDE EXAFS SPECTRA

H. Funke, A. Scheinost, M. Chukalina[1]

[1]Institute of Microelectronics Technology RAS, Chernogolovka, Russia

By applying the wavelet analysis of Extended X-Ray Absorption Fine Structure (EXAFS) spectra to a Zn-Al layered double hydroxide, we could unequivocally identify the presence of Al and Zn atoms at the same distance of approximately 3 Å from the central Zn atom.

Introduction

Layered double hydroxides (LDH) are a class of minerals hosting a wide range of divalent metal cations like Cr^{2+}, Ni^{2+}, Zn^{2+} (M^{2+}). Due to their relatively low solubility at circumneutral pH values, formation of such phases plays an important role in reducing the toxicity of metals in soils, sediments and nuclear waste repositories /1/.

LDH phases consist of layers of edge-sharing metal hydroxide octahedra, where up to 1/3 of the divalent cations are replaced by trivalent Al^{3+}. The resulting net positive layer charge is compensated for by hydrated anions in the interlayer space /2/. Due to their low crystallinity and turbostratic layer structure, LDH are difficult to identify by XRD in environmental media. While EXAFS is much better suited for this purpose, the discrimination from more soluble, simple hydroxide phases is hindered, since the backscattering wave from Al^{3+} is masked by destructive interference with backscattering waves from the heavier M^{2+} /1/.

Our previous theoretical studies have shown that examination of EXAFS spectra by wavelets may reveal the identity of two different atoms at the same distance from an excited atom center /3/.

Hence, we tested the wavelet approach to resolve the Zn and Al atoms in the structure of Zn-Al LDH.

Experimental

The Zn K-edge EXAFS spectrum of a Zn-Al LDH was collected in transmission mode at 20 K on ROBL/ESRF. The spectrum and its FT are shown in figure 1. The FT shows four dominant shells, which can be assigned to the oxygen coordination sphere (O), and to the first, second and third spheres of metal (Zn, Al) neighbors.
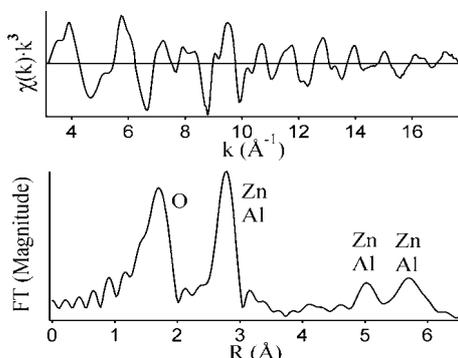
Fig. 1: Zinc K-edge EXAFS function and its FT.

Wavelet analysis

Figure 2 shows the overview wavelet with the Morlet parameter η =15. The two peaks at r = 1.7 and 2.8 Å correspond to the oxygen coordination shell and the first (Zn, Al) shell, respectively.
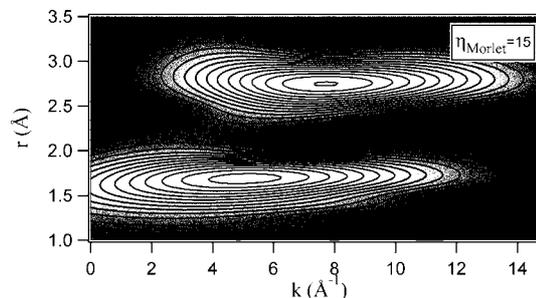
Fig. 2: Overview WT

The detail map with the optimized Morlet parameter η =5.5 in the interval 2.4< r <3.0 Å resolves two maxima at r =2.6 Å, one at k =5.2 Å^{-1} and one at k =7.6 Å^{-1}, thereby clearly indicating the presence of Zn and Al in the first metal shell (Fig. 3).
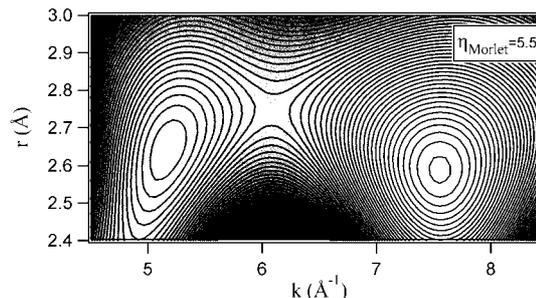
Fig. 3: High resolution WT

Based on the information of the WT, we fitted the FT between 1.0 and 3.5 Å using theoretical paths calculated with FEFF7 (Table 1).

Tab. 1: Fit parameters for Zn-Al LDH

Path	N	R (Å)	σ^2 (Å^2)	ΔE_0 (eV)
Zn-O	6.2	2.09	0.0069	1.6
Zn-Zn	3.7	3.08	0.0051	1.6
Zn-Al	2.8	3.06	0.0064	1.6
Zn-0	4.7	3.56	0.0042	1.6

To the best of our knowledge, this is the first time that both a 3d-metal atom and Al could be fitted together to the first metal shell of LDH phases without constraining Debye-Waller factors nor distances.

This application of the WT to experimental data of a Zn-Al LDH demonstrate the potential of wavelets for distinguishing different atoms at similar distances.

References

/1/ Scheinost, A.C. et al., Geochim. Cosmochim. Acta **63**, 3193 (1999)

/2/ D'Espinose, J.B. et al., Amer. Chem. Soc., **117**, 11471 (1995)

/3/ Funke, H. et al., Report FZR-343, p. 45 (2002); Report FZR-373, p. 43 (2003)

Reactive Transport of Actinides / Radionuclides

URANIUM RETARDATION IN A CHLORITE-QUARTZ-FERRIHYDRITE COLUMN

T. Arnold, B. Hollenbach, D. Grambole[1], F. Herrmann[1]
[1]Institute of Ion-beam Physics and Materials Research

Mikro-PIXE (Particle induced x-ray emission) measurements revealed that adsorbed uranium is heterogeneously distributed within a chamosite chlorite sample through which in a column experiment uranium was flowing through. The determined uranium concentrations ranged from 524 to 1740 ppm.

Introduction

The transport of heavy metal in nature is still not completely understood. Precipitation and adsorption reactions among other processes leads to the retardation of heavy metals and thereby prevent its migration into the adjacent environment. By better understanding such processes cheap and effective geological material may be used as barrier material to prevent the spreading of contaminants.

Experimental

A solution containing 5×10^{-6} M uranium was given at a flow rate of 42 mL/d on a stratified column. The column was approximately 20 cm in length and 3 cm in diameter and was composed of a thin layer, approximately 1.5 cm thick) of chamosite chlorite (grain size 200 to 630 µm) and a thick layer of about 18.5 cm quarz sand (grain size 200 to 630 µm), which was previously coated with ferrihydrite. A vacuum pump was applied at the bottom of the column to generate a light negative pressure to ensure that the column was operated at unsaturated conditions. Every day a sample of about 40 to 45 ml solution was collected at the bottom of the column and analysed for the major cations. After 147 days the experiment was stopped and the column was cut into 40 evenly thick discs which were analysed by acid digestion for their elemental concentration. Disc number 40 represents the top and disc number 1 the bottom of the column.

In addition, two discs, number 40 (chlorite) and 37 (quartz coated with ferrihydrite) were prepared for mikro-PIXE measurements by embedding the sample in epoxy resin and polish the surface.
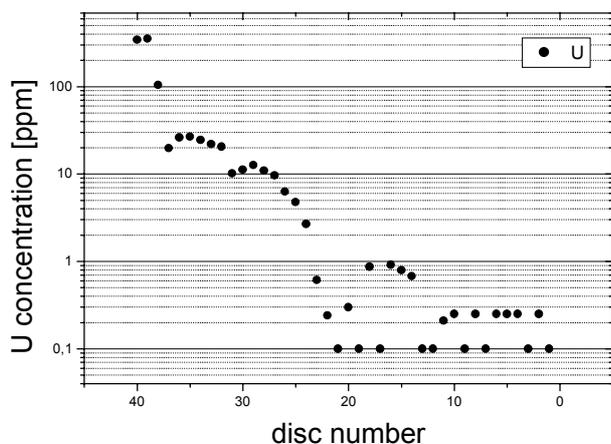
Fig. 1: Uranium distribution in the column.

Results

Figure 1 shows that all of the uranium added to the column was retarded and no uranium was detected in the eluate. Especially the top three layers, which were composed of chamosite chlorite, are characterized by high accumulations of uranium. Within the subsequent layers of quartz coated with ferrihydrite the uranium concentration decreases and becomes from in disc number 23 downwards insignificant, i.e. before half of the length of the column was flown through.

Additional micro-PIXE mapping measurements conducted on disc number 40 showed that the retarded uranium is not homogeneously distributed within the chamosite chlorite. Regions with low Fe concentrations showed high uranium concentrations and vice versa.

low U conc.   high U conc.
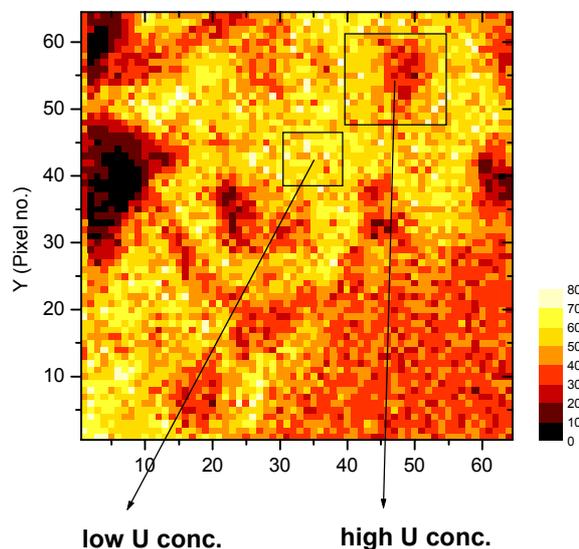
Fig. 2: Fe distribution within the chamosite chlorite in a region of 250 µm × 250 µm. Two areas with low and high U concentrations are shown.

Fig. 2 shows two areas with different uranium concentration. The region with low concentration had 524 ppm uranium and the value for the area with the high concentration was 1740 ppm. Micro-Pixe measurements failed for disc number 37 since the uranium concentrations were below the detection limit. Our results indicate that the uranium retardation within the chlorite cannot exclusively be attributed to adsorption reactions. It seems that the precipitation of a uranium containing phase may also have contributed and is responsible for a heterogeneous distribution within the chlorite.

Acknowledgments

MIGRATION OF URANIUM (IV)/(VI) IN THE PRESENCE OF HUMIC ACIDS IN QUARTZ SAND

J. Mibus, S. Sachs, C. Nebelung, G. Bernhard

The migration of U(IV) and U(VI) in quartz sand in presence of humic acid was investigated by column experiments. Humic acid has a mobilizing effect on the U(VI) transport. Strong indications were found for a similar influence on U(IV). We found that in presence of humic acid both redox species differ in their eluate recoveries by approximately 25 %.

The reliable long-term risk assessment for potential nuclear waste repositories requires detailed knowledge on the migration behavior of actinides in natural aquifers. The colloidal behavior of humic acids (HA) together with their reducing and complexing properties for metal ions may cause an effective transport mechanism for actinides. This work focuses on the influence of HA on the U(IV)/(VI) transport in quartz sand which was studied by column experiments.

Columns (length 25 cm, diameter 5 cm) filled with annealed fine sand were conditioned under N_2 atmosphere with a 0.1 M $NaClO_4$ solution (CO_2-free, pH 7.5) at a Darcy velocity of $(3.6\pm0.5)\cdot10^{-6}$ m s^{-1} for 3 weeks. We studied the transport of U(VI) in HA absence and of U(IV) / U(VI) in HA presence. ^{14}C-labeled HA type M42 /1/, ^{234}U and HTO were used as tracer. U(IV) was prepared by electrochemical reduction. Redox speciation was proven by TTA solvent extraction. Breakthrough curves (BTC) were measured by liquid scintillation (LS). LS data were corrected for ^{232}U daughter nuclides. The concentrations of the reactive substances are listed in Tab. 1. Details are given in /1/.

Tab. 1: Experimental conditions and results.

Exp.	HA (mg/L)	U (mol/L)	Species	R_f	R_{eluate}
1	49.9	-	HA	1.02±0.02	0.91±0.01
2	50.3	-	HA	1.02±0.02	0.92±0.01
3	-	$1.1\cdot10^{-5}$	U(VI)	2.09±0.10	0.43±0.02
4	49.9	$1.0\cdot10^{-5}$	HA	1.05±0.02	0.85±0.01
			U(VI)	1.19±0.02	0.80±0.01
5	50.0	$1.0\cdot10^{-6}$	HA	1.04±0.02	0.90±0.01
			U(VI)	1.11±0.02	0.90±0.06
			U(IV)	1.07±0.02	0.66±0.05

The retardation factors (R_f, Tab. 1) for HA indicate that there is no significant interaction between HA and quartz. The recovery (R_{eluate}, Tab. 1) for HA points to irreversible filtration effects.
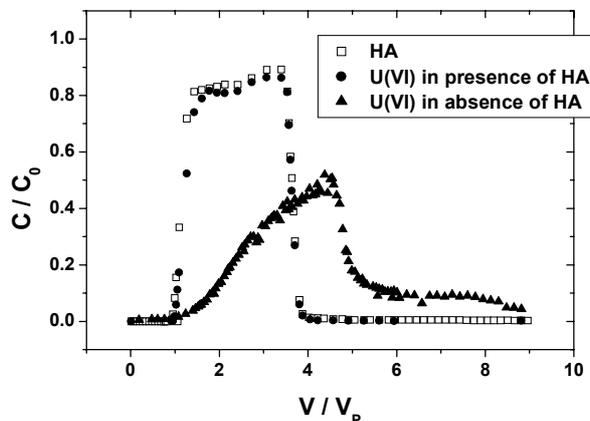
Fig. 1: Breakthrough curves of HA and U(VI).
C: measured and C_0: initial concentration.
V: effluent volume, V_P: effective pore volume.

The U(VI) migration in absence of HA (Fig. 1) is characterized by a kinetically controlled strong retardation which is reflected in the shape of the BTC and the R_f > 1. The low U(VI) recovery is ascribed to sorption processes. However, in HA presence the U(VI) transport is accelerated and the recovery is increased (Fig. 1). Both, HA and U(VI), exhibit slightly different R_f and R_{eluate} values caused by association/dissociation processes in the system HA-U(VI)-quartz. Considering the results reported in /2/, it can be assumed that these processes are kinetically controlled.
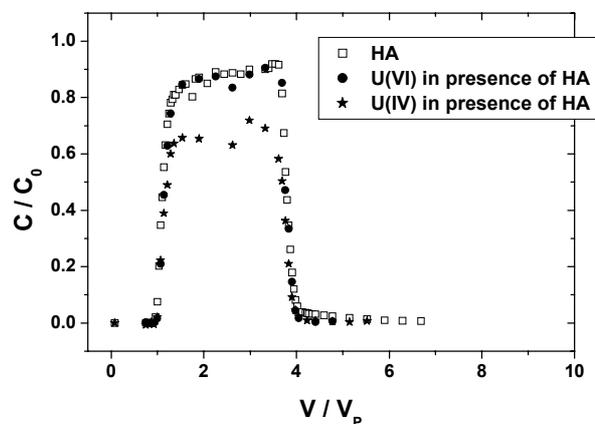
Fig. 2: Breakthrough curves of HA, U(IV) and U(VI).

The portion of U(IV) and U(VI) in the starting solution amounts to 8 % and 92 %, respectively. This ratio was stable over the duration of the experiment and was also found in the effluent solutions, thus indicating that no oxidation occurred in the column. Fig. 2 shows the BTC for HA, U(IV), and U(VI). As with the case of U(IV), the association/dissociation reactions control the transport behavior in presence of HA (R_f > 1). In Exp. 5 R_{eluate} of U(VI) and HA agree very well. This fact refers to a HA bound U(VI) transport. The lower U(IV) recovery points to a stronger interaction with the quartz sand and thus to a more distinct immobilization. Nevertheless, there are strong indications that HA has a mobilizing effect on the U(IV) transport.

It can be concluded that HA affects the migration of both U(IV) and U(VI). In presence of HA U(VI) is significantly mobilized. A similar effect is supposed for U(IV). However, both redox species exhibit a different migration behavior, which is mainly reflected in the different recoveries.

References
/1/ Sachs, S. et al. Report Project No. 02E9299 (2003)
/2/ Artinger, R. et al. J. Contam. Hydr. **58,** 1 (2002)

DETERMINATION OF DIFFUSION PARAMETERS IN COMPACTED KAOLINITE

J. Mibus, R. Küchler[1], M. Lambarki[2]
[1]Institute of Safety Research
[2] RWTH-Aachen University, Department of Engineering Geology and Hydrogeology, Aachen, Germany

Effective transport parameters of compacted kaolinite were determined in a diffusion experiment. An effective diffusion coefficient and a porosity of $(3.6 \pm 0.2) \cdot 10^{-10}$ m^2 s^{-1} and 0.60 ± 0.02, respectively, were found. The results are comparable to those of natural sediments. However, differences in the sorption properties are to be expected.

Clay minerals are main components of many soils, sediments, pelitic rocks, as well as fracture filling material in crystalline rocks. Furthermore, clays are used in geo-engineering, particularly to design hydraulic and geochemical barriers in contaminated sites, landfills or underground repositories for toxic or nuclear wastes. Due to the low permeability of clay molecular diffusion is the main transport mechanism of dissolved or colloidal substances at natural hydraulic gradients. This process has to be studied to assess the long-term behavior of geo-engineered barrier systems.

In order to determine effective transport parameters in kaolinite a diffusion experiment with a conservative tracer was performed. Kaolinite from Hirschau (Germany) was compacted to a dry density of $\rho = 1.1$ g cm^{-3}, filled in a diffusion cell (cross sectional area $A = 78.6$ cm^2, layer thickness $L = 2.1$ cm) and fixed between two filter plates as shown in Fig. 1.
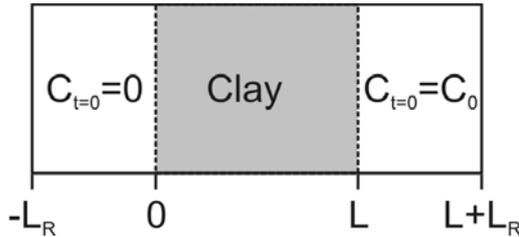
Fig. 1: Schematical set-up of the diffusion experiment

The through-diffusion of tritiated water (HTO) at room temperature was observed using a tracer reservoir of 180 mL with a starting activity of $C_0 = 2.2 \cdot 10^3$ Bq/mL and a tracer free reservoir of the same volume. Both sides were allowed to balance by diffusion and were measured periodically by liquid scintillation counting.

The transient diffusion process is described by Fick's second law

$$\frac{\partial C}{\partial t} = D \frac{\partial^2 C}{\partial x^2} \qquad (1)$$

where C is tracer concentration or activity, t is time, x is distance, and D is the molecular diffusion coefficient. An analytical solution was derived using an eigenfunction expansion to estimate transport parameters. The initial condition for the clay plug is

$$C(0 \le x \le L, t = 0) = 0 \qquad (2)$$

Two variable boundary conditions account for the continuously changing concentrations. For example, for the high concentration side applies

$$C(L,t) = C_0 - \frac{\varepsilon D}{L_R} \int_0^t \frac{\partial C(x,\tau)}{\partial x}\bigg|_{x=L} d\tau \qquad (3)$$

where ε is the porosity of the porous medium. An analogue term exists for the low concentration side.

The measured HTO concentrations as function of time are depicted in Fig. 2.
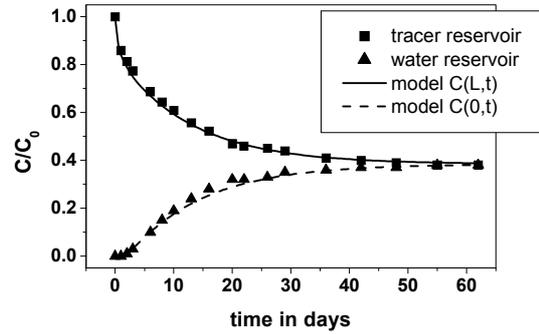
Fig. 2: HTO concentration in both reservoirs versus time

An effective diffusion coefficient $D_e = (3.6 \pm 0.2) \cdot 10^{-10}$ m^2 s^{-1} and a porosity $\varepsilon = 0.60 \pm 0.02$ were determined from the concentration curves. They are in the range of natural clayey sediments /1/. The dependence of D_e from ε and D_0, the diffusion coefficient in free water, is described by the empirical relation $D_e = D_0 \cdot \varepsilon^m$ where m is the cementation factor (cf. /2/). Our experimental results lead to m = 3.5. In consolidated pelitic rocks m ranges between 1.5 and 3.0 /2/ whereas in marine sediments a value of 3.0 was found /1/. This minor difference may origin from compositional and granulometrical properties. Furthermore, a technologically compacted material is likely to offer a texture different from diagenetically matured sediments.

A comparison with long-lasting stationary diffusion experiments using reactive tracers and natural sealing material (loess loam) is of practical relevance. Here D_e was found to be 2.47, 3.04, and $4.14 \cdot 10^{-10}$ $m^2 s^{-1}$ for Cu, Pb, and Zn, respectively. These results indicate that the diffusion parameters in the natural and the engineered barrier material are in the same order of magnitude. However, due to the mineralogical composition it is to be expected that both substances exhibit different sorption properties. For performance assessment both processes, diffusion and sorption, have to be taken into account.

References

/1/ Iversen, N. et al., Geochim. Cosmochim. Acta **57**, 571-578 (1993)
/2/ Van Loon, L.R. et al., Appl. Geochem. **18**, 1653-1662 (2003)

GAS AND VACUUM THERMOCHROMATOGRAPHY OF FISSION PRODUCTS

O.Arndt[1], I. Dillmann[1], K. Eberhardt[1], B. Eichler[2], A. Hohn[2], S. Hübener[2], C. Jost[1], U. Köster[3], K.-L. Kratz[1], H.J. Maier[4], M. Mendel[1], K. Peräjärvi[3], B. Pfeiffer[1], N. Trautmann[1]

[1]Universität Mainz, Institut für Kernchemie, Mainz, Germany; [2]Paul Scherrer Institut, Labor für Radio- und Umweltchemie, Villigen, Switzerland; [3]CERN, ISOLDE, Genève, Switzerland; [4]Ludwig-Maximilians-Universität München, Germany

The chemical behavior of $^{249}Cf(n_{th},f)$ fission products was studied on Ti, Fe, Ni, Nb, Mo, Ta, Re, quartz and sapphire surfaces at the TRIGA Mainz using gas and vacuum thermochromatography. In future a quartz transfer line could be used to retain Cs and In isobars in the on-line separation of Cd beams at ISOLDE.

Introduction

In recent years very neutron-rich isotopes of silver (^{129}Ag [1]), cadmium (^{133}Cd [2]) and indium (^{135}In [3]) have been identified by resonant laser ionization at ISOLDE and their half-lives were measured by detection of beta-delayed neutrons. However, detailed βγ spectroscopy is still hampered by the omnipresent background of huge amounts of surface ionized cesium and indium (in the case of Ag and Cd) isobars. In the present study we investigated various surfaces on their suitability to retain these elements, and, hence, supplement the selectivity of the resonant laser ionization by a chemical pre-separation. Earlier studies [4] proposed quartz surfaces for this purpose.

Experimental

The emphasis of this experiment was on Ag, Cd and In. Hence a ^{249}Cf target was chosen to optimize the production of suitable radiotracers (^{112,113}Ag, ^{117g,m}Cd and ^{117g,m}In) in thermal-neutron-induced fission. The fission products were produced at the TRIGA reactor in Mainz, extracted via a helium gas jet on carbon clusters and collected on a quartz filter. After 1-2 h collection time and ca. 1 h delay to let short-lived nuclides decay, a gamma assay of the filter was made. Radioisotopes of the elements Sr up to the lanthanides were detected. Then the filter was either inserted directly into a quartz or sapphire thermochromatography (TC) column or, for the study of metal surfaces, distilled in a steep temperature gradient (from 1400 K to room temperature within few cm) onto a Nb catcher foil. The piece containing the activity of interest was then inserted into the TC column. The latter consisted either of a bare quartz or sapphire tube with 3 mm inner diameter or of a rolled metal foil inserted into a quartz tube respectively. The samples were heated for 30 minutes in a negative temperature gradient of about –20 K/cm to maximum temperatures of 1325, 1375, 1475 or 1875 K respectively, either in a flow (25 or 50 cm^3/min) of pure He, in a reducing atmosphere of 93% He/7% H$_2$ or after evacuation to vacuum ($<10^{-4}$ mbar). After cooling, the tubes were cut into pieces and the activity distribution was determined with an HPGe detector. The sapphire tube was not cut, but scanned through a Pb collimator.

Results

The distribution of Ag, Cd, In and Cs along a quartz column is shown in Fig. 1 as an example. Cs was not released from the quartz filter even when heated up to 1875 K. In was found to be slightly more volatile on quartz surfaces than Ag. Without H$_2$ addition a second In peak was observed at higher temperatures, proba-

bly corresponding to indium oxide produced from oxygen impurities. As expected, Cd was not retained on any of the surfaces under study, but left the heated zone.
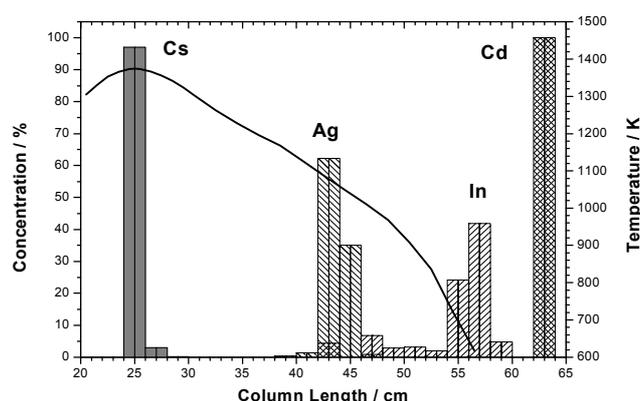
Fig. 1: The deposition of Ag, Cd, In and Cs on quartz surfaces.

Outlook

The results suggest to use for future ISOLDE experiments with Cd beams a quartz transfer line to connect the target to the resonance ionization laser ion source. Hence, background from Cs isobars and of short-lived In isotopes could be suppressed by a large factor.

The same Cs suppression could be achieved when aiming for Ag or In isotopes, but the delay of the latter on a quartz surface will cause excessive delay losses for very short-lived isotopes, hence the Cs retention by a sapphire surface (without temperature-limiting quartz) needs be studied.

References

[1] Kratz, K.L. et al., Hyperfine Interactions **129**, 185 (2000)

[2] Arndt, O. et al., Report IKMz 2003-1, A15., Jahresbericht 2002

[3] Dillmann, I. et al., Eur. Phys. J. **A13**, 281 (2002)

[4] Westgaard, L. et al., J. Inorg. Nucl. Chem. **31**, 3747 (1969)

II. PUBLICATIONS, LECTURES, POSTERS, PH.D. THESES, DIPLOMA, PATENTS, AWARDS

PUBLICATIONS

Books, Journals

Baumann, N., Arnold, T., Geipel, G., Bernhard, G.
TRLFS-investigations of uranium(VI) sorbed on gibbsite and ferrihydrite
Beiheft zum European Journal of Mineralogy **15**, (2003)

Billard, I., Ansoborlo, E., Apperson, K., Arpigny, S., Azenha, M. E., Birch, D., Bros, P., Burrows, H. D., Choppin, G., Coustin, L., Dubois, V., Fanghänel, Th., Geipel, G., Hubert, S., Kim, J. I., Kimura, T., Klenze, R., Kronenberg, A., Kumke, M., Lagarde, G., Lamarque, G., Lis, S., Madic, Ch., Meinrath, G., Moulin, Chr., Nagaishi, R., Parker, D., Planque, G., Scherbaum, F., Simoni, E., Sinkov S., Viallesoubranne, C.
Aqueous Solutions of U(VI) as Studied by Time-Resolved Emission Spectroscopy (TRES) : A Round-Robin Test
Applied Spectroscopy **57**, 1027 (2003)

Geipel, G., Vulpius, D., Acker, M., Bernhard, G., Fanghänel, Th., Nitsche, H.
A System for Time-Resolved Fluorescence Spectroscopy Using Ultrashort Laser Pulses as Excitation Source for Studying the Complexation of Metals with Organic Ligands
Spectrochimica Acta A **60**, 417-424 (2003)

Geraedts, K., Bruggeman, C., Maes, A., Van Loon, L.R., Roßberg, A., Reich, T.
Evidence for the existence of Tc(IV) - humic substance species by X-ray absorption near-edge spectroscopy
Radiochimica Acta **90**, 879-884 (2002)

Günther, A., Bernhard, G., Geipel, G., Reich, T., Roßberg, A., Nitsche, H.
Uranium Speciation in Plants
Radiochimica Acta **91**, 319-328 (2003)

Hennig, C., Reck, G., Reich, T., Roßberg, A., Kraus, W., Sieler, J.
EXAFS and XRD investigations of zeunerite and meta-zeunerite
Zeitschrift für Kristallographie **218**, 37-45 (2003)

Hofmann, T., Baumann, T., Bundschuh,T., von der Kammer, F., Leis, A., Schmitt, D., Schäfer, T., Thieme, J., Totsche, K.U., Zänker, H.
Aquatische Kolloide I: Eine Übersichtsarbeit zur Definition, zu Systemen und zur Relevanz
Grundwasser **8**, 203-210 (2003)

Hofmann, T., Baumann, T., Bundschuh,T., von der Kammer, F., Leis, A., Schmitt, D., Schäfer, T., Thieme, J., Totsche, K.U., Zänker, H.
Aquatische Kolloide II: Eine Übersichtsarbeit zur Probenahme, Probenaufbereitung und Charakterisierung
Grundwasser **8**, 213-223 (2003)

Knechtenhofer, L.A., Xifra, I.O., Scheinost, A.C., Flühler, H., Kretzschmar, R.
Fate of heavy metals in a strongly acidic shooting-range soil: Small-scale metal distribution and its relation to preferential water flow
J. Plant Nutr. Soil Sci. **166**, 84-92 (2003)

Koban, A., Geipel, G., Bernhard, G.
Complex formation between uranium(VI) and α-D-glucose 1-phosphate
Radiochimica Acta **91**, 393 (2003)

Martin, P., Ripert, M., Petit, T., Reich, T., Hennig, C., D´Acapito, F., Hazemann, J.L., Proux, O.
A XAS study of the local environments of cations in (U,Ce)O$_2$
J. Nuclear Mat. **312**, 103-110 (2003)

Merroun, M.L, Benchekroun, K., Arias, J.M., Gonzalez-Munoz, M.T.
Lanthanum fixation by *Myxococcus xanthus*: cellular location and extracellular polysaccharide observation
Chemosphere **52**,113-120 (2003)

Merroun, M.L., Geipel, G., Nicolai, R., Heise, K.H., Selenska-Pobell, S.
Complexation of uranium (VI) by three eco-types of *Acidithiobacillus ferrooxidans* studied using time-resolved laser-induced fluorescence spectroscopy and infrared spectroscopy
Biometals **16**, 331-339 (2003)

Merroun, M., Hennig, C., Roßberg, A., Reich, T., Selenska-Pobell, S.
Characterization of U(VI)-*Acidithiobacillus ferrooxidans* complexes using EXAFS, transmission electron micros-copy, and energy-dispersive X-ray analysis
Radiochimica Acta **91,** 583-591 (2003)

Moll, H., Geipel, G., Reich, T., Bernhard, G., Fanghänel, Th., Grenthe, I.
Uranyl(VI) Complexes with Alpha-substituted Carboxylic Acids in Aqueous Solution
Radiochimica Acta **91**, 11-20 (2003)

Neuweiler, F., d'Orazio, V., Immenhauser, A., Geipel, G., Heise, K.H., Cocozza, C., Miano, T.M.
Fulvic acid-like organic compounds control nucleation of marine calcite under suboxic conditions
Geology 681-684 (2003)

Pollmann, K., Wray, V., Hecht, H.J., Pieper, D.H.
Rational engineering of the regioselectivity of TecA tetrachlorobenzene dioxygenase for the transformation of chlorinated toluenes.
Microbiology **149**, 903-913 (2003)

Raff J., Soltmann U., Matys S., Schnorpfeil M., Böttcher H., Pompe W., Selenska-Pobell S.
Microbial bioremediation of uranium mining waste waters by using sol-gel ceramics
Chemistry of Materials **15(1)**, 240-244 (2003)

Richter, A., Brendler, V., Bernhard, G.
The mineral-specific thermodynamic sorption database RES^{3}T: Concept description, implementation, and application towards contaminated systems
Geochimica et Cosmochimica Acta **67,** A397(2003)

Roßberg, A., Reich, T., Bernhard, G.
Complexation of uranium(VI) with protocatechuic acid - application of iterative transformation factor analysis to EXAFS spectroscopy
Analytical and Bioanalytical Chemistry **376**, 631-638 (2003)

Schmeide, K., Sachs, S., Bubner, M., Reich, T., Heise, K.H., Bernhard, G.
Interaction of Uranium(VI) with Various Modified and Unmodified Natural and Synthetic Humic Substances Studied by EXAFS and FTIR Spectroscopy
Inorg. Chim. Acta **351**, 133-140 (2003)

Soltmann, U., Raff, J., Selenska-Pobell, S., Matys, S., Pompe, W., Böttcher, H.
Biosorption of heavy metals by sol-gel immobilized *Bacillus sphaericus* cells, spores and S-layers
Journal of Sol-Gel Science and Technology **26**, 1209-1212 (2003)

Vallet, V., Moll, H., Wahlgren, U., Szabó, Z., Grenthe, I.
Structure and Bonding in Solution of Dioxouranium(VI) Oxalate Complexes: Isomers and Intra-Molecular Ligand Exchange
Inorganic Chemistry **42**, 1982-1993 (2003)

Walter, M., Arnold, T., Reich, T., Bernhard, G.
Sorption of uranium(VI) onto ferric oxides in sulfate-rich acid waters
Environ. Sci. Technol. **37**, 2898-2904 (2003)

Yakushev, A.B., Zvara, I., Oganessian, Yu.Ts., Belozerov, A.V., Dmitriev, S.N., Eichler, B., Hübener, S., Sokol, E.A., Türler, A., Yeremin, A.V., Buklanov, G.V., Chelnokov, M.L., Chepigin, V.I., Gorshkov, V.A., Gulyaev, A.V., Lebedev, V.Ya., Malyshev, O.N., Popeko, A.G., Soverna, S., Szeglowski, Z., Timokhin, S.N., Tretyakova, S.P., Vasko, V.M., Itkis, M.G.
Chemical Identification and Properties of Element 112
Radiochimica Acta **91**, 433-439 (2003)

Zänker, H., Richter, W., Hüttig, G.
Scavenging and immobilization of trace contaminants by colloids in the waters of abandoned ore mines
Coll. Surf. A: Physicochem. Eng. Aspects **217,** 21-31 (2003)

Proceedings, Reports

Buschmann, H.-J., Jansen, K., Schmeide, K., Richter, A.M., Keil, D., Praschak, D., Best, W.
Integrierter Umweltschutz in der Textilindustrie: Abtrennung von Uranylionen aus Sicker- und Grundwässern mit uranophilen Calixarenen
Abschlussbericht zum Verbundprojekt 0339916-0339919, Forschungszentrum Jülich GmbH (2003)

Geißler, A.
Molekulare Analyse der bakteriellen Diversität in Uranabraumhalden. Wissenschaftlich-Technische Berichte des
Report FZR-377, FZ Rossendorf (2003)

Merroun, M.L., Hennig, C., Roßberg, A., Funke, H., Selenska-Pobell, S., Reich, T.
EXAFS investigations of uranium complexes formed by different bacteria isolated from uranium mining wastes
Report FZR-364, FZ Rossendorf (2003) p.26-30

Moyes, L.N., Jones, M.J., Reed, W.A., Livens, F.R., Charnock, J.M., Mosselmans, J.F.W., Hennig, C., Vaughan, D.J., Pattrick, R.A.D.
Reactions of Neptunium with Mackinawite
ESRF Highlights 2002, 39-41 (2003)

Sachs, S., Heise, K.H., Bernhard, G.
Synthetic Humic Acid Model Substances with Specific Functional Properties for the Use in Complexation and Sorption Experiments with Actinides
Report FZKA 6800, FZ Karlsruhe (2003), p. 51-64

Sachs, S., Schmeide, K., Brendler, V., Heise, K.-H., Bernhard, G.
Untersuchung der Bildung und Verteilung von Huminsäure-Actiniden-Spezies im geochemischen System
Report FZKA-PTE 8, FZ Karlsruhe (2003), p. 257-265

Sachs, S., Schmeide, K., Brendler, V., Krepelová, A., Mibus, J., Geipel, G., Heise, K.H., Bernhard, G.
Investigation of the Complexation and the Migration of Actinides and Non-Radioactive Substances with Humic Acids under Geogenic Conditions. Complexation of Humic Acids with Actinides in the Oxidation State IV Th, U, Np
Final Report, BMWA Project No. 02E9299, Rossendorf, 2003

Scheinost, A.C., Kretzschmar, R., Pfister, S., Roberts, D.R., Sparks, D.L.
Chemical forms of zinc in a smelter-contaminated soil
Science Highlights of the NSLS **2003**, June 18, 2003

Schmeide, K., Sachs, S., Reich, T., Heise, K.H., Bernhard, G.
Determination of Structural Parameters for Th(IV), Np(IV), Np(V) and Pu(III) Humate Complexes by Means of XAFS Spectroscopy
Report FZKA 6800, FZ Karlsruhe (2003), p. 65-77

Schmeide, K., Geipel, G., Heise, K.H., Bernhard, G.
Migration Case Study: Uranium Mining Waste Rock Pile No. 250 in the Region Schlema/Alberoda (Saxony, Germany)
Report FZKA 6800, FZ Karlsruhe (2003), p. 79-98

Vejmelka, P., Lützenkirchen, K., Gompper, K., Nebelung, C. Baraniak, L.
Nuklidmigration im Deckgebirge des ERAM (DGL)
Abschlussbericht BfS-Auftrag 9M 212 230-62

LECTURES

Arnold, T.
Adsorption of uranium on mineral surfaces, in particular secondary Fe-Minerals
DFG Graduiertenkolleg 273, Uni Heidelberg
Heidelberg, Germany, 04.-05.12.2003

Arnold, T.
Untersuchungen zur Sorption von U(VI) auf geologischen Phasen
Institutsseminar Kernchemie Mainz
Mainz, Germany, 19.02. 2003

Arnold, T.
Untersuchungen zur Mineralauflösung von unterschiedlich alterierten Chloriten und deren Einfluss auf die Sorption von U(VI)
GDCh-Jahrestagung Chemie 2003, Fachgruppe Nuklearchemie
München, Germany, 06.-11.10.2003

Arnold, T.
Nachweis adsorbierter U(VI) Oberflächenspezies auf Muskovit mit TRLFS
GDCh-Jahrestagung Chemie 2003, Fachgruppe Nuklearchemie
München, Germany, 06.-11.10.2003

Baumann, N., Arnold, T., Geipel, G., Bernhard, G.
TRLFS-investigations of uranium(VI) sorbed on gibbsite and ferrihydrite
81. Jahrestagung der Deutschen Mineralogischen Gesellschaft
Bochum, Germany, 22.-25.09.2003

Bernhard, G.
Chemische Speziation von Uran und Transfer in Biosysteme
2. Sanierungskolloquium "Transfer von Schwermetallen und Radionukliden in Pflanzen"; Friedrich-Schiller-Universität Jena
Jena, Germany, 13.-14.10.2003

Bernhard, G.
Speziation des Urans in ausgewählten biologischen Systemen
Kolloquium Institut für Interdisziplinäre Isotopenforschung Leipzig
Leipzig, Germany, 02.07.2003

Brendler, V.
ACTINET - Towards a 6th Framework Proposal
3rd ACTINET Workshop
Avignon, France, 06.03.2003

Brendler, V.
ACTAF - Contributions to WP 1 and WP 2 by FZ Rossendorf
ACTAF Workshop
Karlsruhe, Germany, 24.06.2003

Brendler, V.
Pathways towards Recommended Data Sets for Sorption Modelling
4. Koordinierungsgespräch PSI-FZR
Villingen, Switzerland, 20.-21.10.2003

Brendler, V.
Modelle der Schadstoffausbreitung: Wechselwirkungen mit den fest-flüssig-Grenzflächen
Umweltkolloquium HTW Dresden
Dresden, Germany, 06.11.2003

Brendler, V.
Strategien und Konzepte für eine Thermodynamische Standard-Datenbasis - Sichtweise des FZR
Tagung Arbeitskreis „Thermodynamische Standarddatenbasis"
Freiberg, Germany, 12.11.2003

Brendler, V., Richter, A., Arnold, T., Bernhard, G.
Capability of Surface Complexation Models and Databases for Predicting Radionuclide Sorption
9th International Conference on Chemistry and Migration Behaviour of Actinides and Fission Products in the Geosphere (Migration 03)
Gyeongju, Korea, 21.-26.09.2003

Chukalina, M., Golosio, B., Simionovici, A., Somogyi, A., Funke, H.
Accuracy Problem in X-ray Fluorescence Computer Microtomography
17th International Congress on X-Ray Optics and Microanalysis
Chamonix, France, 22.-26.09. 2003

Chukalina, M., Funke, H., Dubrovskii, Yu., Golossio, B., Shapoval, S., Ivanov, D., Volkov, V., Simionovici, A. Somogyi, A.
Wavelet transformation for image analysis and signal processing: some estimations and real applications
6th German-Russian Workshop "Pattern Recognition and Image Understanding" OGRW-6-2003
Katun, Altai Region, Russia, 25.-30.08, 2003

Furrer, G., Ulrich, K.-U.
Aluminum-Oxyhydroxide Flocs in Acid-Impaired Streams
Proc. 7th Intern. Conf. on the Biogeochem. of Trace Elements (ICOBTE)
Uppsala, Sweden, 15.-19.06.2003

Funke, H., Chukalina, M.
HAMA - a computer program for wavelet analysis of EXAFS data
Scientific Software Group, ESRF
Grenoble, France, 22.07. 2003

Funke, H.
Introduction to EXAFS data analysis and the use of wavelets
Moscow State University
Moscow, Russia, 02.09. 2003

Funke, H.
The Rossendorf beamline (ROBL) at the ESRF in Grenoble
Moscow State University
Moscow, Russia, 03.09. 2003

Funke, H.
Wavelet analysis of EXAFS data
Institute of Microelectronics Technology, RAS
Chernogolovka, Russia, 05.09. 2003

Geipel, G.
Laser Induced Spectroscopy - Detection of Actinide Species at Low Concentrations
University of Kyoto
Kyoto, Japan, 21.01.2003

Geipel, G.
Anwendung spektroskopischer Methoden zur Bestimmung von Komplexbildungskonstanten und Spezies
Seminarvortrag, Universität Potsdam
Potsdam, Germany, 22.05.2003

Geipel, G.
Laserinduzierte Spektroskopie: Von der Speziesdetektion zur Fluoreszenzspektroskopie an Mineralien
Geowissenschaftliches Kolloquium Freiberg
Freiberg, Germany, 02.07.2003

Geipel, G.
Laser Induced Spectroscopy - A Tool to Study Interaction of Actinides with Various Ligands at Low Concentrations
5th International Conference on f-Elements
Geneva, Switzerland, 24.-29.08.2003

Geipel, G., Bernhard, G., Nagasaki, S.
Complex Formation of Uranium with 2,5-Dihydroxybenzoic Acid
9th International Conference on Chemistry and Migration Behaviour of Actinides and Fission Products in the Geosphere (Migration 03)
Gyeongju, Korea, 21.-26.09.2003

Geipel, G.
Detection of solid state species by spectroscopic methods
4. Koordinierungsgespräch PSI-FZR
Villingen, Switzerland, 20.-21.10.2003

Hennig, C.
EXAFS investigation of uranium(VI) sorption complexes at the clay mineral surface
Institut de Recherches Subatomiques
Strasbourg, France, 21.05. 2003

Hennig, C.
Speciation of radio elements using X-ray absorption spectroscopy
Ecole des Mines de Nantes
Nantes, France, 17.09. 2003

Hennig, C.
Structure of actinide sorption complexes on clay minerals – an EXAFS study
Institut de Physique Nucleaire
Orsay, France, 21.03. 2003

Hennig, C.
Coordination of actinides in aqueous solution
ESRF User Meeting
Grenoble, France, 12. 02. 2003

Hübener, S.
Thermochromatographische Untersuchungen von Actinidenoxiden
Seminar des Labors für Radio- und Umweltchemie der Universität Bern und des PSI
Bern, Schweiz, 24.01.2003

Jansen, K., Buschmann, H.-J., Schmeide, K., Schollmeyer, E.
Modifizierung von Polyestervliesen mit Calixarenen - Textile Filter für die Abtrennung von Uran aus Gruben- und Sickerwässern
3. Textilveredlertag des Vereins Deutscher Textilveredlungsfachleute e.V.
Erfurt, Germany, 29.-31.05.2003

Kienzler, B., Metz, V., Kelm, M., Nebelung, C., Baraniak, L.
Interactions of Carbon in a Repository Environment
[14]C Workshop NAGRA
Wettingen, Schweiz, 27.-28.10.2003

Klenze, R., Fanghänel, Th., Kim, J.I., Chaix, P., Leroy, M., Bruggeman, A., Brendler, V., Hadermann, J., Grenthe, I., Bruno, J., Stipp, S.L.S., Read, D., Missana, T.
Joint Research on Actinide Sciences in Europe: ACTAF and ACTINET Programmes
9th International Conference on Chemistry and Migration Behaviour of Actinides and Fission Products in the Geosphere (Migration 03)
Gyeongju, Korea, 21.-26.09.2003

Kretzschmar, R., Scheinost, A.C., Vantelon, D., Xifra, I., Knechtenhofer, L., Jäger, F., Flühler, H.
Verlagerung und räumliche Verteilung von Pb und Sb in kontaminierten Schiessplatzböden
Jahrestagung der Deutschen Bodenkundlichen Gesellschaft (DBG)
Frankfurt/Oder, Germany, 30.08. - 07.09. 2003

Merroun, M.L., Hennig, C., Roßberg, A., Geipel, G., Reich, T., Nicolai, R., Heise, K.H., Selenska-Pobell, S.
Molecular and spectroscopic characterization of uranium complexes formed by different bacteria isolated from uranium mining wastes.
International workshop on Biogeochemical controls on the mobility and bioavailability of metals in soils and ground water
Ascona, Switzerland, 02.-07.03.2003

Merroun, M.L.
EXAFS studies of the Pd nanoclusters formed by cells and S-layers of *B. sphaericus* JG-A12 and NCTC 9602
EU Biocat Project Meeting
Technical University of Dresden
Dresden, Germany, 09.10.2003

Mibus, J.
Säulen- und Diffusionsversuche zum reaktiven Transport

4. Koordinierungsgespräch PSI-FZR
Villingen, Switzerland, 20.-21.10.2003

Moll, H., Merroun, M., Stumpf, Th., Geipel, G., Selenska-Pobell, S., Hennig, C., Roßberg, A., Bernhard, G.
Interaction of *Desulfovibrio äspöensis* with Actinides
9th International Conference on Chemistry and Migration Behaviour of Actinides and Fission Products in the Geosphere (Migration 03)
Gyeongju, Korea, 21.-26.09.2003

Nedelkova, M., Radeva, G., Selenska-Pobell, S.
Bacterial Diversity in Water at the Deep-Well Monitoring Site Tomsk-7
International Symposium on Underground Injection Science and Technology
Berkeley, California, USA, 22.- 25.10.2003

Neguljaev, N., Funke, H., Chukalina, M., Scheinost, A., Serdobolskaja, M.
Use of wavelet transform for data analysis of Extended X-ray Absorption Fine Structure (EXAFS) spectra
4th National Conference on Application of X-Ray, Synchrotron Radiation, Neutrons and Electrons for Material Characterization - RSNE-2003
Moscow, Russia, 17.-22.11. 2003

Pollmann, K., Selenska-Pobell, S.
Molecular analyses of S-layer genes and proteins
BIO-CAT Meeting
Marseille, France, 02.05.2003

Pollmann, K., Selenska-Pobell, S.
Molecular analyses of S-layer genes and proteins
BIO-CAT Midterm-Meeting
Chester, England, 17.11.2003

Raff, J., Soltmann, U., Matys, S., Pompe, W., Boettcher, H., Selenska-Pobell, S.
Bacteria-based bioremediation of uranium mining waste waters by using sol-gel ceramics
21. DECHEMA-Jahrestagung
München, Germany, 02.-04.04.2003

Raff, J.
Auf Bakterien basierende Biosanierung von Sickerwässern aus Uranabfallhalden unter Verwendung von Sol-Gel Keramiken
Nanoverbund-Projekttreffen, Institut für Biochemie, TU-Dresden
Dresden, Germany, 08.05.2003

Raff, J.
Untersuchung der Uransorption an freien und immobilisierten Biokomponenten von *Bacillus sphaericus* JG-A12 und *Bacillus sphaericus* NCTC 9602 mittels Röntgenabsorptionsspektroskopie
DFG-Projekttreffen, Institut für Werkstoff-Wissenschaft, TU-Dresden
Dresden, Germany, 30.04.2003

Reich, T., Roßberg, A.
Application of iterative transformation factor analysis to EXAFS spectroscopy
12th International Conference on X-ray Absorption Fine Structure (XAFS 12)
Malmö, Sweden, 22.-27.06.2003

Richter, A., Brendler, V., Bernhard, G.
The mineral-specific thermodynamic sorption database RES[3]T: Concept description, implementation, and application towards contaminated systems
Goldschmidt Conference
Kurashiki, Japan, 7.-12. 09.2003

Roßberg, A.
Anwendung der Faktorenanalyse auf die Röntgenabsorptionsspektroskopie zur Bestimmung der Speziation von Uran in Lösungen (Verleihung des Promotionspreises 2003)
GDCh-Jahrestagung Chemie 2003, Fachgruppe Nuklearchemie
München, Germany, 06.-11.10.2003

Roßberg, A.
Iterative Transformation Factor Analysis (ITFA) of XAS Spectra
Scientific Software Group, ESRF
Grenoble, France, 22.07. 2003

Sachs, S., Krepelová, A., Mibus, J.
Aktuelle Ergebnisse der Untersuchungen zum Redoxverhalten von Huminsäuren und zum Einfluss von Huminsäuren auf die Sorption vierwertiger Actinide im System Quarzsand/Huminsäure/Wasser
Workshop zum Forschungsvorhaben „Untersuchungen über die Komplexierung und die Migration von Actiniden und nichtradioaktiven Stoffen mit Huminsäuren unter geogenen Bedingungen - Komplexierung von Huminsäuren mit Actiniden in der Oxidationsstufe IV Th, U, Np"
Mainz, Germany, 02.-03.04.2003

Sachs, S., Geipel, G., Heise, K. H., Bernhard, G.
Specific Humic Acid Model Substances for the Study of the Redox Behavior of Humic Acids in the Environment
9th International Conference on Chemistry and Migration Behaviour of Actinides and Fission Products in the Geosphere (Migration 03)
Gyeongju, Korea, 21.-26.09.2003

Sachs, S.
Studies on the Redox Stability of U(VI) Humate Complexes Using Synthetic Humic Acids with Distinct Redox Functionalities
Workshop zum Forschungsvorhaben "Humic Substances in Performance Assessment of Nuclear Waste Disposal: Actinide and Iodine Migration in the Far-Field"
Nicosia, Cyprus, 26.-27.10.2003

Scheinost, A.C., Roßberg, A., Pfister, S., Kretzschmar, R., Marcus, M., Newville, M.
Quantitative Zinc Speciation in Soil with XAFS: Evaluation of Iterative Transformation Factor Analysis
12th International Conference on X-ray Absorption Fine Structure (XAFS 12)
Malmö, Sweden, 22.-27.06.2003

Scheinost, A.C., Roßberg, A., Pfister, S., Kretzschmar, R., Marcus, M.
Bindungsformen von Zn in einem mit Filterstaub belasteten Boden: EXAFS-Spektroskopie kombiniert mit Faktoranalyse
Jahrestagung der Deutschen Bodenkundlichen Gesellschaft (DBG)
Frankfurt/Oder, Germany, 30.08.- 07.09. 2003

Schollmeyer, E., Jansen, K., Buschmann, H.-J., Schmeide, K.
Modification of Textile Mats with Calixarenes – Separation of Uranium From Mine and Seepage Waters
4th International Symposium on Polymer Surface Modification
Orlando, USA, 09.-11.06.2003

Schmeide, K.
Np(V) Sorption onto Granite in the Absence and Presence of Humic Acid
Workshop zum Forschungsvorhaben "Humic Substances in Performance Assessment of Nuclear Waste Disposal: Actinide and Iodine Migration in the Far-Field"
Nicosia, Cyprus, 26.-27.10.2003

Schmeide, K.
Anwendung fixierter und unfixierter Calix[6]arene zur Abtrennung von Uran aus wässriger Lösung
Workshop zum Forschungsvorhaben "Abtrennung von Uranylionen aus Sicker- und Grundwässern mit uranophilen Calixarenen – Integrierter Umweltschutz in der Textilindustrie"
Wolfen, Germany, 13.03.2003

Schnorpfeil, M., Raff , J., Selenska-Pobell, S.
Mikrobiologische Grundlagenprobleme von Schwermetall-bindenden S-Layer des *B. sphaericus* JG-A12
Projekttreffen zum NanoVerbund-Projekt: „Biologische Synthese von Metallclustern an Proteinen und deren technische Nutzung", TU Dresden
Dresden, Germany, 08.05.03

Schumacher, M., Scheinost, A.C., Christl, I., Jacobsen, Ch., Kretzschmar, R.
Chemical heterogeneity of mobile soil colloids and dissolved organic matter (DOC) studied by x-ray microscopy and x-ray spectroscopy

17th International Congress on X-Ray Optics and Microanalysis
Chamonix, France, 22.09.-26.09. 2003

Selenska-Pobell, S., Schnorpfeil, M., Raff, J., Pollmann, K., Merroun, M.
Evolutionary aspects of the S-layers of *Bacillus sphaericus*
VAAM-Jahrestagung
Berlin, Germany, 23.-26.03.2003

Selenska-Pobell, S.
Ungewöhnliche Bakterien aus Uranabfallhalden zur Nutzung für Biosanierung und Nanotechnologie
BioMeT vor Ort, FZ Rossendorf
Rossendorf, Germany, 08.07.2003

Selenska-Pobell, S.
Uranium contaminated environments as a reservoir of unusual bacteria prospective for bioremediation and nanotechnology
Internationale Konferenz „Perspektiven der Umweltmikrobiologie; Biodegradation, Biotransformation, Adaptation, Geomikrobiologie"
Freiberg, Germany, 05.-07.10.2003

Selenska-Pobell S.
Heavy metal contaminated environments as a reservoir of unusual bacteria prospective for bioremediation and nanotechnology
Max Plank Institut für Zellbiologie und Genetik
Dresden, Germany, 26.11.2003

Vantelon, D., Scheinost, A.C., Kretzschmar, R., Marcus, M.
A Microspectroscopic Study of Pb Distribution and Speciation in a Contaminated Soil
17th International Congress on X-Ray Optics and Microanalysis
Chamonix, France, 22.09.-26.09. 2003

Vulpius, D.
Fluoreszenzspektroskopische Untersuchung von Komplexgleichgewichten und Protonentransfer im angeregten Zustand
Universität Potsdam, Institut für Chemie, Professur für Physikalische Chemie
Golm, Germany, 22.05.2003

Walter, M., Arnold, T., Bernhard, G.
Sorption von Uran(VI) an Albit - Identifizierung von Uran(VI)-Oberflächenspezies mit spektroskopischen Methoden (EXAFS, TRLFS)
Geochem 2003
Oldenburg, Germany, 27.-28.06.2003

POSTERS

Arnold, T., Krawczyk-Bärsch, E., Brandt, F., Bosbach, D., Bernhard, G.
Effect of secondary Fe-phases on the sorption behavior of U(VI) on chlorite by
9th International Conference on Chemistry and Migration Behaviour of Actinides and Fission Products in the Geosphere (Migration 03)
Gyeongju, Korea, 21.-26.09.2003

Brandt, F., Bosbach, D., Krawczyk-Bärsch, E., Arnold, T., Bernhard, G.
Uranium(VI) Sorption onto Weathered Chlorite and Secondary Phases
9th International Conference on Chemistry and Migration Behaviour of Actinides and Fission Products in the Geosphere (Migration 03)
Gyeongju, Korea, 21.-26.09.2003

Foerstendorf, H., Seidel, W., Heise, K.H., Ortega, J.M., Glotin, F., Prazeres, R.
Photothermal Beam Deflection Using a Free Electron Laser For Infrared Characterization of Environmental Samples
ICAVS-2, The 2nd International Conference on Advanced Vibrational Spectroscopy
Nottingham, U.K., 24.-29.8.2003

Funke, H., Chukalina, M., Roßberg, A.
Wavelet analysis of EXFAS spectra
12th International Conference on X-ray Absorption Fine Structure (XAFS 12)
Malmö, Sweden, 22.-27.06.2003

Gaillard, C., Hesemann, P., Hennig, C., Bauer, A., Billard, I., Moutiers, G., Mariet, C., Labet, A., Lützenkirchen, K.
Complexation of uranium(VI) with F^-, PF_6^- and BF_6^- in aqueous solution. Comparison with ionic liquids
ESRF User Meeting
Grenoble, France, 12.02. 2003

Geipel, G., Vulpius, D., Bernhard, G.
Excited state reactions in studies of complex formation between actinides and organic ligands with laser induced methods
9th International Conference on Chemistry and Migration Behaviour of Actinides and Fission Products in the Geosphere (Migration 03)
Gyeongju, Korea, 21.-26.09.2003

Geißler, A., Tzvetkova, T., Selenska-Pobell, S.
Bacterial diversity and monitoring of *Geobacter* sp. in uranium contaminated soils
Tagung „Perspektiven der Umweltmikrobiologie; Biodegradation, Biotransformation, Adaptation, Geomikrobiologie"
Freiberg, Germany, 05.-07.10.2003

Günther, A., Bernhard, G., Geipel, G., Roßberg, A., Reich, T., Nitsche, H.
Uranium transfer into plants
9th International Conference on Chemistry and Migration Behaviour of Actinides and Fission Products in the Geosphere (Migration 03)
Gyeongju, Korea, 21.-26.09.2003

Hennig, C.
EXAFS investigation of Am(III) and U(VI) Sorption onto smectite and kaolinite
ESRF User Meeting
Grenoble, France, 12.02. 2003

Hennig, C., Reich, T., Kraus, W., Reck, G., Schell, N., Prokert, F.
Combining EXAFS and X-ray powder diffraction to solve structures with heavy atoms
12th International Conference on X-ray Absorption Fine Structure (XAFS 12)
Malmö, Sweden, 22.-27.06.2003

Hübener, S., Opel, K., Zänker, H.
Gerätesystem zur Laser-induzierten Breakdown-Detektion aquatischer Kolloide
GDCh-Jahrestagung Chemie 2003, Fachgruppe Nuklearchemie
München, Germany, 06.-11.10.2003

Jäger, F., Scheinost, A.C., Vantelon, D., Kretzschmar, R.
Einfluss präferentieller Fliesswege auf die Verlagerung von Pb und Sb in einem Schiessplatzboden
Jahrestagung der Deutschen Bodenkundlichen Gesellschaft (DBG)
Frankfurt/Oder, Germany, 30.08. - 07.09. 2003

Jansen, K., Buschmann, H.-J., Schmeide, K., Bernhard, G., Schollmeyer, E.
Polyester Fleece Modified with Calixarenes
Techtextil
Frankfurt, Germany, 07.-10.04.2003

Jansen, K., Buschmann, H.-J., Schmeide, K., Bernhard, G., Schollmeyer, E.
Calixarenmodizifierte Polyestermaterialien - Textile Filter für die Abtrennung von Uran aus Gruben- und Sickerwässern
3. Textilveredlertag des Vereins Deutscher Textilveredlungsfachleute e.V.
Erfurt, Germany, 29.-31.05.2003

Kunicke, M., Kamensky, I.Y., Babanov, Y.A., Funke, H.
Efficient determination of optimal regularization parameter for inverse problem in EXAFS spectroscopy

12th International Conference on X-ray Absorption Fine Structure (XAFS 12)
Malmö, Sweden, 22.-27.06.2003

Merroun, M.L., Raff, J., Hennig, C., Roßberg, A., Reich, T., Selenska-Pobell, S.
X-ray absorption spectroscopy characterization of uranium (VI) complexes formed by *Bacillus sphaericus* JG-A12 and NCTC 9602 and their recrystalized S-layers
VAAM-Jahrestagung
Berlin, Germany, 23.-26.03.2003

Merroun, M.L., Raff, J., Hennig, C., Roßberg, A., Reich, T., Selenska-Pobell, S.
EXAFS investigations of uranium complexes formed by bacterial cells, S-layers and bioceramics
12th International Conference on X-ray Absorption Fine Structure (XAFS 12)
Malmö, Sweden, 22.-27.06.2003

Merroun, M.L., Hennig, C., Roßberg, A., Reich, T., Geipel, G., Selenska-Pobell, S.
Bacterial strains isolated from uranium mining waste piles and their interactions with uranium
9th International Conference on Chemistry and Migration Behaviour of Actinides and Fission Products in the Geosphere (Migration 03)
Gyeongju, Korea, 21.-26.09.2003

Mibus, J.
Uranbergbau ins Labor geholt
Highlights der Physik
Dresden, Germany, 24.-28.06.2003

Mibus, J.
Sicherheit durch Tiefe
Highlights der Physik
Dresden, Germany, 24.-28.06.2003

Moll, H., Merroun, M.L, Stumpf, Th., Geipel, G., Selenska-Pobell, S., Hennig, C., Roßberg, A., Bernhard, G.
Interaction of *Desulfovibrio äspöensis* with actinides
9th International Conference on Chemistry and Migration Behaviour of Actinides and Fission Products in the Geosphere (Migration 03)
Gyeongju, Korea, 21.-26.09.2003

Nebelung, C., Baraniak, L.
Simultanbestimmung von ^{237}Np, ^{233}U und ^{226}Ra mittels Flüssigszintillations-Spektroskopie (LS)
GDCh-Jahrestagung Chemie 2003, Fachgruppe Nuklearchemie
München, Germany, 06.-11.10.2003

Nedelkova, M., Selenska-Pobell, S.
Bacterial and archaeal diversity in waters at the Siberian deep-well monitoring site Tomsk-7
Internationale Konferenz „Perspektiven der Umweltmikrobiologie; Biodegradation, Biotransformation, Adaptation, Geomikrobiologie"
Freiberg, Germany, 05.-07.10.2003

Poineau, F., Fattahi, M., Grambow, B., Hennig, C.
In situ speciation of radio elements by coupled XAFS electrochemistry – preliminary results on speciation of rhenium as analogue of technetium
9th International Conference on Chemistry and Migration Behaviour of Actinides and Fission Products in the Geosphere (Migration 03)
Gyeongju, Korea, 21.-26.09.2003

Pollmann, K., Raff, J., Merroun, M.L., Schnorpfeil, M., Selenska-Pobell, S.
Uranium mining waste pile isolate *Bacillus sphaericus* JG-A12 and its technological applications
Internationale Konferenz „Perspektiven der Umweltmikrobiologie; Biodegradation, Biotransformation, Adaptation, Geomikrobiologie"
Freiberg, Germany, 05.-07.10.2003

Radeva, G., Flemming, K., Satschanska, G., Selenska-Pobell, S.
Archaeal and bacterial populations in soil and water samples from the uranium mill tailings Gittersee/Coschütz

Internationale Konferenz „Perspektiven der Umweltmikrobiologie; Biodegradation, Biotransformation, Adaptation, Geomikrobiologie"
Freiberg, Germany, 05.-07.10.2003

Raff, J., Soltmann, U., Matys, S., Merroun, M.L., Roßberg, A., Hennig, C., Böttcher, H., Pompe, W., Selenska-Pobell, S.
Bacteria-based Bioceramics for Bioremediation of Uranium Mining Waste Waters
103th General Meeting of the American Society for Microbiology (ASM)
Washington, USA, 18.-22.05.2003

Raff, J., Soltmann, U., Matys, S., Böttcher, H., Pompe, W., Selenska-Pobell, S.
Bakterien – Putzkolonne aus der Natur
Hannover-Messe
Hannover, Germany, 06.- 12.04.2003

Raff, J., Schnorpfeil, M., Pollmann, K., Selenska-Pobell, S.
Molecular analysis of the S-layer proteins of *Bacillus sphaericus* strains JG-A12 and NCTC 9602
VAAM-Jahrestagung
Berlin, Germany, 23.-26.03.2003

Reuther, H., Arnold, T., Krawczyk-Bärsch, E.
Quantification of secondary Fe-phases formed during sorption experiments on chlorites
International Conference on the Applications of the Mössbauer Effekt 2003
Muscat, Oman, 21.-25.09.2003

Roßberg, A., Scheinost, A.C.
Structural analysis of metallo-organic complexes in aqueous solutions
12th International Conference on X-ray Absorption Fine Structure (XAFS 12)
Malmö, Sweden, 22.-27.06.2003

Schmeide, K., Geipel, G., Ludwig, R., Heise, K.H., Bernhard, G.
Uranium(VI) Complexation by Calix[6]arenes studied by Time-resolved Laser-induced Fluorescence Spectroscopy (TRLFS)
9th International Conference on Chemistry and Migration Behaviour of Actinides and Fission Products in the Geosphere (Migration 03)
Gyeongju, Korea, 21.-26.09.2003

Schnorpfeil, M., Raff, J., Polmann, K., Merroun, M.L., Selenska-Pobell, S.
Evolutionary aspects of the S-layers of *Bacillus sphaericus*
VAAM-Jahrestagung
Berlin, Germany, 23.-26.03.2003

Seidel, W., Foerstendorf, H., Heise, K.H., Ortega, J.-M., Glotin, F., Prazeres, R.
Infrared Characterization of Environmental Samples by Photothermal Beam Deflection Using a Free Electron Laser
25th Int. Conference on Free Electron Laser and the 10th FEL User Workshop
Tsukuba, Ibaraki, Japan, 08.-12.9.2003

Selenska-Pobell, S., Geißler, A., Merroun, M.L., Schnorpfeil, M., Raff, J., Radeva, G., Flemming, K.
Uranium Mining Wastes as a Reservoir of Unusual Bacteria Prospective for Bioremediation and Nanotechnology
103th General Meeting of the American Society for Microbiology (ASM)
Washington, USA, 18.-22.05.2003

PH.D. THESES

Pollmann, K.
Abbau von chlorierten Toluolen durch natürliche und konstruierte Mikroorganismen
TU Carolo-Wilhelmina Braunschweig, Germany, 2002

DIPLOMA

Brottka, K.
Herstellung von biologisierten Keramiken zur Reinigung Schwermetall-kontaminierter Abwässer
TU Dresden, Germany, 2003

Großmann, K.
Mikroskopische und Geochemische Charakterisierung von Biofilmen
HTW Dresden, Germany, 2003

Swantusch, M.
Experimente zur Sorption von Radionukliden an Tonmineralen
HTW Dresden, Germany, 2003

PATENTS

Selenska-Pobell, S., Soltmann, U., Raff, J., Böttger, H., Kallies, K.-H., Quast, H., Matys, S.
Biokompositmaterial
Patent: DE 101 46 375 A 1 vom 03.01.2003

AWARDS

Pollmann, K.
Abbau von chlorierten Toluolen durch natürliche und konstruierte Mikroorganismen
Fritz-Wagner-Preis, Förderpreis der Biotechnologie der Gesellschaft für Biotechnologische Forschung mbH
Braunschweig, Germany, 2003

Roßberg, A.
Anwendung der Faktorenanalyse auf die Röntgenabsorptionsspektroskopie zur Bestimmung der Speziation von Uran in Lösungen
Doktorandenpreis 2003 der FG Nuklearchemie, GDCh-Jahrestagung Chemie
München, Germany, 06.-11.10.2003

III. SEMINARS, CONFERENCES, WORKSHOPS, TEACHING ACTIVITIES

INSTITUTE SEMINARS (talks of visitors)

Prof. Dr. Siegfried Niese
VKTA Rossendorf
Der Naturforscher Georg von Hevesy in Deutschland
07.01.2003

PD Dr. Gerald Ziegenbalg
TU BA Freiberg, Institut für Technische Chemie
Die in-situ Kristallisation von natürlichen Mineralen - eine neue Möglichkeit zur Schadstoffimmobilisirung und Gesteinsverfestigung
14.01.2003

Dr. Claudia Hanfland
Alfred Wegener Institute for Polar and Marine Research, Geochemistry Section, Bremerhaven
Die Anwendung natürlicher Radionuklide auf marine Fragestellungen
04.02.2003

Dr. Ruth Lewin Sime
Sacramento, USA
Lise Meitner and the Discovery of Nuclear Fission
17.3.2003

Dr. Francis Livens
University of Manchester, Centre for Radiochemistry Research
Environmental and Synchrotron Studies of the Radioactive Elements
25.03.2003

Dr. Friedhelm Enzmann
Johannes Gutenberg Universität Mainz, Institut für Geowissenschaften
Simulation der Migration von Tracern in geklüftet-porösen Medien
01.04.2003

Dr. Robert Eichler
Paul-Scherrer-Institut Villigen
Gaschemische Untersuchung von Transaktinoiden
15.04.2003

Dr. Susanta Lahiri
Saha Institute of Nuclear Physics Kolkata, Chemical Sciences Division
Tracer Packet: A novel concept and its application
10.06.2003

Dr. Jürgen Thieme
Universität Göttingen, Institut für Röntgenphysik
Spektromikroskopie mit Röntgenstrahlen zur Untersuchung kolloidaler Strukturen in Boden und Grundwasser
17.06.2003

Akira Kirishima
Japan Atomic Energy Research Institute, Department of Materials Science
Luminescence study of tetravalent uranium in aqueous solution
02.09.2003

Dr. Resch-Genger
Bundesanstalt für Materialforschung und –prüfung Berlin
Analytische Applikationen der Fluorometrie: Entwicklung von Fluoreszenzstandards und Fluoreszenzmarkern
15.10.2003

PD Dr. Kai Uwe Totsche
TU München, Lehrstuhl für Bodenkunde; Wissenschaftszentrum Weihenstephan
Transport mobiler Sorbenten (MOS) und MOS-gekoppelter Schadstofftransport in der ungesättigten Bodenzone
02.12.2003

Dr. Wolfgang Dedeck
IIF Leipzig
Entdeckung des Neutrons
09.12.2003

INTERNAL SEMINARS (open for the public)

Institutskolloquium aus Anlass des 65. Geburtstages von Dr. Karl Heinz Heise
10.09.2003

Pötter, H.
Aspekte der Dünnschichtchromatographie

Neuweiler, F.
Heise's Wirkung auf die moderne Karbonatsedimentologie

Sachs, S.
Zum Einfluss von Huminsäuren auf das Migrationsverhalten von Actiniden in der Umwelt

Foerstendorf, H.
Ausgewählte Methoden der Schwingungsspektroskopie in der Radiochemie
Konventionelle FT-IR Messungen und erste Untersuchungen am Freie Elektronen Laser
18.11.2003

CONFERENCES / WORKSHOPS (organized by Institute of Radiochemistry)

5. Sitzung des Arbeitskreises "Kolloide" der Wasserchemischen Gesellschaft in der GDCh
Rossendorf, Germany, 14.03.2003

Sachs, S.
Synthetische Huminsäuren als Beispiel für Modellsubstanzen in der Kolloidforschung

EXAFS Workshop
Rossendorf, Germany, 19.-24.04.2003

Roßberg, A.
EXAFS-Arbeitstechniken

Workshop "Humic Substances in Performance Assessment of Nuclear Waste Disposal: Actinide and Iodine Migration in the Far-Field"
Rossendorf, Germany, 12.-13.05.2003

Sachs, S.
Studies on the Influence of Humic Acid Phenolic OH Groups on the Redox Behavior of Humic Substances

Workshop BMWA-Verbundprojekt "Migration von Actiniden im System Ton, Huminstoff, Aquifer"
Dresden, Germany, 05.-06. 11.2003

Mibus, J.
Einfluss von Huminsäuren auf die Migration von U(IV)/U(VI) in Quarzsand

Sachs, S.
Untersuchungen zur Redoxstabilität von U(VI)-Humaten synthetischer Huminsäuren mit ausgeprägter Redox-funktionalität

5th ROBL Radiochemistry Workshop
Rossendorf, Germany, 08.12.2003

Funke, H., Chukalina, M., Roßberg, A., Scheinost, A., Walter, M.
Wavelet-Analyse von EXAFS-Spektren: Ausgewählte Beispiele

Günther, A., Roßberg, A.
Spektroskopische Charakterisierung von U-Spezies in Pflanzen

Hennig, C.
A new goniometer for polarized XAFS experiments at ROBL – comparison of spectral features at the uranium L1 and L3 edges

Hennig, C., Tutschku, J.
First uranium L3 XAFS measurements with spectro-electrochemical cell

Koban, A., Geipel, G., Roßberg, A., Bernhard, G.
Spektroskopische Untersuchungen zur Komplexierung von U(VI) mit Zuckerphosphaten

Merroun, M., Pollmann, K., Raff, J., Aichmayer, B., Scheinost, A., Selenska-Pobell, S.
EXAFS studies of the Pd nanoclusters formed by cells and S-layers of *Bacillus sphaericus* JG-A12 and NCTC 9602

Merroun, M., Raff, J., Roßberg, A., Hennig, C., Scheinost, A., Selenska-Pobell, S.
EXAFS characterization of the uranium complexes formed by bacterial cells and S-layers

Roßberg, A.
Monte-Carlo Transformation-Factor-Analysis – eine neue Strategie zur EXAFS Datenanalyse

Roßberg, A.
Probleme bei der U-L$_{III}$-EXAFS-Datenanalyse biologischer Proben

Scheinost, A., Leckelt, M., Johnson, A., Somogyi, A., Vantelon, D.
Speciation of antimony and uranium in soil and sediment samples: Making use of high energy, low temperature and micrometer resolution

Scheinost, A., Roßberg, A., Hennig, Ch., Funke, H.
Technische Neuerungen am und um den RCH-Messplatz: UV-Vis, 13-Elementdetektor, Spektrendatenbank, Mikrofokussierung, Halter etc.

Workshop "Auswertung von EXAFS-Daten"
Rossendorf, Germany, 11.12.2003

Roßberg, A.
Faktorenanalyse

Funke, H.
Wavelet

Scheinost, A.
EXAFS Workshop

TEACHING ACTIVITIES

Bernhard, G.
Radiochemie – Radiochemische Methoden / Radiochemistry – Radiochemical Methods
Technische Universität Dresden
Summerterm 2003

Bernhard, G.
Umweltanalytik (Spurenanalytik) / Environmental Analysis (Trace Analysis)
Technische Universität Dresden
Summerterm 2003

Bernhard, G.
Umweltchemie (Umwelt-Stoffe-Energie) / Environmental Chemistry (Environment-Substance-Energy)
Technische Universität Dresden
Winterterm 2003/2004

IV. PERSONNEL

PERSONNEL

Director

Prof. Dr. F.-P. Weiß (acting, until October 31, 2003)
Prof. Dr. G. Bernhard (since November 01, 2003)

Administrative Staff

G. Kreusel   H. Pospischil

Scientific Staff

Dr. T. Arnold*	Dr. C. Hennig	Dr. A. Richter*
Dr. N. Baumann*	Dr. S. Hübener	Dr. W. Richter
DGP N. Betzl*	Dr. A. Koban[+]	Dr. A. Roßberg
DC D. Birnstein	Dr. K. Krogner	Dr. S. Sachs*
Dr. V. Brendler	Dr. M. Merroun[+]	Dr. A. Scheinost
Dr. H.-J. Engelmann*	Dr. J. Mibus[+]	Dr. K. Schmeide*
Dr. H. Foerstendorf	Dr. H. Moll*	Dr. S. Selenska-Pobell
Dr. H. Funke	DC C. Nebelung	Dr. J. Tutschku*
Dr. G. Geipel	Dr. K. Pollmann[+]	Dr. K.-U. Ulrich*
Dr. A. Günther*	Dr. J. Raff[+]	Dr. H. Zänker
Dr. K.H. Heise		

Technical Staff

S. Brockmann	St. Henke	DI(BA) K. Muschter
DI(FH) C. Eckardt	B. Hiller	H. Neubert
D. Falkenberg	DI(FH) R. Jander	DI(FH) R. Nicolai*
DBC K. Flemming	W. Knebel	A. Rumpel
DI(FH) H. Friedrich	M. Leckelt*	R. Ruske
Ch. Fröhlich	DI(FH) M. Meyer	DI(FH) U. Schaefer
DI(FH) G. Grambole	Ch. Müller	DI(FH) St. Weiß
DI(FH) S. Heller*	I. Muschter	DI(FH) M. Wenzel*

Graduate Students

DB K. Brottka	DI A. Krepelova	M. Swantusch
DGE A. Geißler	DB M. Nedelkova	DI(FH) D. Vulpius
DI(FH) K. Grossmann*	DC K. Opel	DM M. Walter

Trainee

T. Birk	Y. Lange	I. Schubert
M. Heilig	C. Möckel	U. Siewert
Ch. Jungnickel	I. Müller	Ch. Stange
M. Kaufmann	I. Ossowski	Ch. Wendel
St. Knauer	St. Protze	Y. Zaruba

[+] post doc	DC: Dipl.-Chem.	DBC: Dipl.-Biochem.	DGP: Dipl.-Geophys.
* term contract	DI: Dipl.-Ing.	DB: Dipl.-Biol.	DGE: Dipl.-Geoökol.
	DM: Dipl.-Mineral.		

Guest Scientists

B. Aichmayer	Institute of Metal Physics, University of Leoben, Austria
V. Baxter-Plant	School of Biological Sciences, University of Birmingham, UK
M. Brennerova	Institute of Microbiology, Academy of Sciences, CZ
M. Chukalina	Institute of Microelectronics Technology, RAS, Chernogolovka, Russia
I. Mikheenko	School of Biological Sciences, University of Birmingham, UK
S. Nagasaki	Institute of Environmental Studies, Graduate School of Frontier Science, University of Tokyo, Japan
G. Radeva	Institute of Molecular Biology, Sofia, Bulgaria
M. Rousset	Centre National de la Recherche Scientifique, Marseille, France
G. Satchanska	Institute of Molecular Biology, Sofia, Bulgaria
C. Walther	Institut für Nukleare Entsorgung, Forschungszentrum Karlsruhe, Germany

V. ACKNOWLEDGMENTS

Four projects were supported by Deutsche Forschungsgemeinschaft (DFG):

- Heterogene Reaktionsmechanismen und deren Kinetik an Schichtsilikatoberflächen
  Contract No.: DFG BE 2234/4-2

- Komplexierung von Uranyl- und Neptunylionen mit phenolischen Monomeren des natürlichen Ligninabbaus als Grundlage für die Beschreibung der Radionuklidausbreitung
  Contract No.: DFG BE 2234/3-2

- Kolloidgetragener Transport von Uran und anderen radiotoxischen Schwermetallen in oxischen Bergwerks- wässern
  Contract No.: DFG ZA 238/2-1, 2-2

- BIOCERE mit spezifischer Metallbindungsaktivität
  Contract No.: DFG SE 671/7-1

Two projects were supported by the Bundesamt für Strahlenschutz (BfS):

- Sorptionsexperimente im Deckgebirge des Endlagers für radioaktive Abfälle Morsleben (ERAM)
  Contract No.: BfS 9M 212230-62

- Wechselwirkung mit Oberflächen
  Contract No.: BfS WS 1011

One project was supported by AMD Saxony Manufacturing GmbH:

- Aufbau, Inbetriebnahme und Erprobung einer Messapparatur zur Low-Level-Alphaspektrometrie
  Joint project of FZR and INE FZ-Karlsruhe
  Contract No.: AMD 51000018867